“SAPIENZA” UNIVERSITÀ DI ROMA

Dottorato di ricerca in

Biologia Cellulare e dello Sviluppo

XX ciclo

“Dystrophic *mdx* mice exhibit structural and molecular alterations of sympathetic neurons and their muscular targets”

Dottorando: Lombardi Loredana

Docente guida: Prof.ssa Paola Paggi

ABBREVIATIONS

ACh	acetylcholine
BDNF	brain derived neurotrophic factor
BSA	bovine serum albumine
CNS	central nervous system
CREB	cyclic-AMP response element binding
DAB	diaminobenzidine
DGC	dystrophin-associated glycoprotein complex
DMD	Duchenne muscular dystrophy
EBD	Evans blue dye
ERK	extracellular signal-regulated kinase
HPRT	hypoxantine-phospo-rybosil-transferase
IF	intermediate filament
JNK	Jun amino-terminal kinase
kDa	kiloDalton
MAPK	mitogen activated protein kinase
mdx	murine X-linked muscular dystrophy
MEK	MAPK kinase
MMLV-RT	moloney murine leukemia virus reverse transcriptase
MMP	metalloproteinase
nAChR	nicotinic acetylcholine receptor
NCAM	neural cell adhesion molecule
NF	neurofilament
NF-L	light molecular mass neurofilament protein
NF-M	medium molecular mass neurofilament protein
NF-H	high molecular mass neurofilament protein
NGF	nerve growth factor
NGS	normal goat serum
nNOS	neuronal nitric oxide synthase
NO	nitric oxide
NRIF	neurotrophic receptor interacting factor
NT3	neurotrophin 3
NT4/5	neurotrophin 4/5
p75NTR	p75 neurotrophin receptor

PAP	peroxidase-anti-peroxidase
PB	phosphate buffer
PBS	phosphate buffered saline
PI3K	phosphoinositide 3-kinase
PNS	peripheral nervous system
PSA-NCAM	polysialic acid neural cell adhesion molecule
RT	room temperature
SCG	superior cervical ganglion
SEM	standard error of the mean
SIF	small intensely fluorescent
T-OH	tyrosine hydroxylase
Trk	receptor tyrosine kinase
WGA-HRP	horseradish peroxidase conjugated with wheat germ agglutinin
wt	wild-type

INDEX

INTRODUCTION

INTRODUCTION

1. Duchenne muscular dystrophy and dystrophin

1.1 Duchenne muscular dystrophy

Duchenne muscular dystrophy is a fatal X-linked inherited disease with an incidence of 1 in 3300 male births. It is caused by large deletions or duplications in the dystrophin gene that disrupt the translational reading frame leading to the complete loss of the full-lenght protein. In allelic disorder Becker muscular dystrophy the translational reading frame is preserved, resulting in the production of an incomplete but partially functioning protein (reviewed in Mehler, 2000). DMD is characterized by progressive muscle weakness, leading to death at around an age of 20 years, usually because of cardio-respiratory complications (reviewed in Blake et al., 2002). Many DMD patients also show signs of cognitive impairment (reviewed in Anderson et al, 2002) and autonomic dysfunctions (Yotsukura et al., 1995). From a histological point of view, necrotic or degenerating muscle fibers, often grouped in clusters, are seen in all postnatal DMD muscle biopsies even before muscle weakness is clinically observed. This occurs together with inflammatory cells. In the early phase of the disease a regenerative process is ongoing. However in later phases, the regenerative capacity of the muscles appears to be exhausted and muscle fibers are replaced by connective and adipose tissue (reviewed in Deconinck & Bernard, 2007). Lack of dystrophin in cardiac muscle cells is responsible for cardiomyopathy and cardiac conduction abnormalities in DMD patients (reviewed by Blake et al., 2002). Smooth muscle cells are also altered, at least in certain regions, such as the gastrointestinal tract (Bensen et al., 1996). Many hypotheses have been proposed to explain the pathophysiological processes responsible for DMD. The so-called “mechanical hypothesis” is based on the observation that the absence of the scaffolding protein dystrophin or of members of the dystrophin-associated glycoprotein complex compromises the sarcolemma integrity of muscle fibers in DMD, particularly during sustained contractions (Petrof et al., 1993). Indeed, in muscle cells, dystrophin is localized at costameres, composed of cytoskeletal proteins that act as mechanical couplers to distribute contractile forces generated in the sarcomere. It has been shown that the absence of dystrophin and the consequent loss of the DGC is responsible for the disruption

of the costameric lattice leading to membrane fragility (Rybakova et al., 2000), which is also suggested by the increased membrane permeability of dystrophic muscles to small molecules and dyes (Straub et al., 1997). Another important and widely explored hypothesis is the altered calcium homeostasis in dystrophic muscle fibers. All the data support the hypothesis that when mechanical stress induces micro-lesions in the fiber membrane, high influx of extracellular calcium occurs through calcium leak channels, overriding the capacity of the cell to maintain physiological calcium concentrations. Sustained increase in cytosolic calcium concentration leads to activation of proteases, which, in turn, can lead to cell death (Alderton & Steinhardt, 2000). There are often other contributing factors such as altered regeneration, inflammation, impaired vascular adaptation and fibrosis (reviewed in Deconinck & Bernard, 2007).

With regard to the involvement of the nervous system, it is noteworthy that Duchenne himself in 1861 reported that many DMD patients showed altered cognitive functions. According to Sekiguchi (2005), CNS disorders can be divided into two categories: the intellectual and/or cognitive impairment and the psychiatric disorders. Even though initial data from DMD brain autopsies showed no abnormalities (Dubowitz & Crome, 1969), by using more sophisticated techniques it has become possible to observe slight cortical atrophy, neuronal loss and dendritic abnormalities in cortical and sub-cortical brain areas, as well as cerebellar hypometabolism (reviewed in Anderson et al., 2002).

1.2 *Dystrophin and the dystrophin-associated glycoprotein complex*

Dystrophin is a large cytoskeletal protein whose loss is responsible for Duchenne muscular dystrophy (Hoffmann et al., 1987). The DMD gene is located on the short arm of the X chromosome, at Xp21. The expression of the full-length dystrophin (Dp427, a protein of molecular mass 427 kDa) is controlled by three tissue specific promoters, whose names reflect the major site of expression: B, brain, M, muscle and P, Purkinje cells (Fig.1). The DMD gene has also internal promoters that drive the expression of shorter non-skeletal muscle protein products of 260 kDa (Dp260), 140 kDa (Dp140), 116 kDa (Dp116) and 71 kDa (Dp71). These proteins consist of the C-terminal domains of dystrophin, but lack progressively greater parts of the N-terminal regions of Dp427 (Fig.1); Dp71 is detected in many

non-muscle tissues, including brain, liver, lung and kidney, while the other isoforms are primarily expressed in central and peripheral nervous system (reviewed in Blake et al., 2002).

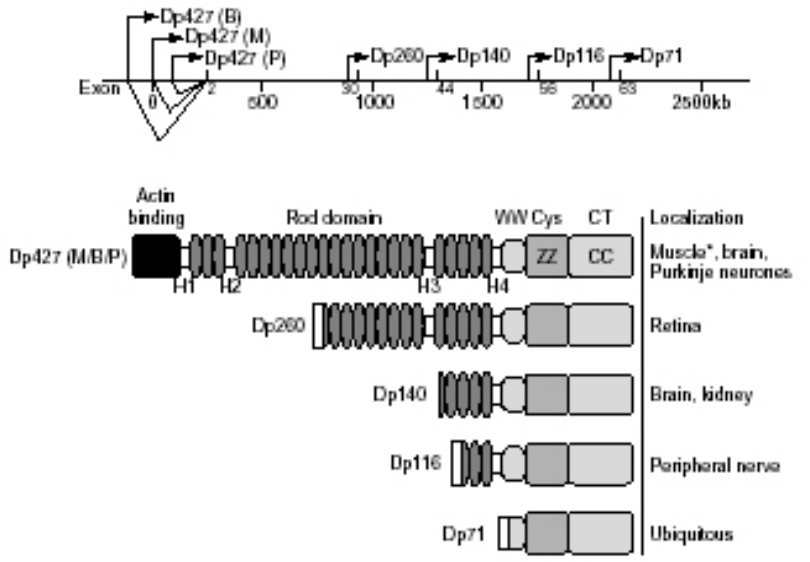

Figure 1. The dystrophin gene and protein isoforms (from Blake & Kroger, 2000)

Dystrophin is a member of the β-spectrin/α-actinin protein family. Dystrophin major domains are homologues to those present in cytoskeletal proteins belonging to this family. Dystrophin N-terminal domain is a functional actin binding domain; the central rod domain consists of 24 triple helical spectrin-like repeats interspersed with four putative hinge domains, that together are thought to confer dystrophin an elongated and flexible shape; the cysteine-rich domain comprises different modules for protein-protein interactions, namely a EF hand-like, a WW and a ZZ module; the C-terminal domain is unique to dystrophin and its closest homologues utrophin and dystrobrevins and contains two polypeptide stretches that form α-helical coiled coils (Fig.1) (reviewed in Ervasti, 2007).

Utrophin is an autosomal gene product with high homology to dystrophin, in fact its primary structure is similar to dystrophin throughout its length especially in the N- and C-terminal domains. A number of utrophin shorter C-terminal isoforms have also been described. It is widely expressed in nearly all tissues, including skeletal and smooth muscle, lung, kidney and the nervous system. In fetal and regenerating muscle cells, utrophin is distributed all along the sarcolemma, while in adult muscle it is confined to myotendinous and neuromuscular junctions, where it

is thought to stabilize postsynaptic AChRs (reviewed in Blake et al., 2002). Many studies have demonstrated that utrophin overexpression can compensate for the absence of dystrophin in muscle cells. However, biochemical differences between utrophin and dystrophin actin binding have been identified (reviewed in Ervasti, 2007). Moreover, it is likely that dystrophin isoforms and utrophin fulfill distinct roles in non-muscle tissues (Haenggi & Fritschy, 2006).

1.2.1 The dystrophin-associated glycoprotein complex in muscle cells

In muscle cells, dystrophin is localized to the cytoplasmic face of the sarcolemma, where it is part of a large protein complex (Campbell & Kahl, 1989), called the dystrophin-associated glycoprotein complex (Fig.2). This complex spans the muscle cell membrane and physically links the cellular actin-based cytoskeleton to the extracellular matrix, stabilizing the sarcolemma and helping to resist the stresses that develop particularly during muscle contraction or stretch (reviewed in Blake et al., 2002). Nevertheless, it is becoming clear that, beyond its structural functions, the DGC also plays an important role in signal transduction, in non-muscle tissues, through its interactions with many cytoplasmic signaling proteins (Rando, 2001). Furthermore, it is involved in physiological phenomena such as brain development, synaptic plasticity and ion homeostasis (reviewed in Haenggi & Fritschy, 2006). The DGC is composed of three subcomplexes: the dystroglycan, the sarcoglycan and the cytoplasmic complex. The dystroglycan complex, a central component of the DGC, primarily involved in sarcolemma stabilization, is composed by α- and β-dystroglycan; a single dystroglycan gene produces a precursor protein that is afterwards proteolytically processed into extracellular α-dystroglycan and single-pass transmembrane β-dystroglycan, which remain non-covalently associated (Ibraghimov-Beskrovnaya et al., 1993). β-dystroglycan is directly linked to the cysteine-rich domain of dystrophin through its C-terminal domain and interacts with α-dystroglycan through its N-terminal domain. α-dystroglycan binds to many extracellular matrix proteins such as laminin, perlecan and agrin. Moreover, dystroglycan interacts with the signaling proteins Grb2 and Caveolin-3, and might thus have a role in intracellular signal transduction (reviewed in Rando, 2001), and with rapsyn, a protein that, at the neuromuscular junction, is required for clustering of AChRs (Cartaud et al., 1998).

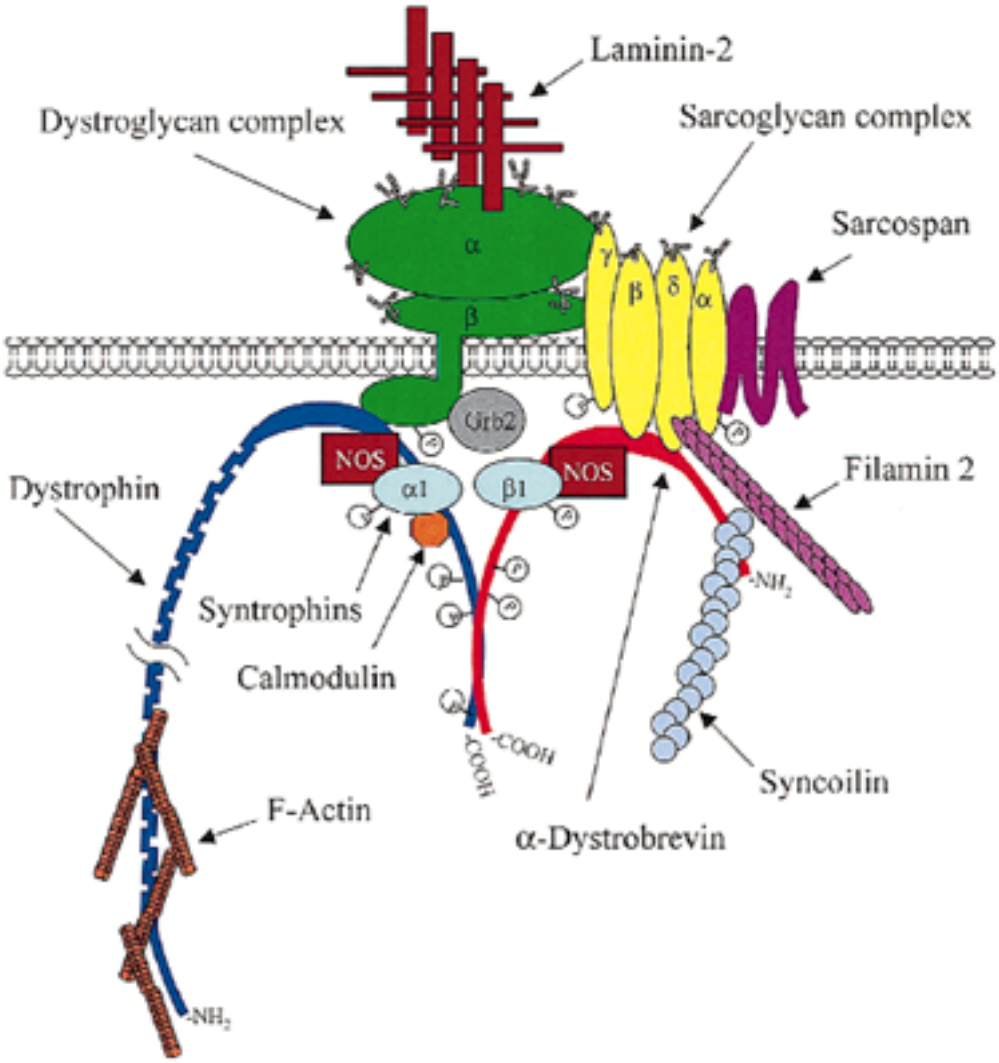

Figure 2. The dystrophin-associated glycoprotein complex in muscle cells (from Rando, 2001)

The sarcoglycan/sarcospan complex is made up by four transmembrane glycoproteins (α-, β-, γ- and δ-sarcoglycan in skeletal and cardiac muscle) and by a small transmembrane protein named sarcospan; it is necessary for the DGC stabilization, in fact mutations in any of the sarcoglycan isoforms result in the absence or severe reduction in the remaining components of the complex and are the primary defects in some forms of human limb-girdle muscular dystrophy (reviewed in Blake et al., 2002). The main components of the cytoplasmic complex are dystrobrevins and syntrophins. Dystrobrevin belongs to the dystrophin-related protein family and two isoforms, α- and β-dystrobrevin, are encoded by different genes, though only the former is highly expressed in skeletal muscle, and both present multiple splice-variants. Dystrobrevins interact with dystrophin and utrophin,

the binding occurring at the coiled-coil C-terminal domains of each protein, and dystrophin-dystrobrevin and utrophin-dystrobrevin complexes contain syntrophin binding sites (Sadoulet-Puccio et al., 1997). Moreover, dystrobrevin C-terminal domain contains many tyrosine kinase consensus sites, suggesting that the protein-protein interactions might be modulated by tyrosine phosphorylation (reviewed in Rando, 2001). The syntrophin family is composed of five members, encoded by different genes and able to bind both dystrophin and dystrobrevin; they are considered adaptor proteins: they have been shown to interact with a number of signaling molecules and membrane proteins through their PDZ domain, including nNOS, acquaporin 4, inwardly rectifying potassium channels, voltage-gated sodium channels and stress-activated protein kinase 3 (reviewed in Haenggi & Fritschy, 2006).

1.2.2 The dystrophin-associated glycoprotein complex in the nervous system

In the brain, dystrophin shows a region-specific expression pattern: it is expressed in the cerebral cortex, cerebellum and hippocampus, localized at post-synaptic densities (Lidov et al., 1990). Members of the DGC complex are also present in specific neurons, astrocytes and radial glia, usually associated with either dystrophin or utrophin; moreover, dystrophin shorter isoforms Dp140 and Dp71 are both highly expressed in brain (reviewed in Haenggi & Fritschy, 2006). Localization of dystroglycan in the brain showed that it is widely expressed in postsynaptic densities and in the endfeet of perivascular astrocytes (Zaccaria et al., 2001); α-dystroglycan interactions with extracellular matrix proteins are thought to be important in synapse stabilization, while β-dystroglycan cytoplasmic domain is needed for rapsyn to associate with AChRs (reviewed in Culligan & Ohlendieck, 2002). In addition, this complex is able to bind brain-specific ligands such as neurexins, presynaptic membrane-associated proteins whose Ca^{2+}-dependant binding with α-dystroglycan might mediate intercellular cell adhesion at the synapse (Sugita et al., 2001). α- and β-dystrobrevin are both expressed in the CNS, both in glial cells and hippocampal neurons, in association with Dp427 and utrophin (reviewed in Culligan & Ohlendieck, 2002). With regard to syntrophins, two brain-specific syntrophins have recently been described, and, even though their function is not yet clear, they are likely to function as syntrophin isoforms in muscle cells

(reviewed in Culligan & Ohlendieck, 2002). Finally, it is known that Dp116 is present in glial cells of the peripheral nervous system (Byers et al., 1993).

1.3 Animal models for Duchenne muscular dystrophy

The discovery of dystrophin led to the recognition of mutations in orthologous genes in other animals. Their study dramatically increased our knowledge of DMD pathogenetic mechanisms and allowed initial testing of putative treatments for patients. Although animals, such as GMRD (golden retriever muscular dystrophy) dogs and FXMD (feline X-linked muscular dystrophy) cats exist, the *mdx*/*mdx* mice are the smallest and easiest to handle. The *mdx* mouse was initially identified because of raised serum creatine kinase levels (a characteristic shared with human patients), that is an indicator of muscle damage (reviewed in Blake et al., 2002). It lacks full-length dystrophin (Dp427) because a mutation in exon 23 of the gene leads to the appearance of a stop codon which prematurely terminates the translation of dystrophin, while the short isoforms are normally produced (Sicinsky et al., 1989). Moreover, all components of the DGC are extremely reduced (reviewed in De La Porte et al., 1999). Even though *mdx* mice are largely used as a model for human DMD, the progressive muscle-wasting disease is present in these animals in a much milder form than in humans. Their life span is not reduced compared to controls, there is minimal fibrosis and fatty replacement in their muscle cells, and cellular necrosis is compensated by regeneration of muscle fibers, with degeneration-regeneration cycles peaking between 4 and 8 postnatal weeks of age (reviewed by De La Porte et al., 1999). Why dystrophic mice and humans show such diverse characteristics is still controversial and many possible explanations have been proposed, such as the different size and the different regenerative capacity that involves satellite cells and transcription factors expression (reviewed by Durbeej & Campbell, 2002), and utrophin compensation for the lack of dystrophin in *mdx* mice skeletal muscle (Grady et al., 1997). Recently a comparison of studies in mice and humans has highlighted no remarkable differences between *mdx* mice and DMD patients at least in the expression of proteoglycans, muscle growth factors, integrins, caveolin-3, nNOS and calcineurin (reviewed by Fadic, 2005), suggesting that further investigations are needed.

In *mdx* mice, both skeletal and cardiac muscle show membrane fragility and increased permeability to small molecules, necrotic fibers are typically grouped in clusters and the amount of degenerating tissue varies depending on the considered muscle (Straub et al., 1997; Danialou et al., 2001). It has been suggested that this could be due to many factors, namely muscle activity level and diameter of the fibers (Boland et al., 1995). The most affected skeletal muscle is the diaphragm, which well reproduces the degenerative changes observed in human muscular dystrophy (Stedman et al., 1991). *Mdx* smooth muscles show no morphological signs of cell necrosis or muscle fibrosis, but a reduction in gastrointestinal smooth muscle thickness has been observed, that could reflect a mild smooth muscle atrophy (Boland et al., 1995). From a functional point of view, *mdx* mice present altered electric and motor activity in various regions of the gastrointestinal tract, that are likely to depend on altered nitric oxide production by smooth muscle cells (Mulè et al., 1999, 2001, 2006); altered biomechanical properties of carotid arteries have been also demonstrated in these animals (Dye et al., 2007). As for the nervous system alterations, it appears that the lack of full-length dystrophin in *mdx* mice is correlated with a slight degree of cognitive impairment (reviewed by Anderson et al., 2002). It has been shown that nicotine doses needed to increase memory in a passive avoidance memory task were higher in *mdx* than in wt mice, suggesting that central nAChRs might be down regulated in dystrophic animals (Coccurello et al., 2002). Histological evidences demonstrated architectural changes of the cortico-spinal system in the cerebral cortex of *mdx* mice, namely a reduction in the number of the cortico-spinal neurons and in their average diameter relative to wt animals (Sbriccoli et al., 1995). Dystrophin is enriched in the postsynaptic densities of cerebral cortex, hippocampus and cerebellum (Lidov et al., 1993); Knuesel and colleagues (1999) demonstrated that in these brain areas dystrophin co-localizes with $GABA_A$ receptor subunits and that synaptic clustering of $GABA_A$ receptors is markedly reduced in *mdx* mice, suggesting that dystrophin may play an important role in the clustering or stabilization of such receptors. Increased sensitivity of *mdx* hippocampal pyramidal neurons to hypoxia-induced loss of synaptic transmission (Mehler et al., 1992) and reduced long-term depression in dystrophic cerebellar Purkinje cells (Anderson et al., 2004) have been also demonstrated. Moreover,

dystrophin deficiency leads to severe injury of glial endfeet and to blood-brain barrier breakdown in *mdx* mice brain (Nico et al., 2003).

2. The sympathetic superior cervical ganglion

The superior cervical ganglion is part of the autonomic sympathetic nervous system and belongs to the paravertebral sympathetic chain, which lies close to the vertebral column. The SCG is localized in the cervical region, dorsally to the branching of the common carotid artery (Fig.3). Its large size and accessibility make it a favorite research model.

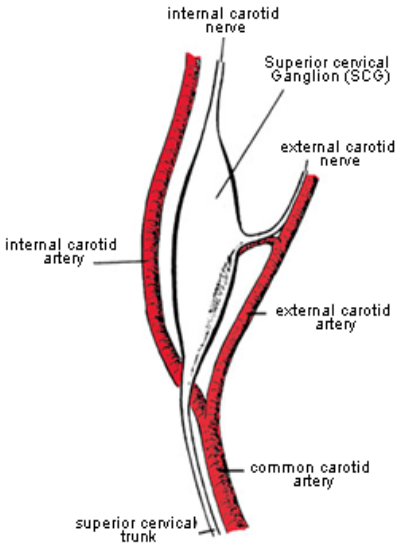

Figure 3. Schematic representation of the superior cervical ganglion: localization, afferent and efferent nerves

Sympathetic ganglion cells are isolated from their environment by a thick capsule of connective tissue, which is continuous over afferent and efferent nerves. Sympathetic ganglia receive a rich blood supply from vessels that enter the ganglion over both the pre- and the post-ganglionic nerve pathways (reviewed in Dail & Burton, 1983). Superior cervical ganglion neurons are reached by preganglionic input from neurons located mainly in the intermediolateral column of the last cervical and the first seven thoracic spinal cord segments: preganglionic neurons project to the SCG through the superior cervical trunk (reviewed in Baluk, 1995). Superior cervical ganglion neurons project to their targets through two postganglionic nerves (Fig.3): the internal carotid nerve that innervates iris, pineal gland and tissues in the cranium, such as smooth muscle cells of some arteries, and the external carotid nerve that innervates heart and submandibular glands

(Fig.4) (reviewed by Dail & Burton, 1983); moreover, a small population of neurons sends axons caudally through the superior cervical trunk (Bowers & Zigmond, 1979). Within the ganglion, neurons tend to be localized near the exit of their postganglionic nerve fibers (Bowers & Zigmond, 1979).

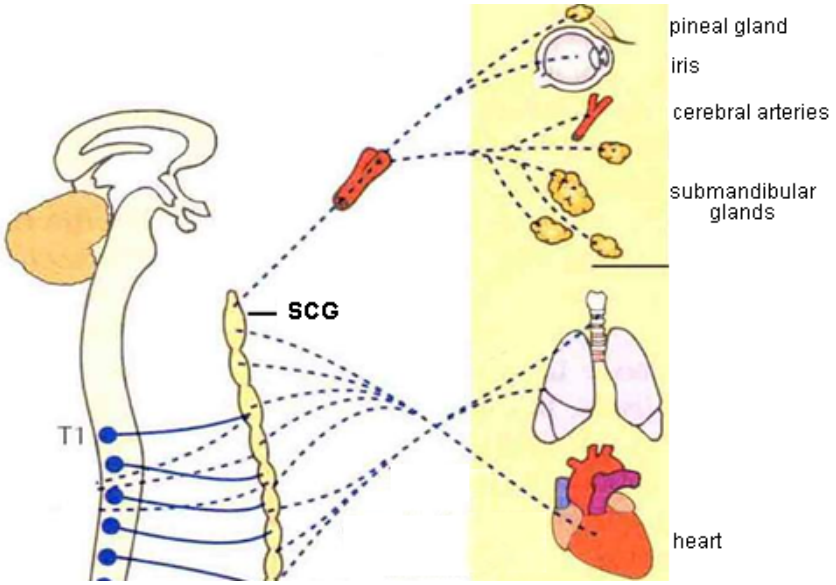

Figure 4. SCG target organs (modified from Berne & Levy, 2002)

Superior cervical ganglion neurons are called “principal” and are typical multipolar neurons with a complex array of processes, and they are almost entirely enclosed by satellite cells. The covering of satellite cells is only deficient at synapses sites on both soma and dendrites (reviewed by Dail & Burton, 1983). Like all sympathetic ganglion neurons, SCG neurons are noradrenergic and contain dense-core catecholamine vesicles in their cytoplasm (reviewed by Dail & Burton, 1983). SIF cells, with very high amount of catecholamines are also present in sympathetic ganglia, but there still is no general agreement as to their function: they have been proposed to mediate a chemoreceptor function for substances in the blood, to act as interneurons or to have a paracrine role (reviewed in Baluk, 1995).

The main neurotransmitter released by presynaptic terminals is acetylcholine and its binding to nAChRs elicits rapid excitatory postsynaptic potentials in ganglionic neurons (reviewed in Taxi & Eugène, 1995). This neurotransmitter interacts with different nAChRs subtypes: heteromeric receptors containing the α3 subunit associated with the β4 and/or β2 subunits and the homomeric α7 receptors

(Del Signore et al., 2002; 2004). Moreover, in the SCG, muscarinic receptors are also present: ACh binding to M_1 muscarinic receptors induces slow excitatory postsynaptic potentials and its binding to M_2 muscarinic receptors induces inhibitory postsynaptic potentials (reviewed in Taxi & Eugène, 1995). In SCG, presynaptic terminals release, besides ACh, many neuropeptides, namely vasointestinal peptide, enkefalins and substance P that are neuromodulators and can also induce delayed excitatory postsynaptic potentials (reviewed in Taxi & Eugène, 1995). It is now clear that signals traveling along the preganglionic nerves are not simply relayed by postganglionic nerves to the effector tissues, but are distributed, integrated and/or modified before reaching the final target (reviewed in De Biasi, 2002).

2.1 Development of the superior cervical ganglion

During development, principal neurons of sympathetic ganglia acquire the appropriate match of input from preganglionic neurons in the spinal cord and establish synaptic contacts with peripheral target tissues. Superior cervical ganglion neurons, like all sympathetic neurons, SIF cells and adrenal chromaffin cells, derive from embryonic neural crest cells (reviewed in Francis & Landis, 1999). Precursors migrate ventrally from the neural crest to form a column of sympathetic ganglion primordia near the dorsal aorta, undergo specification, commence acquisition of noradrenergic properties and then coalesce to form the definitive sympathetic ganglia, among which the rostrally located SCG (reviewed in Glebova & Ginty, 2005). The initial outgrowth of the single axon from principal ganglion neurons occurs soon after the withdrawal from the cell cycle and axons do not branch until they reach their targets. Dendritic arbor development follows shortly after the beginning of axon outgrowth (reviewed in Wright, 1995). Contacts between preganglionic and postganglionic neurons and between postganglionic neurons and peripheral targets begin to form before birth, but develop and mature postnatally (reviewed in Wright, 1995). Developmental neuron death occurs in the first postnatal weeks: neurons die by apoptosis and this results in the loss of 30-40% of the neurons present at birth, in the rat SCG (Wright et al., 1983). Thus, death of SCG neurons occurs during the developmental period in which neurons are establishing synaptic contacts with their targets and afferents. Many factors

contribute to the establishment of synaptic contacts, as well as their maintenance throughout life, thus influencing development and survival of SCG neurons themselves. Preganglionic input (Black et al., 1971; Black & Mytilineou, 1976), neuronal activity and non-neuronal cells (reviewed in Wright, 1995) may all regulate development of SCG neurons. Nevertheless, it is the interaction of sympathetic neurons with their peripheral target organs that primarily influences neuronal development and survival and allows to maintain neuronal morphology and connections. The release by peripheral targets of neurotrophic factors and their subsequent retrograde transport to neuronal somata is the main mechanism involved in this essential function.

2.1.1 Role of target organs and neurotrophins in the development of the superior cervical ganglion

The classical "neurotrophic hypothesis", formulated to explain the observed developmental cell death, states that in order to ensure the optimal amount of target innervation, neurons are initially overproduced during development. Once they innervate their targets, compete for limiting amount of target-derived neurotrophic factors. Consequently, those neurons that do not obtain sufficient amounts of neurotrophins die by apoptosis (Oppenheim, 1991). The foundation for this hypothesis was laid by the pioneering work by Hamburger and Levi-Montalcini back in 1949 which demonstrated that neuronal survival is strictly dependent on target-derived trophic factors. These studies led, in the 1960s, to the identification of the first neurotrophic factor, named nerve growth factor, as the neurotrophic factor for sensory and sympathetic neurons (reviewed in Bennett et al., 2002). Subsequently, it has been found that NGF is only a member of a low-molecular-mass protein family of growth factors, called the neurotrophic family, which includes NGF, BDNF, NT3 and NT4/5. It is now well established that, besides many aspects of development such as cell fate decisions, axon growth, dendrite pruning, patterning of innervation and protein expression, neurotrophins regulate also maintenance and function of the whole vertebrate nervous system (reviewed in Huang & Reichardt, 2001).

Neurotrophins are synthesized as precursor forms called proneurotrophins, which are intracellularly cleaved by furin or proconvertases to yield mature neurotrophin dimers (reviewed in Nykjaer et al., 2005). Proneurotrophins can also

be secreted and cleaved by extracellular proteases such as metalloproteinases and plasmin (Lee et al., 2001). Neurotrophins are able to bind to two types of transmembrane receptors (Fig.5): the Trk and the p75NTR receptors, thus giving rise to different and sometimes opposite signalling pathways. In fact, while Trk receptors transmit positive signals such as enhanced survival and growth, p75NTR (p75) transmits both positive and negative signals (reviewed in Kaplan and Miller, 2000).

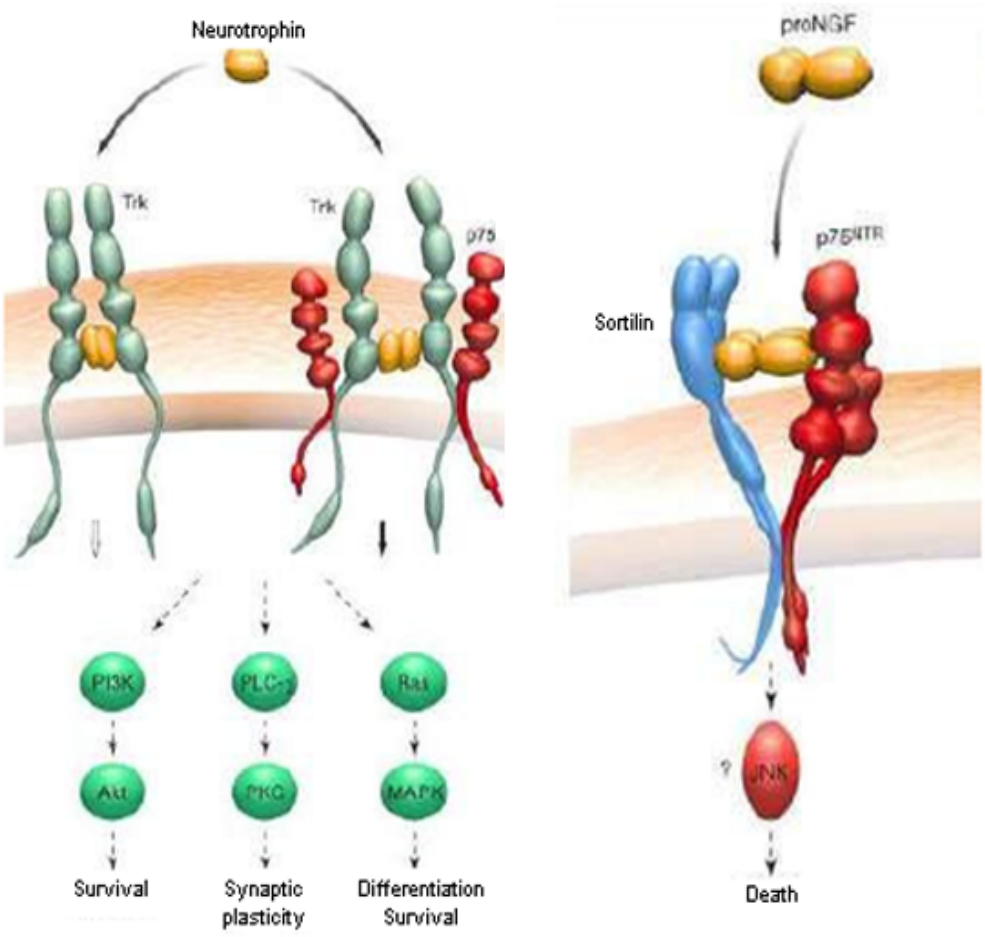

Figure 5. Neurotrophins: ligands and receptors (from Nykjaer et al., 2005)

Each neurotrophin binds with high affinity to a specific receptor of the Trk family: NGF to TrkA, BDNF to TrkB and NT3 to TrkC. NT3 can also bind to TrkA and TrkB (reviewed in Zweifel et al., 2005). Ligand binding induces dimerization of Trk receptors and their autophosphorylation at specific tyrosine residues in the cytoplasmic domain. This, in turn, leads to the recruitment of various downstream effectors and the activation of numerous signal transduction cascades that support

growth and survival (reviewed in Huang & Reichardt, 2003) (Fig.5). Trks use at least two mechanisms to signal survival: the Ras-PI3K-Akt-induced suppression of apoptotic pathways and the MEK/MAPK activation of anti-apoptotic proteins (reviewed in Kaplan and Miller, 2000). It is interesting to note that distinct effector pathways may be activated by neurotrophin signalling in different cellular compartments, that is in axon terminals, or after retrograde transport, in neuronal soma (Watson et al., 2001). The mechanism that has been proposed to explain Trks retrograde signalling is the "signalling endosome model" (Campenot, 1994). According to this hypothesis, neurotrophins are synthesized by target tissues and the binding to their specific Trk receptor in axon terminals leads to endocytosis of a ligand-receptor complex and to formation of signalling endosomes; the downstream signals must be retrogradely conveyed to the cell body where they support neuronal survival. The signalling endosome is retrogradely transported along the axon via a cytoskeleton-based transport machinery (reviewed in Howe and Mobley, 2003). In support of this model, it has been shown, in compartmentalized cultures, that inhibition of Trk kinase activity, both in the distal axons compartment or the cell bodies compartment, attenuates or eliminates accumulation of Trk signalling events (Senger & Campenot, 1997), activation of the transcription factor CREB (Riccio et al., 1997; Watson et al., 2001) and cell survival (Ye et al., 2003; Heerseen et al., 2004). Disruption of neurotrophin endocytosis (Ye et al., 2003) and pharmacological or molecular disruption of dynein-dependent microtubule transport (Heerseen et al., 2004) also leads to neuronal apoptosis. *In vivo*, target-derived NGF is detected in cell bodies in early endosomes together with TrkA and activated ERK and the amount of retrograde transport of activated TrkA is influenced by the amount of NGF present in the target (Delcroix et al., 2003). Most of the reviewed papers focus on NGF and its tyrosine kinase receptor TrkA, since NGF is the principal sympathetic and sensory neuron target-derived neurotrophic factor. During development, sympathetic neurons only become dependent on NGF about the time their axons first reach their target (reviewed in Bennett et al., 2002). In this period, in sympathetic target tissues NGF is expressed at levels corresponding to innervation density. Moreover, increasing the available NGF during development rescues sympathetic neurons that normally die, whereas decreasing NGF levels

with NGF antisera causes destruction of the sympathetic nervous system (reviewed in Francis & Landis, 1999).

The role of p75 in sympathetic neuron development is, instead, still controversial, because it has been shown to play different functions depending on cell types and developmental stages (reviewed in Hempstead, 2002). p75 is a member of the tumour necrosis factor receptor superfamily and binds all neurotrophins equally well (reviewed in Nykjaer et al., 2005). p75 can modulate ligand affinity and specificity of Trk receptors (Fig.5): indeed, responsiveness to limiting concentrations of NGF depends on the relative levels of TrkA and p75 and their ability to form high affinity binding sites (Lee et al., 1994; Esposito et al., 2001). Both NGF and NT3 bind TrkA, but p75 expression restricts TrkA signalling to NGF (Mischel et al., 2001), enabling developing sympathetic neurons to switch sensitivity from NT3 to NGF and to support TrkA internalization and retrograde transport (Kuruvilla et al., 2004). Nevertheless, a well established function of p75 is to promote cell death, by inducing the activity of the JNK-p53-Bax apoptosis pathway (Aloyz et al., 1998) and of other proteins that regulate cell death, such as NRIF (Casademunt et al., 1999; Kenchappa et al., 2006). Ligand-dependent activation of p75 has been shown to cause apoptosis of a number of different cell types (reviewed in Kaplan and Miller, 2000), including neonatal sympathetic neurons (Bamji et al., 1998). In sympathetic neurons, examination of a possible apoptotic role for p75 has focused on BDNF, which is produced by both sympathetic ganglia (Causing et al., 1997) and their targets (Maisonpierre et al., 1990a; Kohn et al., 1999). BDNF signals only through p75 in these neurons because they do not express the BDNF Trk receptor, TrkB (reviewed in Glebova & Ginty, 2005). Nevertheless, a number of studies have shown that p75 only mediates apoptosis when TrkA is inactive or suboptimally activated, leading to the conclusion that TrkA activation silences p75 apoptotic signalling in sympathetic neurons (Bamji et al., 1998; Majdan et al., 2001). Recently, it has become evident that the pro-forms of neurotrophins, proneurotrophins, are able to bind p75 with higher affinity than that exhibited by mature neurotrophins (Lee et al., 2001), particularly when p75 forms a complex with sortilin, a member of the family of Vps10p-domain receptors (Nykjaer et al., 2004; Teng et al., 2005). Pro-NGF induces apoptosis of p75-expressing cells (Fig.5), including sympathetic neurons and oligodendrocytes, and is unable to

stimulate TrkA-mediated survival (Lee et al., 2001). The proneurotrophin pro-NGF is expressed *in vivo* by both sympathetic neurons (Hasan et al., 2003; Jansen et al., 2007) and peripheral targets (Bierl et al., 2005).

It is now clear that sympathetic neuron development is an elaborate chain of intricate events, composed by distinct temporal and spatial elements that lead, through a coordinated process, from neuron specification to axon growth and maturation. During embryonic development, at least one other member of the neurotrophin family is needed for proximal axon extension, NT3 (Kuruvilla et al., 2004), that, together with artemin, a vascular-derived neurotrophic factor, (Honma et al., 2002), mediates sympathetic axon growth along the vasculature. Final target innervation is instead controlled by NGF (Glebova & Ginty, 2004): once the axons reach target tissues, the increased availability of NGF and the higher selectivity of TrkA for NGF over NT3, due to up-regulation of p75, possibly cause NGF to become the dominant survival factor (Francis & Landis, 1999); in addition, although both NT3 and NGF signal through TrkA to mediate axon growth, only NGF can support retrograde TrkA signalling in sympathetic neurons (Kuruvilla et al., 2004). Control of sympathetic neuron survival and death during development by neurotrophins and their receptors has been well characterized (Fig.6).

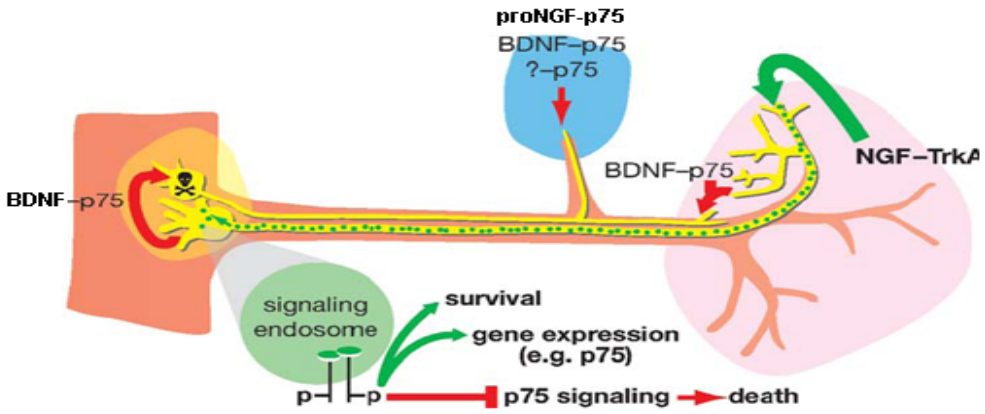

Figure 6. Control of sympathetic neuron survival and death during development (from Glebova & Ginty, 2005)

It is, thus, possible to propose a model for the events that control sympathetic neuron survival (Glebova and Ginty, 2005). NGF expressed by target tissues binds TrkA on axon terminals, where it is endocytosed as a ligand-receptor complex and transported to the cell body in a signalling endosome. In neuronal soma, NGF

supports survival, also by regulating gene expression. One of the genes upregulated by NGF is p75 (Wyatt & Davies, 1995), which may have a proapoptotic function. TrkA activation suppresses prodeath p75 signalling (Majdan et al., 2001), thus ensuring cell survival. However, if a neuron does not obtain adequate NGF to sustain prosurvival TrkA signalling after p75 induction, such suppression will not occur. p75 may then promote cell death in response to ligands such as BDNF or proNGF from the target or from the neurons themselves (Glebova and Ginty, 2005).

2.2 Dystrophin and the organization of the SCG intraganglionic synapses

Previous work of our laboratory has shown that in the autonomic superior cervical ganglion dystrophin co-localizes with β-dystroglycan and nAChRs at the intraganglionic postsynaptic apparatus (De Stefano et al., 1997; Zaccaria et al., 1998). After SCG postganglionic nerve crush, it has been observed by immuno-electron microscopy that the disassembly of the intraganglionic synapses was preceded by a rapid decline in the percentage of postsynaptic specializations immunopositive for β-DG, dystrophin and the α3 subunit of the nAChR. When axotomized neurons began to regenerate their axons, the number of intraganglionic synapses, as well as that of postsynaptic specializations immunopositive for the aforementioned proteins, increased. This suggests that the dystrophin-dystroglycan complex might play a role in the injury-induced disassembly and subsequent reassembly of the postsynaptic apparatus, possibly being involved in the stabilization of nAChR clusters (Zaccaria et al., 1998). In the SCG of *mdx* mice, that lack full-length dystrophin, a selective and significant reduction in intraganglionic postsynaptic specializations immunopositive for α3nAChRs (Del Signore et al., 2002; Zaccaria et al., 2000) and for α- and β-dystroglycan (Zaccaria et al., 2000) compared with the wt have been found. This strongly indicates that the absence of dystrophin at the intraganglionic postsynaptic apparatus of *mdx* mouse SCG interferes with the presence of both dystroglycan and nAChRs clusters at these sites, possibly affecting fast intraganglionic transmission. Moreover, the different nAChR subtypes present in the SCG of wt and *mdx* mice were characterized. Two types of receptors were found: one containing the α3 subunit associated with the β2 and/or β4 subunits and another one containing the α7 subunit (Del Signore et al.,

2002). Only α3, β2 and/or β4 nAChRs were drastically reduced at the intraganglionic postsynaptic specializations of *mdx* mouse SCG, further demonstrating a dystrophin-dependant stabilization of this subtype of receptor at the postsynaptic apparatus. Conversely, dystrophin was not involved in stabilization of the α7 containing nAChRs, as the percentage of α7-immunopositive synapses is similar in both wt and *mdx* mouse SCG (Del Signore et al., 2002). Thus, in the autonomic SCG the dystrophin-dystroglycan complex is involved in the disassembly-reassembly of the postsynaptic apparatus consequent to axotomy and in the stabilization of the α3 containing AChRs.

3. Axonal transport and neuronal cytoskeleton

Neurons are highly polarised cells with a long and thin axon that typically grows very far from the cell body. They also have multiple thick dendrites that remain comparatively short. Cytoskeletal elements play key architectural roles and contribute significantly to the acquisition and maintenance of such asymmetrical cellular morphologies (reviewed in Baas & Buster, 2003). Moreover, communication and active transport between the cell periphery and the cell centre and vice versa are required (reviewed in Chevalier-Larsen & Holzbaur, 2006). Neurons depend on molecular transport for all these cellular functions.

The cytoskeleton is an aggregate structure formed by three classes of cytoplasmic structural proteins: microtubules (tubulins), microfilaments (actins) and intermediate filaments. They are all dynamic rather than passive structural elements (reviewed in Brady et al., 1999). Microtubules are nearly ubiquitous components of the cytoskeleton in eukaryotes and are very abundant in the nervous system. They are hollow tubes 25 nm in diameter, whose walls comprise 13 protofilaments formed by a linear arrangement of globular subunits, that is heterodimers of α- and β-tubulin. Each protofilament thus consists of a series of α- and β-tubulin dimers organized in a polar fashion, giving the microtubule a “plus” (fast growing) and a “minus” (slow growing) end (reviewed in Brady et al., 1999). In neurons, microtubules are differently arranged in the axonal and dendritic compartments: along the axon, they are organized in a polar array, with the microtubule “plus” end directed outward and the microtubule “minus” end directed toward the cell centre. Differently, they are found in mixed polarities in dendrites (reviewed in Chevalier-Larsen & Holzbaur, 2006). Microfilaments are composed by actin, which is universally present in eukaryotes. Microfilaments are present throughout the cytoplasm in the form of short filaments from 4 to 6 nm in diameter, often bundled into networks. In neurons, actin microfilaments are most abundant in presynaptic terminals, dendritic spines, growth cones and the subplasmalemmal cortex (reviewed in Brady et al., 1999). Intermediate filament proteins constitute a superfamily of 5 classes, which have specific cell type and developmental stage patterns of expression. They are named after the characteristic diameter of 8-10 nm, that is intermediate between actin filaments and microtubules. IF share a

characteristic ~310 amino acid α-helical domain containing a hydrophobic repeat essential for assembly. Head and tail segments flank this central rod, and are markedly divergent in length and sequence among the various members of the family (reviewed in Lee & Cleveland, 1996). Assembly of IF involves the formation of two coiled-coil dimers of protein subunits in order to form an antiparallel tetramer. The lateral and longitudinal association of tetramers makes up the final filament (reviewed in Lariviere & Julien, 2003). The neurofilament proteins are the most abundant IF type in adult neurons. They are made up by the copolymerization of the NF-light (NF-L, 68 kDa), medium (NF-M, 140 kDa) and heavy (NF-H, 180-200 kDa) molecular mass proteins (reviewed in Lariviere & Julien, 2003). They are obligate heteropolymers requiring NF-L with either NF-M or NF-H for proper polymer formation (Lee et al., 1993). Unlike other IFs, NFs have characteristic “side arms” extending from the filament backbone that appear to form bridges between filaments (Hirokawa et al., 1984); these side arms are formed by NF-M and NF-H carboxy-terminal regions. NF-H and, even though to a less extent, NF-M tails contain many repeats of lysine-serine-proline (KSP); the serines in the KSP domains are heavily phosphorylated in axons (Julien & Mushynski, 1983). NFs have a role in modulating the radial growth of large myelinated axons: this is important for normal nerve function because calibre is the principal determinant of conduction velocity (reviewed in Lariviere & Julien, 2003). Phosphorylation of multiple KSP repeats in NF-H and NF-M C-terminal domains can influence axon calibre: phosphorylation increases neurofilaments negative charge that causes increased NF spacing (de Waegh et al., 1992). Neurofilaments also contribute to axon branch stability (Smith et al., 2006).

Organelles generally move very short distances along actin filaments and the molecular motors that drive this transport are myosins (reviewed in Chevalier-Larsen & Holzbaur, 2006). Actin-based organelle transport is particularly important in regions of axons and dendrites that are not rich in microtubules, such as dendritic spines and the leading edge of the axonal growth cone (reviewed in Baas & Buster, 2003).

The rapid and robust movement of organelles and membrane-associated proteins along microtubules within the axon is referred to as “fast axonal transport”. This kind of transport occurs both in the anterograde and retrograde directions, that

is from the cell body to the periphery and from the periphery to the soma, respectively. Microtubules act as railways for fast axonal transport. Proteins belonging to the kinesin superfamily drive plus-end directed motility along microtubules and are thus the anterograde motors. Cytoplasmic dynein is the major motor driving retrograde transport, because it produces force towards the minus end of microtubules (reviewed in Chevalier-Larsen and Holzbaur, 2006). *In vivo*, the dynactin accessory complex is required for most of dynein functions (reviewed in Mallik & Gross, 2004). Among the most critical cargos transported by dynein in neurons are neurotrophic signalling molecules (reviewed in Chevalier-Larsen and Holzbaur, 2006). Activated Trk receptors are associated with vesicles that travel in the retrograde direction via a dynein-driven transport mechanism (Bhattacharyya et al., 2002) and a dynein-dependent transport is required for Trk-activated retrograde survival signals (Heerssen et al., 2004).

Slow axonal transport is the movement of the proteins that comprise the cytoskeleton itself, which must be conveyed from their site of synthesis within the cell body down the length of the axon (reviewed in Baas & Buster, 2003). It consists of two subcomponents, the faster of which has a transport rate of 2-3 mm/d and contains actin, actin-associated proteins and a huge array of cytosolic proteins. The slower component has a transport rate of 0.25 mm/d and contains most of the tubulin, the neurofilament proteins and proteins known to associate with microtubules and neurofilaments (Black & Lasek, 1980). Early studies of slow axonal transport utilized pulse-chase experiments and revealed that transported proteins moved distally through the axon; the waves of transported proteins spread as they moved down the axon, suggesting some asynchrony in the rates of movement of individual elements within each component of slow transport (reviewed in Baas & Buster, 2003). The first opportunity to follow the movement of cytoskeletal proteins in living neurons in culture came with the addition of fluorescent tags to cytoskeletal proteins that, microinjected into neurons, typically filled a neurite (reviewed in Brady, 2000). A patch on the neurite could be “photobleached” and monitored for slow synchronous movement. Surprisingly, the movement did not occur (reviewed in Baas & Buster, 2003). Recently, by widening the parameters of the live-cell imaging paradigm, it has become possible to explain and reconcile the results of previous studies (reviewed in Baas et al., 2006). Such

result has been obtained by employing much longer “photomarks” or natural gaps in the neurofilament array, with image acquisition every several seconds instead of minutes. It has been shown that both neurofilaments (Wang et al., 2000; Yan & Brown, 2005) and microtubules (Wang & Brown, 2002) do move as polymers. The vast majority of the polymers are in a “pausing” state at any given moment, while roughly 10% of them undergo bouts of rapid movements. The slow rate of slow axonal transport is thus the result of this fast but relatively infrequent movement. Neurofilaments and microtubules also move bi-directionally, that is in both the anterograde and retrograde directions (Wang et al., 2000; Wang & Brown, 2002; Theiss et al., 2005). These observations also indicate that the motors for slow transport are actually fast motors, and hence are probably already identified motors, such as cytoplasmic dynein and members of the myosin and kinesin families. Indeed, He et al., (2005) showed that dynein is responsible for the retrograde transport of neurofilaments, consistent with a “cargo” model for neurofilament transport. According to this model, neurofilaments move in ways analogous to the movement of vesicles along microtubules. One or more microtubule-associated motor proteins associate with neurofilaments and carry their cargo along microtubules (Shah et al., 2000; reviewed in Brady, 2000). Instead, cytoplasmic dynein is a major participant in the anterograde transport of microtubules, therefore supporting the “sliding filament” model for axonal microtubule transport (He et al., 2005). According to this model, microtubules move down the axon by pushing against the actin cytomatrix (Ahmad et al., 1998). In this view, the cargo domain of the cytoplasmic dynein molecule is associated with the actin cytomatrix, leaving the motor domain available to interact with microtubules (reviewed in Baas & Buster, 2003). It is also possible for cytoplasmic dynein to move microtubules along other microtubules (Ahmad et al., 1998; Hasaka et al., 2004; Ahmad et al., 2006). Retrograde microtubule and anterograde neurofilament movements use motors other than cytoplasmic dynein. These motors are probably members of the kinesin (Yabe et al., 1999; Shah et al., 2000; Theiss et al., 2005) and myosin (Jung et al, 2004) families of motor proteins.

4. AIM OF THE PROJECT

In mouse sympathetic SCG, dystrophin is localized at the postsynaptic apparatus of a number of intraganglionic synapses (De Stefano et al., 1997), where, together with the transmembrane glycoprotein dystroglycan, it stabilizes the nicotinic acetylcholine receptors containing the α3 subunit (α3nAChR) (Zaccaria et al., 1998; Del Signore et al., 2002). In *mdx* mouse SCG, because of the lack of dystrophin Dp427, the number of α3nAChR-containing synapses is significantly reduced with respect to the wt (Zaccaria et al., 2000), suggesting alterations in the fast intraganglionic synaptic transmission. Changes in sympathetic neuron activity may, therefore, contribute to episodes of autonomic dysfunction described in DMD patients, such as heart rate alteration (Yotsukura et al., 1995). However, ganglionic neurons may also be affected by the damages induced by the lack of Dp427 in SCG target organs, such as the cardiac muscle. Dilated cardiomyopathy has been observed in DMD patients and *mdx* mice (Grady et al., 1997; Coral-Vazquez et al., 1999; Megeney et al., 1999). Many of the events characterizing neuronal life are indeed influenced by neuron-target multiple interactions (Introduction, chapter 2). Among these, cell body size and dendritic arborization (Voyvodic, 1989; Andrews et al., 1996), synapse formation and plasticity (Personius and Balice Gordon, 2000; Schinder and Poo, 2000), neurotransmitter secretion (Liou et al., 1999) and neuron survival (reviewed in Bennett et al., 2002). Previous observations of our group showed that the number of synapses per area are reduced in *mdx* mouse SCG compared to the wt and that the *mdx* mouse SCG is smaller than the wt.

The aim of the present work is to analyze whether the lack of Dp427 in *mdx* mice may affect SCG neurons directly and/or indirectly by damaging their target organs. With its dual innervation of muscular (heart, iris, arterial wall) and non-muscular (submandibular and pineal glands) targets, the SCG is an excellent *in vivo* model to evaluate the effects on sympathetic neurons exerted by each type of peripheral target, that may be differently affected by the dystrophic pathology. We counted SCG neuron number and assessed the extension and distribution of adrenergic innervation in SCG peripheral target organs, in wt and *mdx* mice. We also investigated the structural and functional effects of the lack of full-length dystrophin on *mdx* mouse SCG peripheral targets, both muscular and non-

muscular. Finally, we analyzed the expression of proteins involved in neuron development and survival and in axon growth, such as trophic factors, trophic factors receptors, and molecules responsible for axonal retrograde transport.

5. MATERIALS AND METHODS

5.1) Animals

We used male wild-type (C57BL/10) and genetically dystrophic (C57BL/10 *mdx*/*mdx*) mice (Jackson Laboratories, Bar Harbor, Maine, USA) P0, P5, P10, P15, P21 and young adult 6–7 weeks old. The age of 6–7 weeks falls within the time interval of 4–8 weeks during which, in *mdx* mice, intense cycles of skeletal muscle degeneration/regeneration occur. The animals were housed and handled in accordance with the guidelines laid down by the European Community Council Directive (86/609/EEC of 24 November 1986) and the American Society for Neuroscience.

5.2) Determination of SCG neuron number

To determine the number of ganglionic neurons, we used SCG dissected from three wild-type and three *mdx* mice at each postnatal date considered. P5, P10 and P15 mice were anesthetized with isoflurane (Merial, Milano, Italy), killed by decapitation and the ganglia, rapidly dissected, were fixed by immersion in 2.5% glutaraldehyde in 0.1M cacodylate buffer, pH 7.4 for 2 h at 4°C. Differently, adult and P21 animals were deeply anesthetized by intraperitoneal injection of chloral hydrate (400 mg/Kg body weight), perfused transcardially through the ascending aorta with oxygenated Ringer's solution at pH 7.3, followed by the same fixative as above. The SCGs were removed and, together with those fixed by immersion, were processed for standard light and electron microscopy. All specimens were post-fixed in 2% osmium tetroxide in 0.1M cacodylate buffer for 1 h at 4° C, dehydrated through an ascending series of ethyl alcohol and propylene oxide, with a 20 min step in 2% uranyl acetate dissolved in 70% ethanol, and embedded in Epon 812. The ganglia were cut in 2 μm thick serial semithin sections from the caudal to the rostral regions and stained with 0.1% Toluidine Blue in 0.1% borax. For each series, nucleolated neurons were counted at a Zeiss Axiophot light microscope in one of every five sections (P5, P10 and P15) or one of every ten sections (P21 and 6-7 weeks old), taking into account the morphometric development of SCG neurons.

The numbers obtained from each section were summed. This method minimized the risk of counting the same neuron twice, although the actual final number may be underestimated. Two experimenters performed the count blind (not knowing the genotype) and independently to verify its reproducibility. The final number of neurons from each group of animals is reported as the mean ± SEM and the differences were analyzed using Student's *t*-test.

5.3) Immunocytochemistry

5.3.1) Primary antibodies. Extension and distribution of adrenergic fibers in the SCG peripheral targets were evaluated by tyrosine hydroxylase (T-OH) immunostaining using an affinity purified rabbit polyclonal antibody (Chemicon International Inc., Temecula, CA, USA) diluted 1:100. T-OH is the rate-limiting enzyme in catecholamine synthesis (Levitt et al., 1965) and a measure of the functional activity of SCG neurons (Black & Mytilineou, 1976). Dystrophin immunolocalization in heart, iris and submandibular gland cryo-sections was carried out using a polyclonal guinea pig antiserum against a recombinant dystrophin protein (N-terminal residues 1–246) (Knuesel et al., 1999), which recognizes only the full-length dystrophin, kindly provided by Dr. M. Fritschy (University of Zurich, Switzerland), diluted 1:3000. The presence of Dp427 in smooth muscle cells of iris and submandibular gland was verified by co-localization with smooth muscle actin, using a rabbit polyclonal antibody (Abcam Limited, Cambridge, UK) diluted 1:100.

5.3.2) Immunocytochemistry procedure. T-OH was revealed in the hearts, irises and submandibular glands of three wild-type and three *mdx* mice at P0, P5, P10 and 6–7 weeks of age. P0, P5 and P10 mice were killed by decapitation following isoflurane anesthesia and the heart, irises and submandibular glands were rapidly dissected and fixed by immersion in 4% paraformaldehyde in 0.1 M PB for 2 h at 4°C. Adult wild-type and *mdx* mice were, instead, anesthetized and perfused with the same fixative as above. After perfusion, the heart, irises and submandibular glands were removed. All specimens were cryoprotected for 36 h in 30% sucrose at 4°C, rapidly frozen and cut on a cryostat into 12 μm thick sections, collected on subbed glass slides. Immunolabeling for T-OH in heart and submandibular gland was performed using the PAP procedure as described previously (De Stefano et al.,

1997). Due to the presence of black pigmentation, T-OH immunoreactivity in the iris was detected using a secondary antibody Cy3^{TM}-conjugated affinityPure F(ab)2 fragment goat anti-rabbit IgG (H + L) diluted 1:400 or a Cy2^{TM}-conjugated affinityPure F(ab)2 fragment goat anti-rabbit IgG (H + L) diluted 1:100 (Jackson Immunoresearch Laboratories Inc., West Grove, PA, USA). Iris cryostat sections were first incubated for 1 h at RT in a blocking solution containing 10% NGS, 1% BSA and 0.2% Triton X-100 in 0.1 M PB, pH 7.4. After a rinse in buffer, the specimens were incubated for 36 h with the anti-T-OH antibody diluted in 1% NGS, 1% BSA and 0.1% Triton X-100 in 0.1 M PB, pH 7.4 and coverslipped with 3:1 glycerol:PBS. Full-length dystrophin and smooth muscle actin were revealed in two 6–7 weeks old wt and two *mdx* mice. Tissue preparation and Dp427 immunostaining were performed as described by Vannucchi et al. (2002). Briefly, animals were anesthetized with isoflurane and killed by decapitation. Hearts, irises and submandibular glands were rapidly dissected, frozen in TissueTek® O.C.T. compound on dry ice and kept at -80°C until use. 10 μm cryostat sections were cut from each sample, collected on electrostatic glass slides and immersed horizontally in a Petri dish containing 50 ml of fixative (2% formaline in 0.1 M PB, pH 7.4). After a 2 min rinse in PBS, the sections were incubated in a blocking solution of PBS containing 4% NGS and 0.5% Triton X-100, for 15 min at RT. After a 3 x 10 min rinses in PBS, the specimens were incubated overnight at 4°C with the guinea pig dystrophin antibody diluted in the same medium used for blocking, rinsed again and then incubated with the secondary antibody Alexa Fluor® 594 goat anti-guinea pig IgG (H + L) (10 μg/ml) (Molecular Probes, Inc., Eugene, OR, USA). Iris and submandibular gland sections were further rinsed and incubated, overnight at 4°C, with the antibody to smooth muscle actin, successively revealed with a secondary antibody Cy2^{TM}-conjugated affinityPure F(ab)2 fragment goat anti rabbit IgG (H + L) (Jackson Immunoresearch Laboratories Inc.) diluted 1:100. Sections were coverslipped with glycerol:PBS and viewed at a Zeiss Axiophot fluorescence microscope. Control sections from all specimens were obtained by omitting the primary antibody.

5.4) Retrograde labeling of superior cervical ganglion neurons by wheat germ agglutinin injection and quantitative analysis

Neurons projecting to the submandibular gland and to the iris were visualized by retrograde labeling with WGA-HRP. Five μl of 2% WGA-HRP diluted in 2% dimethylsulfoxide and sterile saline solution were injected, under deep anesthesia with chloral hydrate, into the right submandibular gland of three wild-type and three *mdx* adult mice. Five injections of 1 μl each were administered to different areas of the glands using a 30 $^{1/2}$ gauge needle connected, through a polyethylene tube (PE-20), to a Hamilton syringe. To label neurons projecting to the iris, 3 μl of 5% WGA-HRP were injected through the corneal limbus, using the same device, into the anterior eye chamber (in the proximity of the iris) of three wild-type and three *mdx* adult mice. To minimize the excessive dilution of the tracer and its outflow from the anterior eye chamber by the regular replacement of the aqueous humor, 10-15 min before retrograde labeling the eyes were injected with 2% methylcellulose diluted in sterile saline solution (Pescosolido et al., 1998). Methylcellulose does not degrade or trigger any immunitary response and forms polymers that reduce and/or block the outflow of aqueous humor by temporarily obstructing Schlemm's canal and its collectors. Eighteen hours after the injection into either the submandibular gland or the anterior eye chamber, the mice were anesthetized and perfused with a fixative composed of 1% paraformaldehyde and 1.5% glutaraldehyde in 0.1 M PB, pH 7.4. After dissection, the SCG were cryoprotected overnight in 30% sucrose and cut into 15 μm thick serial sections collected free-floating in three wells. Each well thus contained a complete series of sections separated from each other by 30 μm. The WGA-HRP within neuronal cell bodies was visualized by the usual DAB reaction. Sections from submandibular glands were also cut and processed as above to verify the homogeneous distribution of the WGA-HRP injections. After DAB reaction, all sections were collected on glass slides and coverslipped with Eukitt balsam. WGA-HRP labeled neurons were counted at a light microscope. For each ganglion, the final number of neurons was represented as the mean ± SEM of the counts performed on the single series of sections collected in the three wells. Differences between counts were statistically evaluated by Student's *t*-test.

5.5) Biochemistry

5.5.1) *Primary antibodies*. The mouse monoclonal antibody Dys1 (Novocastra, Newcastle upon Tyne, U.K.), diluted 1:15, was used in the biochemical characterization of Dp427. Dys1 is directed against the dystrophin mid rod domain and recognizes the full-length dystrophin of 427 kDa. Expression of T-OH was evaluated using the same antibody used for immunocytochemistry (diluted 1:100). In addition, other antibodies used for Western blots were as follows: rabbit anti mouse-NGF (diluted 1:500) was from Alomone Labs (Israel); rabbit anti TrkA, used at a concentration of 2 μg/ml, was from Abcam Limited (Cambridge, UK); rabbit anti phospho-TrkA (diluted 1:800) was from Sigma; mouse anti p75 (diluted 1:100) was kindly provided by Dr. L. Manni; rabbit anti NF-L and anti NF-M, diluted 1:5000 and 1:10000 respectively, were from Immunological Sciences (Rome, Italy); rabbit anti NF-H (diluted 1:1000) was from Sigma; mouse monoclonal (SMI-36) recognizing the phosphorylated form of 200 kDa neurofilament heavy protein was from AbCam Limited (Cambridge, UK) and was diluted 1:1000; rabbit anti dynein heavy chain (R-325) was from Santa Cruz Biotechnologies and it was used diluted 1:1000; mouse monoclonal anti actin (0.75 μg/ml) was from Boehringer Mannheim Biochemica.

5.5.2) *Preparation of tissue extracts*. Mice were anesthetized with isoflurane and killed by decapitation. The hearts, irises, submandibular glands and SCGs were quickly removed on ice, frozen and stored at –80°C until use. The whole hearts and submandibular glands were homogenated in RIPA buffer containing 50 mM Tris/HCl pH 7.6, 150 mM NaCl, 1 mM EDTA, 1% SDS, 1%Triton X-100, 1 X inhibitor cocktail (Sigma), 1 mM PMSF, 0.2 mM Na_3VO_4 and 1 mM NaF, with a ground-glass micro-homogenizer kept in ice. Irises and SCGs were pooled and then homogenized as described for hearts and submandibular glands. After centrifugation (15,000 x g for 15 min at 4°C), a measured aliquot of the supernatants was used to determine protein concentration using the Micro BCA kit (Pierce, Rockford, IL, USA). Other aliquots of the samples were boiled for 1 min after addition of 4 x loading buffer (200 mM Tris/HCl pH 6.8, 4% SDS, 30% glycerol, 4% β-mercaptoethanol, 4% blue bromophenol) and analyzed by sodium dodecyl sulphate-polyacrylamide gel electrophoresis (SDS-PAGE) and immunoblotted.

5.5.3) *Electrophoresis and immunoblotting*. Equal amounts of proteins were separated by SDS-PAGE on 6-15% (for Dp427 revelation), 15% (for NGF

revelation), 4% (for dynein revelation) and 7.5% (for the revelation of all the other proteins) acrylamide gels. Molecular mass standard mixture containing myosin (205 kDa), β-galactosidase (116 kDa), phosphorylase b (97.4 kDa), bovine albumin (66 kDa), egg albumin (45 kDa) and carbonic anhydrase (29 kDa) was used (Sigma-Aldrich s.r.l., Milano, Italy). In another set of experiments, Molecular Weight Standard Mixture (Sigma), containing precisely sized recombinant proteins of molecular mass 150, 100, 75, 50, 35, 25, 15 kDa, was used. Hi-Mark Prestained High Molecular Weight Standard (Invitrogen), containing proteins of molecular mass 500, 279, 251, 164 and 121 kDa was used only for 4% polyacrilamide gels. Proteins were then transferred onto nitrocellulose membranes using a solution containing 50 mM Tris/HCl, 380 mM glycine, 0.1% SDS and 20% methanol and Ponceau S (Sigma) staining was used to verify similar protein loading between wt and *mdx* mouse samples. Non-specific binding sites were blocked with 5% dry milk in TTBS 1X (20 mM Tris/HCl at pH 7.5, 500 mM NaCl, 0.05% Tween 20) and the membranes were then incubated overnight at 4°C with the primary antibody, diluted in 3% BSA and 0.05% NaN_3 in TTBS. After a thorough wash in buffer, the membranes were incubated for 1h at RT with an anti-mouse or anti-rabbit IgG secondary antibody, both conjugated with horseradish peroxidase (Promega Italia, Milano, Italy), diluted 1:15000 and 1:10000 respectively, in 2.5% dry milk in TTBS. Membranes were then developed using enhanced chemiluminescence (ECL) (Pierce, Rockford, IL, USA). The positive bands were visualized by exposure of the membrane to X-OMAT films (Kodak). Densitometric analysis of band intensities was carried out using ImageQuant 5.2 (Amersham Biosciences Europe, Cologno Monzese, Italy) program. At least three western immunoblots were used for each analysis. Actin was used as internal standard. A ratio of each protein of interest to actin was obtained; results were expressed as *mdx* protein level/wt protein level for animals of the same age. Data were evaluated for statistical significance using Student's t-test; differences were accounted as statistically significant if $p \leq 0.05$.

5.6) Standard electron microscopy

6-7 weeks old and P10 wt and *mdx* mice were deeply anesthetized and perfused as described in the 5.2 Section. After fixation, the salivary glands, hearts, irises and SCGs were removed, cut in small pieces and processed following the

same protocol described above. Ultrathin (60-70 nm thick) sections were cut on a Reichert ultramicrotome, stained with 4% uranyl acetate followed by 0.2% lead citrate and viewed under a Philips EM208S transmission electron microscope at 80 kV.

5.7) Evans Blue injection

Evans Blue is a dye used to look for changes in plasma membrane permeability, which is an early sign of the dystrophic pathology in muscle cells (Mokri & Engel, 1975). Four wild-type and four *mdx* mice at P10 and 6-7 weeks of age were injected into the peritoneum with tetrasodium diazo salt Evans blue dye (Sigma-Aldrich) (50 μl/10 g of body weight), dissolved in PBS at a concentration of 0.5 mg EBD/0.05 ml PBS and filtered through a 0.2 μm pore-sized filter. Successful dye injection was indicated by the blue color of mouse paws and ears. Animals were anesthetized with isoflurane and killed by decapitation 5-6 h after injection and visually inspected for dye uptake in the skeletal muscles. Femoral quadriceps muscles (used as positive control tissue), hearts, irises and submandibular glands were removed and fixed in 8% formaline in 0.1 M PB, pH 7.4, for 2 h at 4°C. After a brief wash in PB, the specimens were cryoprotected overnight in 30% sucrose and cut on a cryostat in 10 μm thick sections collected on subbed slides. Sections were postfixed in ice-cold acetone at -20°C for 10 min, washed, mounted with glycerol:PBS 3:1 and viewed under an Axiophot Zeiss fluorescence microscope using the rhodamine filter.

5.8) Real-time RT-PCR

Wt and *mdx* P5, P10 and 6-7 weeks old mice were killed by decapitation following isoflurane anesthesia and SCGs, hearts, irises and submandibular glands were collected, frozen and stored at -80°C until use. Total RNA was isolated from hearts and submandibular glands using TRI Reagent (Sigma, Milano, Italy), according to the manufacturer's instructions. The yield and integrity of the purified RNA were assessed by spectrophotometric analysis at 260 nm and electrophoresis on ethidium bromide-stained 1.3% agarose-formaldheyde gels, respectively. RNA was additionally purified of genomic DNA using DNA-free kit (Ambion Inc, Austin,

TX, USA), according to the manufacturer's instructions. Total RNA was isolated from pools of SCGs and irises using the RNeasy Micro Kit (Quiagen, Milan, Italy), following the manufacturer's instructions. 2 μg of total RNA was reverse-transcribed using random hexanucleotides as primers, 25 U of RNAsin and 200 U of MMLV-RT (all from Promega). 1/50 of the cDNA thus obtained was real-time PCR amplified in a 25 μl reaction mixture containing 1x SYBR Green JumpStart Taq ReadyMix (Sigma) and 0.3 mM of each primer in an iCycler iQ Real-Time Detection System (Bio-Rad, Milano, Italy). Each sample was amplified in duplicate. Amplification was carried out for 30-35 cycles (30 sec at 95°C, 30 sec at 55°C and 45 sec at 72°C). The primers used are listed in Table I. Amplicons were detected after each elongation step and were analyzed using the iCycler iQ software (Bio-Rad). A melting curve was obtained after completion of the cycles to verify the presence of a single amplified product. HPRT was used as the internal standard (Steel & Buckley, 1993); amplification efficiencies of HPRT and of all genes of interest were set to be approximately equal. Comparative expression levels were calculated by the $2^{-\Delta\Delta Ct}$ method (Livak & Schmittgen, 2001). Data were statistically analyzed by Student's t-test; differences were considered statistically significant if $p \leq 0.05$.

5.9) Measurements of NGF by Elisa

Wt and *mdx* P5, P10 and 6-7 weeks old animals were killed by decapitation following isoflurane anesthesia and hearts and irises were collected, frozen and stored at -80°C until use. Homogenization buffer contained 10 mM Tris/HCl pH 7.4, 100 mM NaCl, 1 mM EDTA, 1mM EGTA, 0,1% Triton X-100, 1 mM PMSF and 1X inhibitor cocktail (Sigma). Irises were pooled, suspended in 200μl buffer and sonicated at a frequency of 30 kHz for 30 sec, while hearts were sonicated at a frequency of 30 kHz for 40 sec in a volume established on their wet weight (100μl buffer for 10mg tissue). Sonication was carried out by using a UP100H Ultrasonic Processor (Dr. Hielsher GmbH, Teltow, Germany). Samples were stored at -20°C until use. Measurement of NGF was performed using E_{max} ImmunoAssay System (Promega), according to the manufacturer's instructions. Plates were read at 450 nm. Tissue NGF values were normalized against the protein concentration of each sample and expressed as pg NGF/mg protein. Results were expressed as the ratio *mdx* NGF level/wt NGF level, for age-matched mice. Data were evaluated for

statistical significance using Student's t-test; differences were accounted as statistically significant if $p \leq 0.05$.

Table I. Oligonucleotide primers used for real-time RT-PCR

GENE	lenght of amplicon	PRIMER *(5' to 3')*
NGF	144 bp	Fw: CCAAGCTCACCTCAGTGTCTG Rev: GTTCTGCCTGTACGCCGATC
TrkA	104 bp	Fw: TGGACGGTAACAGCACATCAAG Rev: AAGGAAGAGGGCGGCAGAG
p75	104 bp	Fw: CCTGCCTGGACAGTGTTACG Rev: CACACAGGGAGCGGACATAC
caspase 6	130 bp	Fw: TTCCTCATGTGCTACTCTGTCG Rev: GCAGCTCCGTGAACTCCAG
NF-L	114 bp	Fw: GTCTCCTCCTCGCTGTCC Rev: CTTGAGGTCGTTGCTGATGG
NF-M	82 bp	Fw: AAGGTTGAGGAAGTGGCTGTC Rev: CGGGTGATTTGGGCATAGGG
NF-H	96 bp	Fw: GTGGTTCCGAGTGAGGTTGG Rev: CGCCGGTACTCAGTTATCTCC
□-actin	143 bp	Fw: CCCAGGCATTGCTGACAGG Rev: GCTGGAAGGTGGACAGTGAG
tubulin α1	129 bp	Fw: GTATGCCAAGCGTGCCTTTG Rev: TCCACAGAATCCACACCAACC
tubulin β3	136 bp	Fw: CGCCTTTGGACACCTATTCAGG Rev: ACACTCTTTCCGCACGACATC
Cdk5	76 bp	Fw GTGACCTGGACCCTGAGATTG Rev TTGCGGCTGTGACAGAATCC
p35	81 bp	Fw: GCAAGAACGCCAAGGACAAG Rev: CTGACACCGCCACGATCC
dynein HC1	120 bp	Fw: GCACCTCATCCCACAGACAC Rev: CGCACATCTTGGAGTAACTTGG
kinesin 5A	117 bp	Fw: ATGGAGAGAATGTGCCTGAGAC Rev: GTGCGATGCGTACCACAATG
N-CAM	112 bp	Fw: GCTGTGATTGTCTGTGATGTGG Rev: TGTTGGACAGGACTATGAACCG
L1-CAM	97 bp	Fw: GCAGCAAGGGTGGCAAATAC Rev: CTGTACTCGCCGAAGGTCTC
neuropilin	99 bp	Fw: TGTCCGAATCAAACCTGTATCC Rev: CCCAACATTCCAGAGCAAGG
tenascin C	80 bp	Fw: GAGCCAGCAAGCCACAACC Rev: TGACAGCAGAAACACCAATCCC
HPRT	160 bp	Fw: AGTCCCAGCGTCGTGATTAG Rev: CCATCTCCTTCATGACATCTCG

6. RESULTS

6.1 Neuron number in the SCG of P5, P10, P15, P21 and 6–7 weeks old wt and mdx mice

No evident difference in neuronal organization, shape or staining affinity was observed between serial semithin sections of 6–7 weeks old wt and *mdx* mouse SCG. However, a cell count revealed significantly ($p<0.01$) fewer neurons (36%) in the SCG of *mdx* than of wt mice (Table 1). Since no dying neurons were observed, we performed cell counts at different postnatal dates: P5, P10, P15 and P21. As shown in Table 1, the number of neurons decreased between P5 and P15 in both wild-type and *mdx* mouse SCG, as a consequence of the naturally occurring cell death (Wright et al., 1983). However, while at P5 no statistically significant difference was revealed between the numbers of neurons of wt and *mdx* mouse ganglia (Table1), in the SCG of P10 *mdx* mice there were significantly fewer ($p<0.01$) neurons than in the wt and their numbers further decreased at P15 (Table 1). Thus, the greater neuronal loss observed in *mdx* than in wt mice occurred early after birth and overlapped with the physiological neuronal death.

Table 1
Number of neurons in the superior cervical ganglion of wt and *mdx* mice at different postnatal dates

	wt	***mdx***
P5	7915 ± 393	8450 ± 67
P10	6583 ± 76	4676 ± 74**
P15	5977 ± 106	3984 ± 3**
P21	6157 ± 301	3688 ± 138**
6-7 weeks	5204 ± 74	3339 ± 24**

At each time point, the number of neurons is reported as the mean ± SEM of the number of neurons counted in three SCGs. At P5, wt and *mdx* mouse SCGs have the same number of neurons. At P10, the number of ganglionic neurons in both wt and *mdx* mice decreases significantly compared with P5 ($p<0.05$, wt; $p<0.01$, *mdx*), coinciding with the naturally occurring cell death. However, in *mdx* mice, the number of neurons is significantly lower than in the wt animals (**$p<0.01$) and remains so throughout the time frame considered. Differences were analyzed by Student's t test.

6.2 T-OH immunolocalization and biochemical evaluation in SCG target organs of P0, P5, P10 and 6–7 weeks old wt and mdx mice

To investigate whether, with the loss of ganglionic neurons observed in *mdx* mice, the pattern of peripheral target innervation was affected, we used T-OH immunostaining to label the sympathetic fiber network in the heart and iris (SCG muscular targets) and submandibular gland (SCG non-muscular target) of wild-type and *mdx* mice. The distribution of T-OH-immunopositive nerve fibers in the heart was variable, being more abundant in sections from the atrium and inner ventricular wall, revealing regions more richly innervated than others in both wt and *mdx* mice, depending on the plane of cut. However, analysis of sections from the same heart regions revealed that, compared with the wild-type (Fig. 1A), the extension of the sympathetic fiber network and axonal branching was reduced in *mdx* mice (Fig. 1B). This reduction was strikingly evident in the iris of *mdx* mice (Fig. 2A, wt; Fig. 2B, *mdx*). Due to its small size, which enables sections of the whole structure to be obtained, iris is a much easier specimen to analyze than the heart. A different situation was found in the submandibular gland, where no significant difference was observed in the bulk extension of the sympathetic innervation between wt (Fig. 3A) and *mdx* (Fig. 3B) mice, the whole gland being reached by numerous trunks of T-OH immunopositive fibers. However, at high magnification, the adrenergic fibers appeared mostly clustered in large bundles and only a few thin axonal sprouts were observed in *mdx* mice (Fig. 3D), revealing a reduction in axonal defasciculation and terminal sprouting compared with the wt (Fig. 3C). To evaluate whether these differences preceded or followed the neuronal loss observed in *mdx* mouse SCG, we performed T-OH immunolabeling on tissue sections from P5 and P10 wt and *mdx* mice. At P5, when no difference in neuron number between wt and *mdx* mouse SCG was observed, the adrenergic innervation in the heart (Fig. 1C, wt; Fig. 1D, *mdx*), iris (Fig. 2C, wt; Fig. 2D, *mdx*) and submandibular gland (Fig. 3E, wt; Fig. 3F, *mdx*), although immature, had already the same characteristics described in the 6–7 weeks old animals. These patterns of innervation were more evident in P10 wt (Fig. 1E, heart; Fig. 2E, iris; Fig. 3G, submandibular gland) and *mdx* (Fig. 1F, heart; Fig. 2F, iris; Fig. 3H, submandibular gland) mice. In addition, as the result of the decrease in neuron numbers during naturally occurring cell death, the amount of T-

OH immunopositive nerve fibers in both wt and *mdx* mice was progressively reduced from P5 to adulthood, a phenomenon that can be better appreciated in wt mouse irises. The differences observed between wt and *mdx* mice were also found in the levels of T-OH detected by Western immunoblot analysis (Fig. 4). In the hearts, irises and submandibular gland of 6–7 weeks old (Fig. 4A), P5 (Fig. 4B) and P10 (Fig. 4C) mice, T-OH antibody recognized a clear band at approximately 60 kDa. At all postnatal dates examined, the intensity of the T-OH band was clearly higher in wt mouse iris and heart compared to the *mdx*. A similar result was also obtained for submandibular gland homogenates from 6-7 weeks old mice, while no differences were observed between wt and *mdx* mice of P5 and P10. These results indicate that the decrease in T-OH content is not only a consequence of the drastic reduction in the adrenergic innervation of SCG muscular targets, but also of the impaired defasciculation and terminal axon sprouting described in submandibular glands.

T-OH immunolabeling was also performed in the submandibular gland and iris in P0 mice, long before the appearance of the differences in neuron number between wt and *mdx* mouse SCG. We chose to immunolabel for T-OH only the iris and the submandibular gland (Fig 4), as the heart does not receive a massive innervation from the SCG (Pardini et al., 1989) and the extension of the adrenergic fibers network is greatly variable in different areas, as previously observed (Fig.1). Bulk adrenergic innervation in iris and submandibular gland of both wt and *mdx* P0 mice was lower than that observed at P5, clearly showing a still immature fiber network. Moreover, areas of targets are not completely innervated and axons are more clustered in bundles than in P5 mice. Fig. 5A and 5B show that at P0, in areas that are already innervated, the density of adrenergic fibers is comparable between wt (Fig. 5A) and *mdx* (Fig. 5B) submandibular glands. In addition to these common alterations, in *mdx* mouse iris (Fig. 5D) the net of adrenergic innervation is already lower than that of wt animals (Fig. 5C), suggesting that some of the axons of *mdx* mouse SCG neurons never reach their targets.

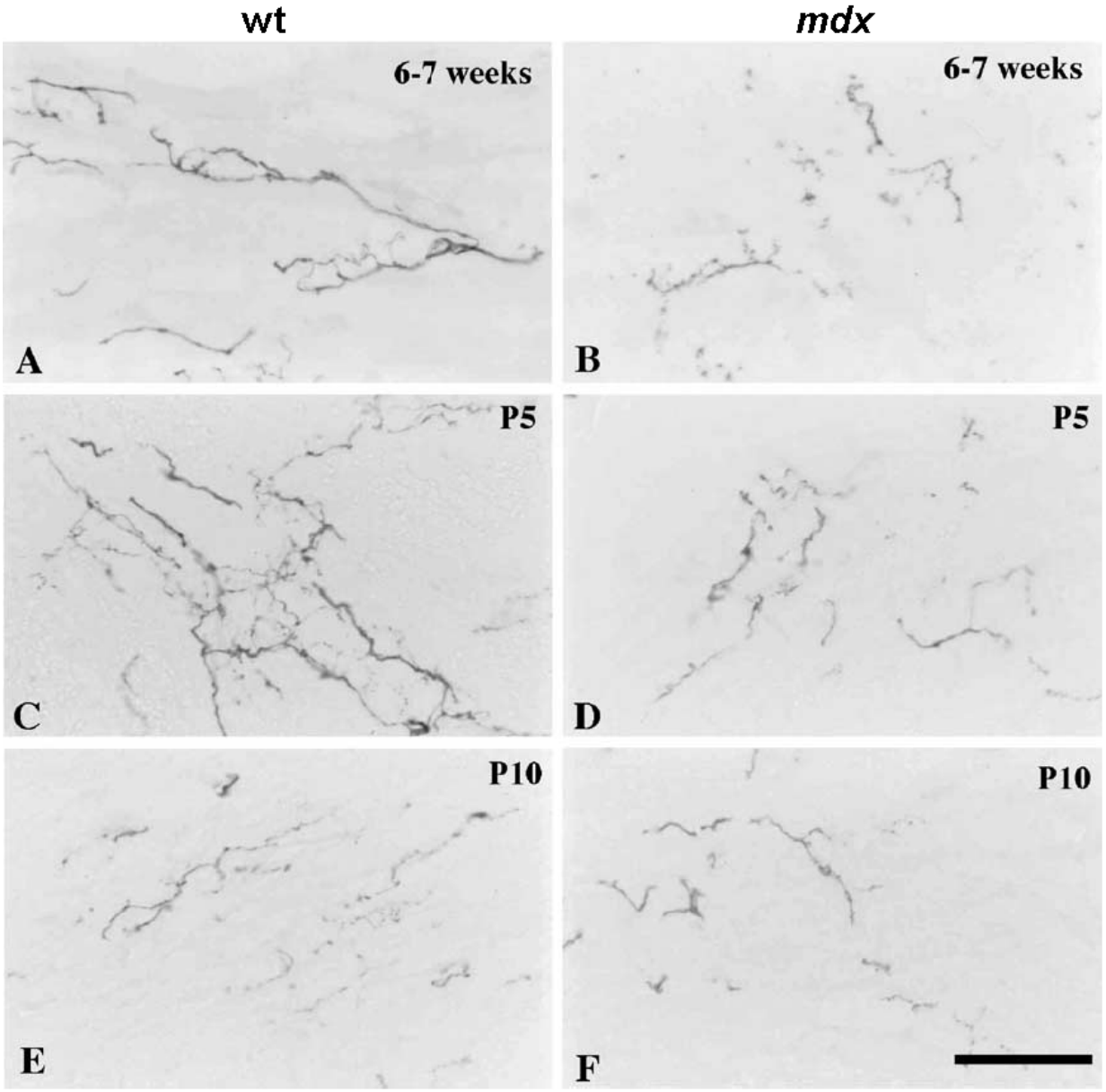

Fig. 1. T-OH immunolabeling showing adrenergic innervation in the heart of P5, P10 and 6– 7 weeks old wt and *mdx* mice. In adult wt mice (A), adrenergic axons innervating the ventricular muscular wall branch in thin and varicose terminal fibers. In *mdx* mice (B), the extension of the adrenergic innervation is strongly reduced compared with the wild-type and nerve fibers are visibly atrophic. This diversified pattern of innervation is also observed at P5 (C: wt; D: *mdx*) and P10 (E: wt; F: *mdx*). Scale bar: 50 μm.

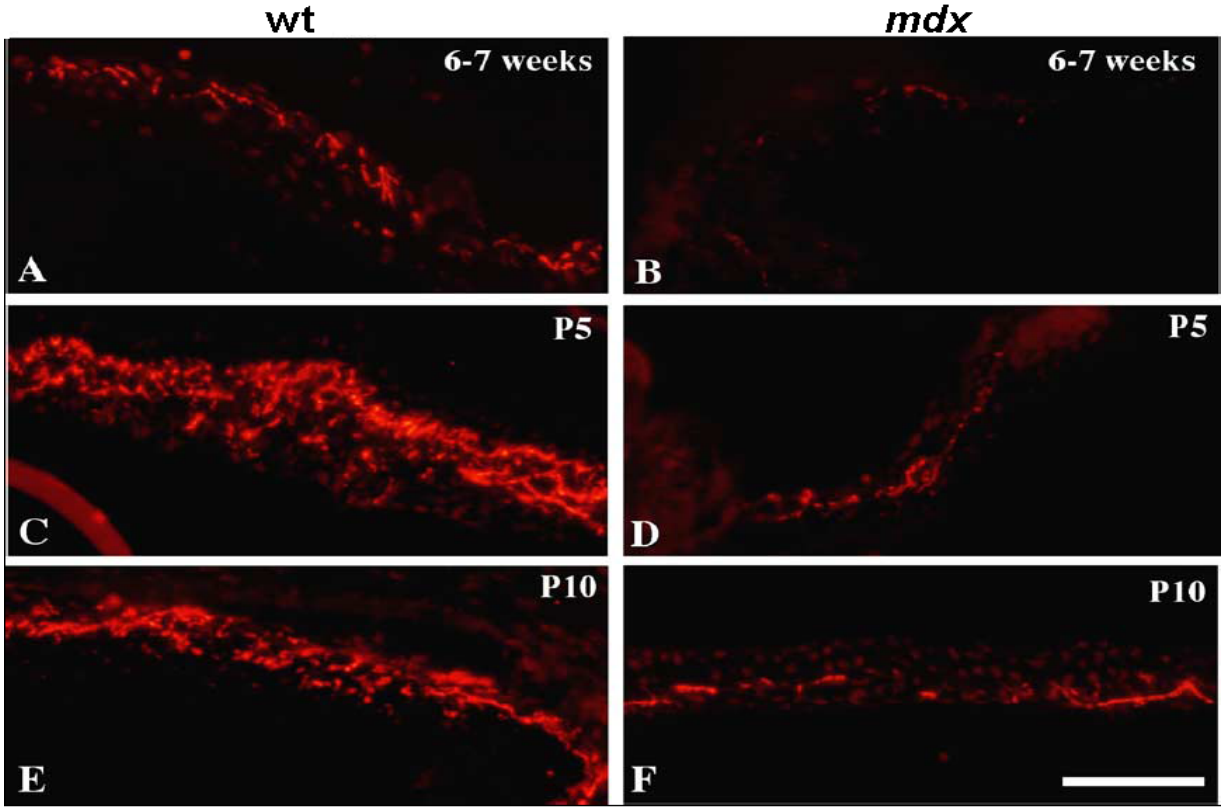

Fig. 2. T-OH immunolabeling showing adrenergic innervation in the iris of P5, P10 and 6–7 weeks old wild-type and *mdx* mice. Adrenergic innervation is dramatically reduced in the irises of 6–7 weeks old *mdx* mice (B) as well as at P5 (D) and P10 (F) with respect to the wt mice of matching ages (A: 6–7 weeks; C: P5; E: P10). Scale bar: 80 μm.

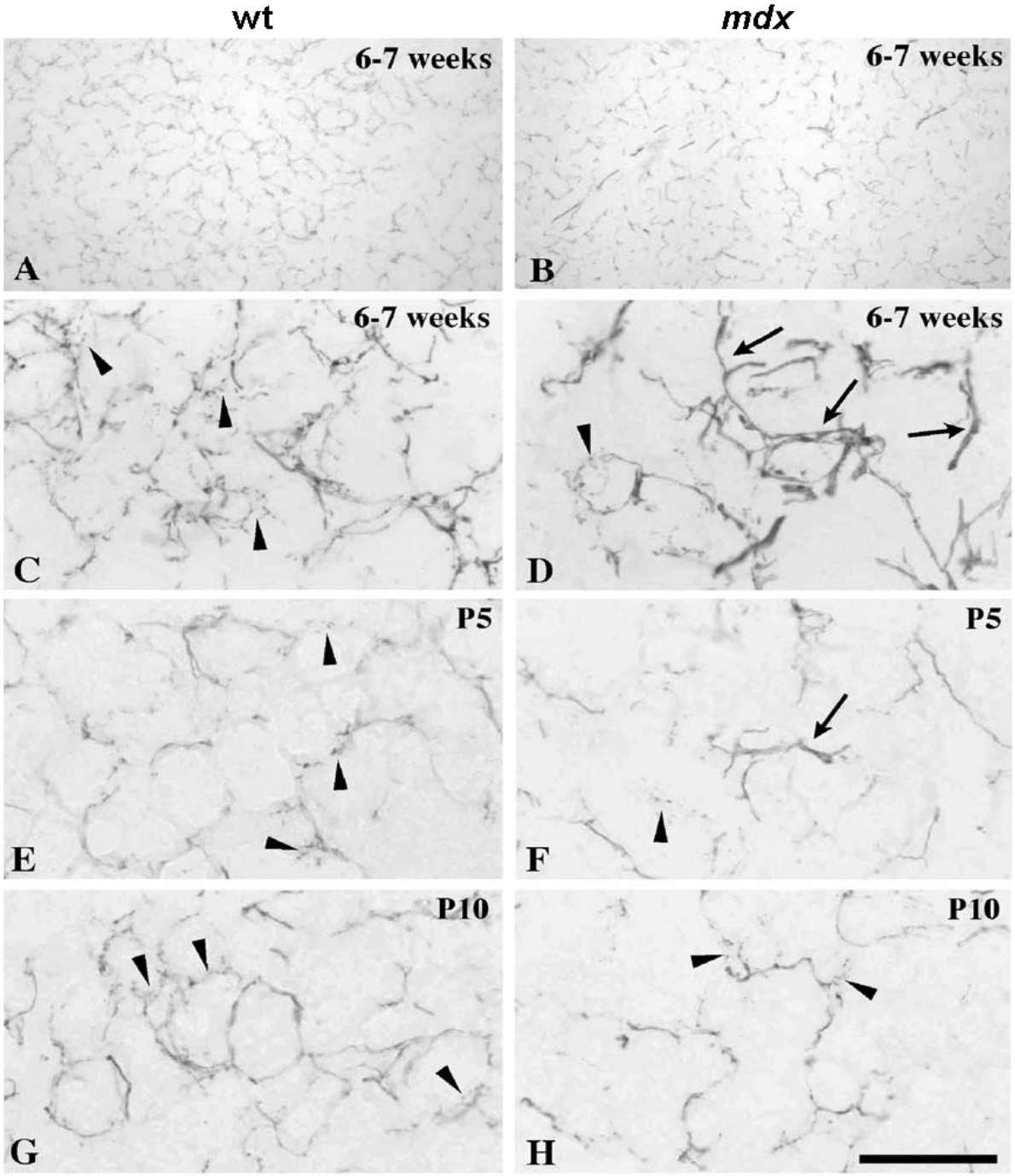

Fig. 3. T-OH immunolabeling showing adrenergic innervation in the submandibular gland of P5, P10 and 6–7 weeks old wt and *mdx* mice. Bulk adrenergic innervation in adult wt (A) and *mdx* (B) mice is comparable and a rich net of T-OH immunopositive axons pervades the glands. However, at higher magnification, it can be seen that, while terminal axons in wt mice (C) give rise to numerous thin and varicose sprouts (some indicated by arrowheads), in *mdx* mice (D) axonal defasciculation and terminal sprouting are impaired. Axons appear clustered, forming large bundles (arrows) that only occasionally emanate to thinner branches (arrowhead). Between P5 (E) and P10 (G), in wt mice T-OH immunopositive axons progressively surround the acini in the submandibular glands with thin and varicose axonal sprouts (arrowheads). Adrenergic innervation of *mdx* mouse glands, instead, is much less developed at both P5 (F) and P10 (H), being characterized by large axonal bundles (arrow) and poor terminal sprouting (arrowheads). Scale bar: A, B: 160 μm; C–H: 50 μm.

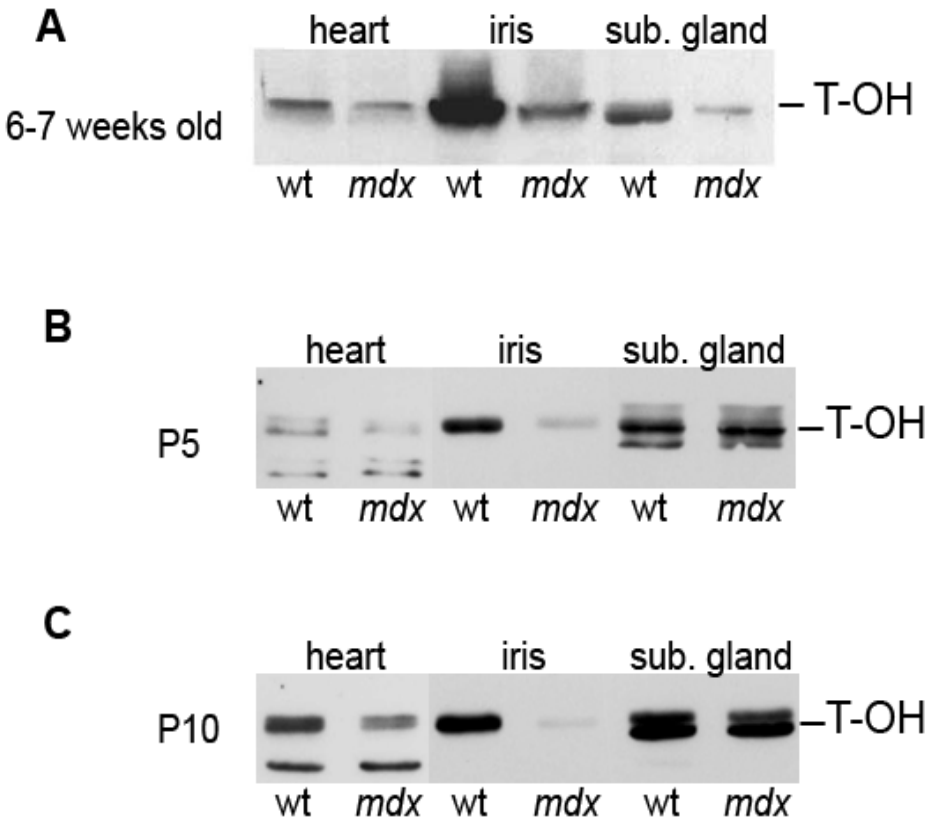

Fig. 4. Western immunoblot analysis of T-OH in heart, iris and submandibular gland of P5, P10 and 6-7 weeks old wt and *mdx* mice. T-OH antibody recognizes a 60 kDa band. The intensity of the T-OH band shows a decrease in all tissue extracts from adult *mdx* mice compared with the wt of the same age (A). In P5 (B) and P10 (C) tissue extracts, T-OH antibody shows a drastic decrease in muscle tissues, which is particularly evident in the iris, in *mdx* mice compared to the age-matched wt. The difference in the T-OH band intensity is not appreciable in P5 and P10 submandibular glands. Equal amounts of proteins were loaded in wt and *mdx* lanes, in each target and in a particular stage.

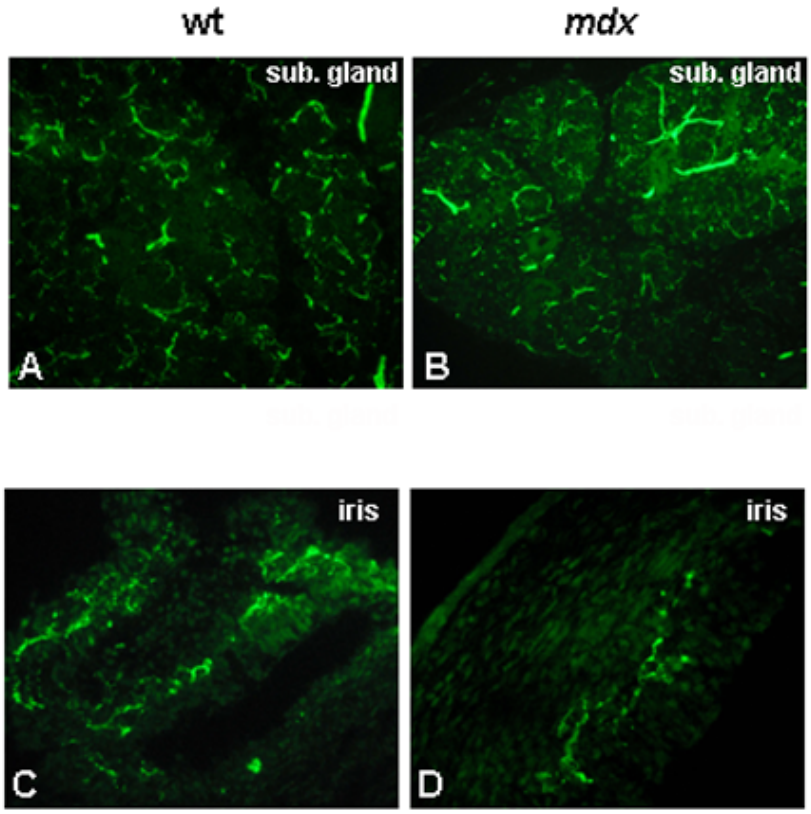

Fig. 5. T-OH immunolabeling showing adrenergic innervation in the submandibular gland and iris of P0 wt and *mdx* mice. In submandibular gland bulk adrenergic innervation is similar in wt (A) and *mdx* (B) mice, even though it is still immature and many axons are clustered in bundles. Adrenergic innervation is dramatically reduced in the irises of P0 *mdx* mice (D) with respect to the wt mice (C).

6.3 Retrograde labeling of SCG neurons by WGA-HRP injection in the submandibular gland and in the anterior eye chamber of 6–7 weeks old wt and mdx mice

In the heart and iris of *mdx* mice, atrophy of the nerve fibers and poor axon terminal sprouting were associated with a drastic decrease in the extension of the sympathetic network, suggesting the selective loss of SCG neurons projecting to the muscular targets. To investigate this hypothesis, we retrogradely labeled ganglionic neurons by injecting WGA-HRP in the submandibular gland and into the anterior eye chamber, close to the iris. The heart was not used in this experiment since an efficient injection of WGA-HRP was impossible on account of the vast area that would need to be injected and to the limited adrenergic innervation supplied by the SCG compared to that of other sympathetic ganglia (Pardini et al., 1989). After unilateral tracer injection in the submandibular gland, no significant difference was seen between the number of labeled neurons in wt (537±11) and *mdx* (555±47) mouse SCG, the brown staining coloring the cell cytoplasm (Fig. 6A and higher magnification in panel C, wt; Fig. 6B and higher magnification in panel D, *mdx*) and emerging axons (Fig. 6C, wt; Fig. 6D, *mdx*). Labeled neurons were distributed throughout the ganglion, with no specific compartmentalization (Fig. 6A, wt; Fig. 6B, *mdx*), and were mostly arranged in small clusters (Figs. 6A,C, wt; Figs. 6B,D, *mdx*). On the contrary, the number of retrogradely labeled SCG neurons after tracer injection into the anterior eye chamber of wt mice (54.5±1) was significantly higher ($p= 0.01$) than that in *mdx* (32±2) mice. Also in this case, neurons were not distributed in accordance with any specific compartmentalization in either wt (Fig. 6E) or *mdx* (Fig. 6F) mice.

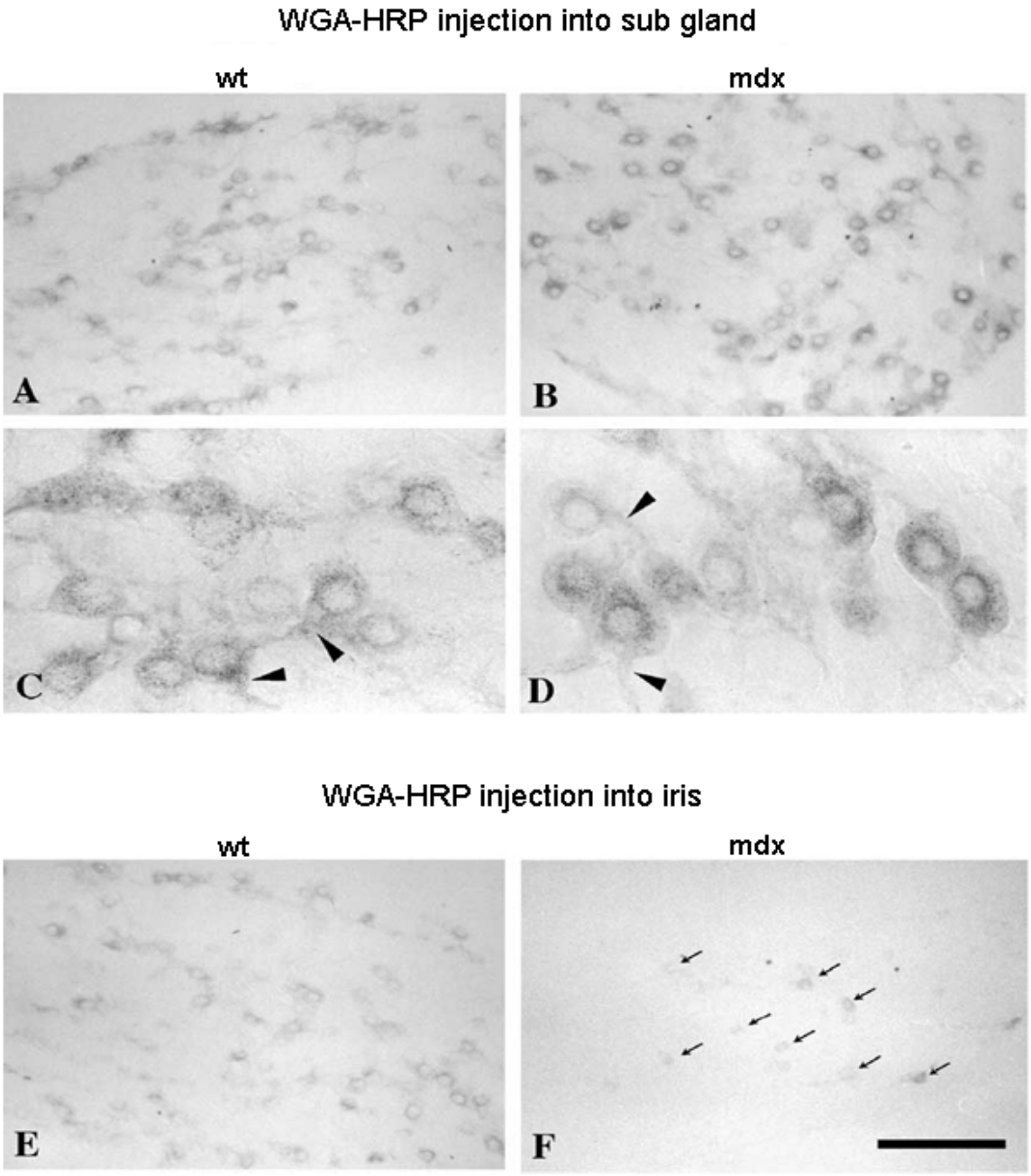

Fig. 6. WGA-HRP retrogradely labeled neurons in the SCG of wt and *mdx* mice after unilateral tracer injection in the submandibular gland and anterior eye chamber. (A–D) WGA-HRP injection in the submandibular gland. Numerous neurons in the ipsilateral ganglion are labeled in both wt (panel A and higher enlargement in panel C) and *mdx* (panel B and higher enlargement in panel D) mice. Labeled neurons are distributed throughout the ganglion with no specific compartmentalization. The reaction product fills the cell bodies and emerging axons (arrowheads in panels C, D). (E, F) WGA-HRP injection into the anterior eye chamber, in proximity of the iris. Several neurons are labeled in the ipsilateral ganglion of wt mice (E), while only a few pale cells (some indicated by arrows) are observed in the *mdx* mouse SCG (F). The difference in labeling intensity observed between neurons projecting to the submandibular gland and those projecting to the iris, in both wt and *mdx* mice, could be due to excessive dilution of the tracer by the aqueous humor. Scale bar: A,B,E,F: 130 μm; C,D: 50 μm.

6.4 Presence and distribution of full-length dystrophin and its biochemical evaluation in SCG target organs of 6–7 weeks old wt and mdx mice

The results obtained so far indicate a loss, in *mdx* mice, of neurons projecting to the muscular targets, which is possibly related to structural and/or functional alterations of muscle cells consequent to the lack of Dp427. We therefore examined, by Western immunoblot and immunocytochemistry, the expression of Dp427 in the heart, used as a positive control, the iris and the submandibular gland, in which the expression of dystrophin is unknown. The Dys1 monoclonal antibody recognized a predominant band at about 427 kDa, corresponding to Dp427, in all wt mouse tissue extracts examined by Western immunoblot (Fig. 7A). In the iris and, less clearly in the submandibular gland, a band at a lower molecular weight than 427 kDa was also present, possibly corresponding to the 405 kDa form described for smooth muscle cells (Hoffman et al., 1988; Feener et al., 1989). The 427 kDa band was absent from the corresponding tissue extracts of *mdx* mice (Fig. 7A). The distribution of Dp427 in the same organs was successively investigated with the light microscope by using the guinea pig polyclonal antiserum together with smooth muscle actin antibody. As expected, Dp427 clearly decorated the profile of cardiomyocytes in wild-type mouse heart sections (Fig. 7B), but not those of *mdx* mice (Fig. 7I), confirming the specificity of the immunoreactivity. Dystrophin immunolabeling was also observed in wt mouse iris (Fig. 7C) and submandibular gland (Fig. 7F), but never in the respective *mdx* specimens (Fig. 7L, iris; Fig. 7M, submandibular gland). In the iris, Dp427 was expressed by a number of cells, some of them identified as smooth muscle cells (Figs. 7C–E). However, as only thin portions of these cells were visible through the iris black pigmentation and dystrophin expressed by smooth muscle cells is supposed to have a patterned distribution, co-localization of Dp427 and smooth muscle actin was seldom observed. In the submandibular gland, numerous Dp427-positive cells of different shapes were widely distributed over the entire gland tissue (Fig. 7F). Among these, there were the vascular smooth muscle cells and the myoepithelial cells encircling the secretory ducts, identified by their position and immunostaining with smooth muscle actin (Figs. 7F–H and insets). Dp427 immunolabeling was also observed in the acinar cells, specifically located close to their luminal side (insets to Figs. 7F-H) where secretory vesicles are clustered.

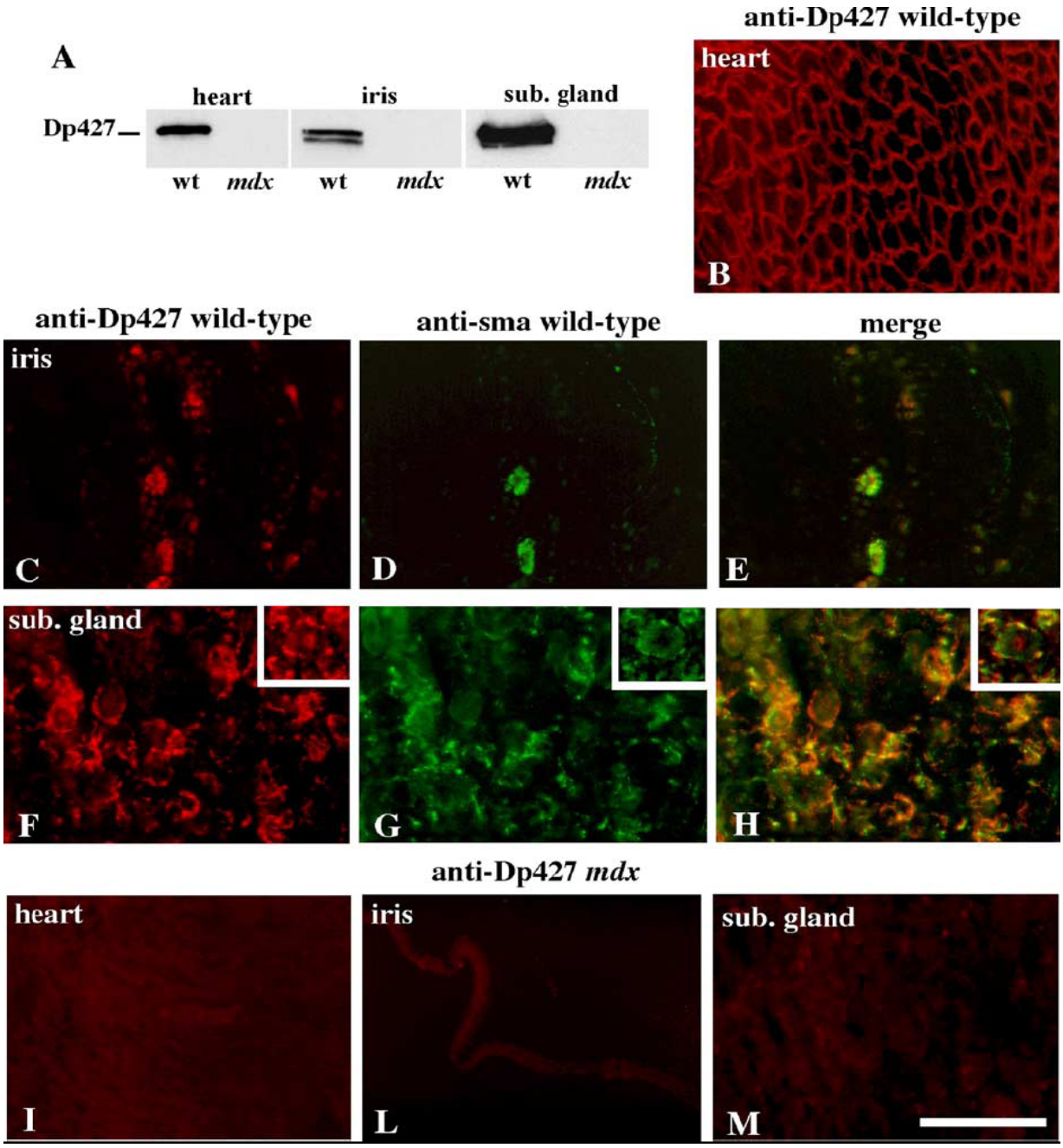

Fig. 7. Dp427 Western immunoblot analysis (A) and immunolocalization (B–M), with or without smooth muscle actin (sma), in the heart, iris and submandibular gland of wild-type and *mdx* mice. (A) Samples of tissue extracts were analyzed by electrophoresis on 6-15% gradient gels using the Dys1 monoclonal antibody against dystrophin. Dys1 reveals a band corresponding to the Dp427 in the heart, iris and submandibular gland extracts of wt mice. This band is lacking in the corresponding tissue extracts from *mdx* mice. The second band observed in the iris lane may represent the dystrophin isoform of 405 kDa characteristic of smooth muscle cells. In wt mice, full-length dystrophin immunolabeling (red) characteristically decorates the profile of cardiomyocytes (B), as well as of several cell types in the iris (C) and submandibular gland (F). Smooth muscle actin immunolabeling (green) in both iris (D) and submandibular gland (G) shows co-localization with Dp427 in a number of cells (merge in panel E: iris; H: submandibular gland). Insets to panels F–H show a transverse section of a secretory acinus displaying dystrophin immunoreactivity within its cells, close to the luminal plasma membrane where secretory vesicles are clustered. No Dp427 immunolabeling is observed in sections of *mdx* mouse heart (I), iris (L) and submandibular gland (M). Scale bar: 100 μm.

6.5 Ultrastructural analysis of SCG target organs in P10 and 6–7 weeks old wt and mdx mice

To investigate whether and when the absence of Dp427 in *mdx* mice induced ultrastructural alterations in the SCG target organs, ultrathin sections of hearts, irises and submandibular glands from P10 and 6–7 week-old wt and *mdx* mice were examined with the electron microscope. In P10 *mdx* mice (data not shown), when SCG neuron loss has already began, we did not observe degeneration, or prominent ultrastructural alterations, of either iris smooth muscle cells, or heart cardiomyocytes, or any of the cell types in the submandibular gland compared to the wild-type mice. Instead, in contrast to the wt (Fig. 8A and higher magnification in panel B), the hearts of 6–7 weeks old *mdx* mice contained several muscle fibers, or portions thereof, with different degrees of alteration, such as disarrangement of the Z-lines (Fig. 8C), hypercontraction of sarcomeres (Fig. 8D), impoverishment of the myofibrillary content (Fig. 8E) and loss of contractile elements in some regions (Fig. 8F). Altered mitochondria with crests separated by a swollen matrix were often observed (Fig. 8E) and large intercellular spaces containing fagocitized cell debris were present (not shown). *Mdx* mice of the same age did not present degeneration, or evident ultrastructural alterations, of either iris smooth muscle cells (not shown), or myoepithelial cells in submandibular glands (not shown).

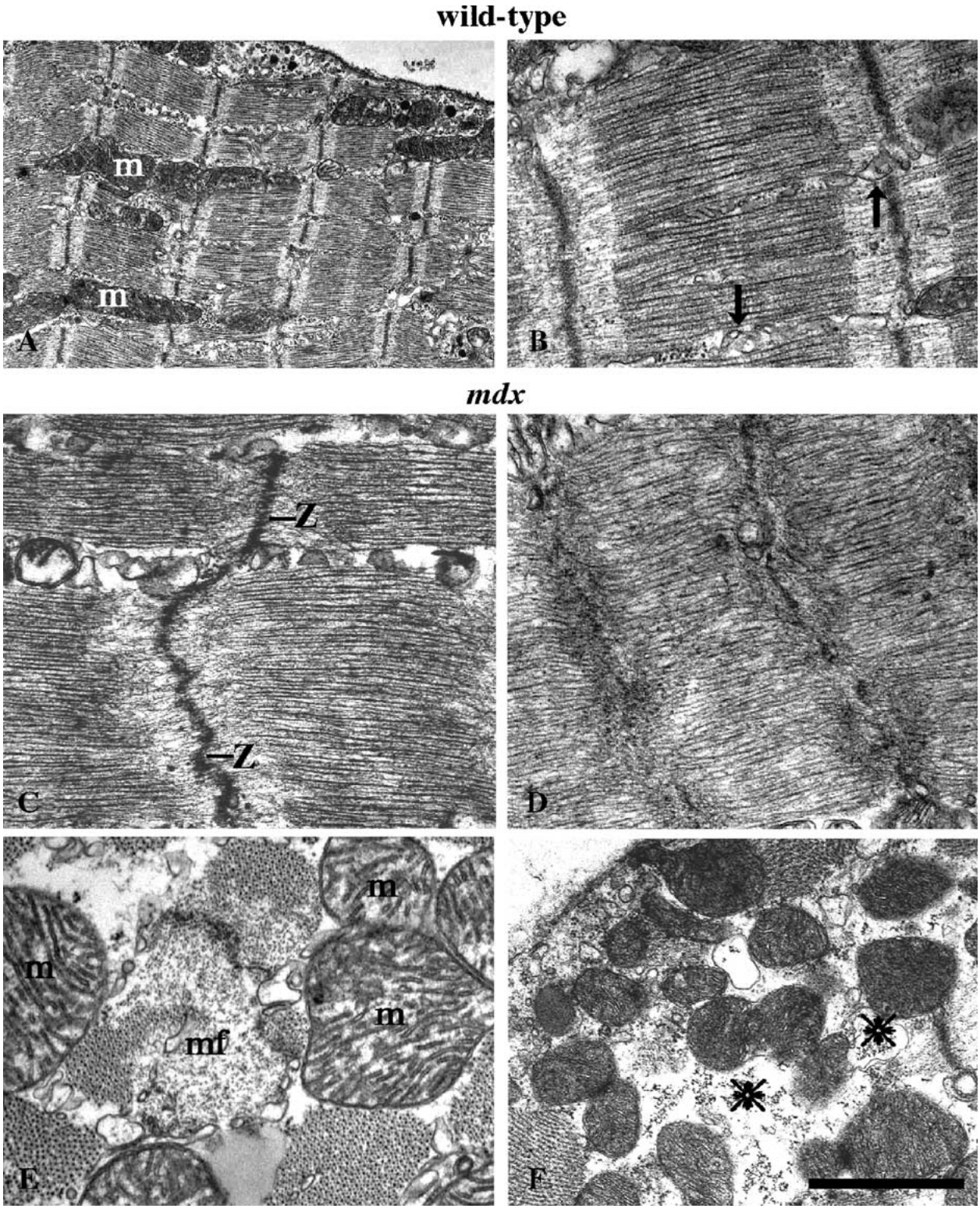

Fig. 8. Ultrastructure of cardiomyocytes in 6–7 weeks old wt (A, B) and *mdx* (C–F) mice. (A, B) Cardiomyocytes show perfectly aligned sarcomeres characterized by regularly alternating bands and lines. Large mitochondria (m) and transverse tubules (arrows) are indicated. (C–F) In *mdx* mice of matching age, numerous cardiomyocytes show progressive sarcomere alteration with disarrangement of the Z-line (Z in panel C), sarcomere hypercontraction (D) and myofibril disruption (mf in panel E). Swollen mitochondria (m) are indicated in panel E. Areas empty of myofibrils are observed (asterisks in panel F). Scale bar: A: 2.5 μm; B–E: 1 μm; F: 2.8 μm.

6.6 Evans blue staining in the SCG muscular targets of P10 and 6–7 weeks old mdx mice

As we had not revealed degeneration or apparent dystrophin-related ultrastructural alterations of cardiomyocytes and iris smooth muscle cells of P10 *mdx* mice, we looked for changes in plasma membrane permeability by intraperitoneal injection of EBD in P10 and adult wild-type and *mdx* mice. This is an early sign of the dystrophic pathology in muscle cells (Mokri & Engel, 1975), that is not always easily detectable at the ultrastructural level, but that is severe enough to induce functional alterations in dystrophic muscle cells. Heart cryosections from adult *mdx* mice showed a variable number of muscle fibers labeled with EBD, preferentially distributed in clusters within the thick muscular wall of ventricles (Fig. 9A). Numerous EBD-positive cardiomyocytes were already visible at P10 (Fig. 9B), when no detectable ultrastructural alterations were observed. In addition, scattered EBD labeled cells, possibly smooth muscle cells, were present in the iris of both adult (Fig. 9C) and P10 (Fig. 9D) *mdx* mice. Cryosections of skeletal muscles of the same *mdx* mice (Fig. 9E, adult; Fig. 9F, P10) from which the hearts and irises had been dissected, used as controls for successful injections, contained several EBD-positive fibers, or portions thereof, which occurred either singly or in clusters. In age-matched wild-type mice, no labeling of cardiac (Fig. 9G), iris or skeletal muscles (not shown) was observed, nor there were cells labeled in the submandibular glands of either wt (Fig. 9H) or *mdx* mice (Fig. 9I).

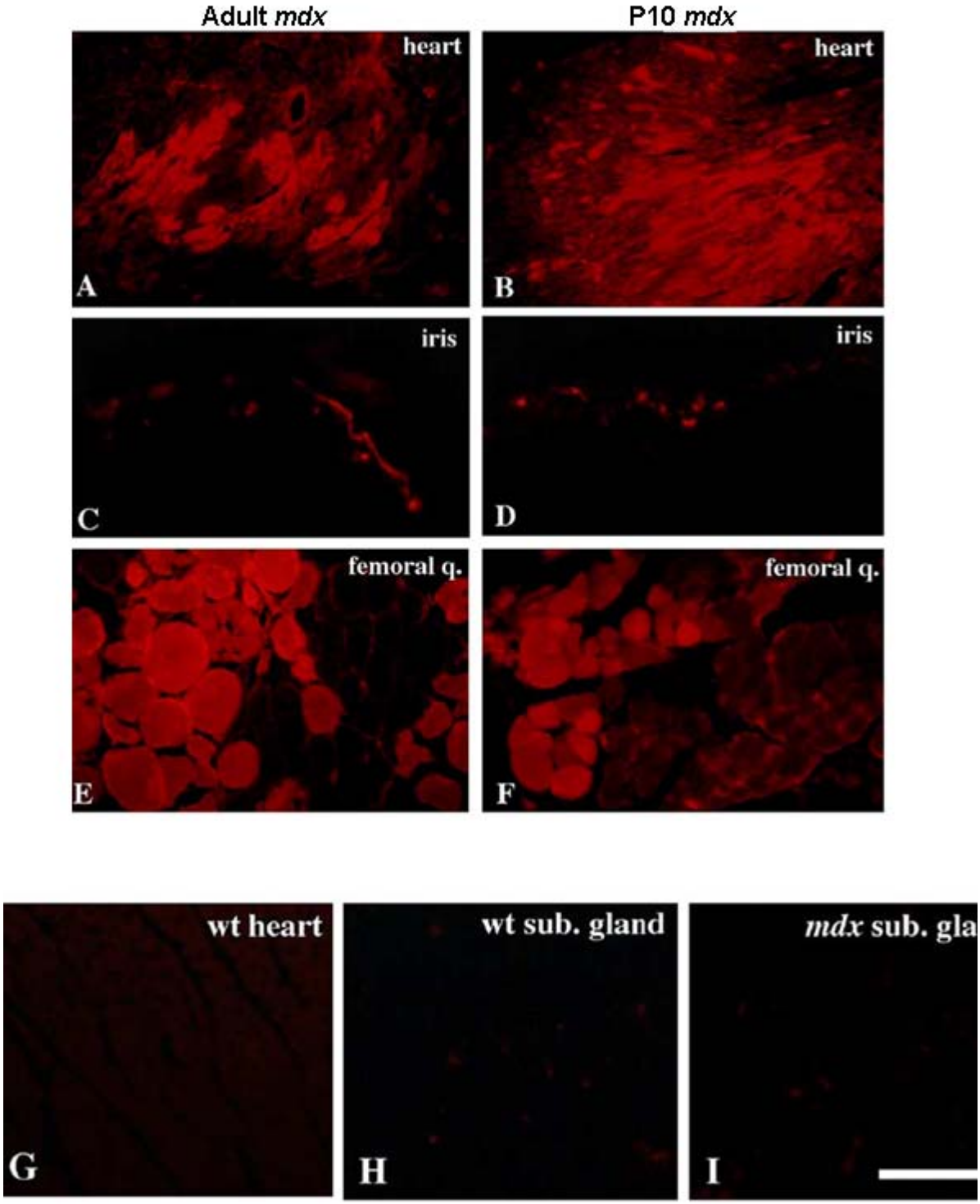

Fig. 9. Evans blue staining in heart, iris and skeletal muscle of 6–7 weeks old and P10 *mdx* mice. Large clusters of cardiomyocytes are labeled in both 6–7 weeks old (A) and P10 (B) mouse heart. A few cells, presumably smooth muscle cells, are also stained in the iris (C: 6–7 weeks; D: P10). Femoral quadriceps of the same animals from which hearts and irises were dissected, used as positive controls of the Evans blue staining, show numerous clusters of labeled fibers (E: 6–7 weeks; F: P10). No labeling is observed in sections of wt mouse heart (G), as well as in wt (H) and *mdx* (I) mouse submandibular glands. Scale bars: A,B,G–H: 160 μm; C– F: 80 μm.

6.7 mRNA levels of proteins involved in SCG neurons survival and axonal growth in wt and mdx P5, P10 and 6-7 weeks old animals

The results obtained so far show that in *mdx* mice the lack of Dp427 affects directly SCG neuron axon growth and terminal sprouting. Although these alterations allow to some neurons to survive, it can be hypothesized that when they combine with structural and/or functional damages of SCG muscular targets, neuronal loss occurs. To further investigate mechanisms possibly involved in both selective neuronal death and impaired defasciculation and terminal sprouting in *mdx* mouse, we analyzed, by real-time RT-PCR, in SCG and/or its peripheral targets, the mRNA levels of proteins of various functional categories: molecules involved in sympathetic neuron death and survival; cytoskeletal components and associated proteins; adhesion molecules and extracellular matrix proteins involved in neuritic outgrowth (Table 2B). NGF mRNA level in SCG peripheral targets was also considered (Table 2A). Based on the previous data, we focused on three postnatal stages: P5, when the neuron number in SCG is still similar between dystrophic and wt animals; P10, when SCG neuron number in *mdx* mice is already significantly reduced compared to controls; and 6-7 weeks old animals, when SCG neuron number in *mdx* mice is 36% lower than in wt animals and intense cycles of skeletal muscle degeneration/regeneration occur in dystrophic mice. Results are summarized in Tables 2A and 2B. As for SCG targets, we found that NGF mRNA level is significantly lower in the heart of P5 and in the submandibular gland of 6-7 weeks old *mdx* mice relative to age-matched controls (Table 2A). Only a few of the analyzed mRNA are differentially expressed between wt and *mdx* mouse SCG (Table 2B). Among these, there are p75 and TrkA NGF receptors; light, medium, and high molecular mass NF proteins, as well as Cdk5, a kinase known to phosphorylate NFs; α1 and β3 tubulin subunits; the retrograde transport motor dynein heavy chain 1 and the extracellular matrix protein tenascin. It is interesting to note that most of the reported alterations are evident in P5 and P10 mice, that is when excessive neuronal death is observed in *mdx* mouse SCG, during the period of the natural occurring neuron death. In addition, the mRNA level of the apoptosis marker caspase 6 in P5 *mdx* mouse SCG is higher relative to the age-matched wt, and this is consistent with the observation that more neurons die in *mdx* SCG compared to the wt during the physiological programmed cell death. On the basis of

our PCR results, we went further to analyze protein levels of most of the genes for which we had observed an altered level of mRNA. In particular, we focused on NGF and its receptors and on cytoskeletal elements to investigate the mechanisms responsible for the selective neuron death and the intrinsic defects of *mdx* mouse SCG neurons.

Table 2A. NGF mRNA levels in SCG peripheral targets of P5, P10 and 6-7 weeks old *mdx* mice relative to age-matched controls (mRNA level *mdx*/mRNA level wt)

		P5	P10	6-7 weeks
NGF	iris	0.85 ± 0.39	0.94 ± 0.26	1.35 ± 0.24
	heart	0.55 ± 0.09 (*)	1.23 ± 0.27	0.94 ± 0.32
	sub. gland	1.32 ± 0.48	0.96 ± 0.33	0.58 ± 0.23 (*)

Table 2B. mRNA levels in SCG of P5, P10 and 6-7 weeks old *mdx* mice relative to age-matched controls (mRNA level *mdx*/mRNA level wt)

		P5	P10	6-7 weeks
proteins involved in neuron death and survival	TrkA	1.27 ± 0.07 (*)	0.93 ± 0.21	1.25 ± 0.18
	p75	0.64 ± 0.07 (**)	0.64 ± 0.16 (**)	1.42 ± 0.44
	NGF	1.19 ± 0.58	1.74 ± 0.53	1.15 ± 0.29
	caspase 6	1.56 ± 0.12 (*)	1.52 ± 0.25	1.26 ± 0.18
cytoskeletal components and associated proteins	NF-L	0.81 ± 0.17	0.90 ± 0.02 (*)	0.60 ± 0.14 (*)
	NF-M	0.59 ± 0.07 (*)	0.68 ± 0.20	1.31 ± 0.42
	NF-H	0.66 ± 0.11 (*)	0.85 ± 0.14	0.88 ± 0.20
	β-actin	1.01 ± 0.18	1.16 ± 0.14	1.16 ± 0.28
	tubulin-α1	1.03 ± 0.08	1.53 ± 0.13 (**)	1.63 ± 0.69
	tubulin-β3	0.95 ± 0.10	1.48 ± 0.16 (**)	1.09 ± 0.28
	Cdk5	1.21 ± 0.10	1.01 ± 0.04	0.69 ± 0.08 (*)
	p35	1.05 ± 0.05	1.18 ± 0.08	0.68 ± 0.2
	dineyn HC1	0.86 ± 0.02 (*)	0.84 ± 0.07	1.13 ± 0.44
	kinesin 5A	0.95 ± 0.07	0.82 ± 0.17	0.70 ± 0.20
adhesion and extracellular matrix proteins	N-CAM	1.03 ± 0.08	1.13 ± 0.15	0.74 ± 0.19
	L1-CAM	0.94± 0.10	0.87 ± 0.09	1.10 ± 0.49
	neuropilin	0.98 ± 0.08	0.96 ± 0.17	0.86 ± 0.19
	tenascin C	1.26 ± 0.04 (**)	1.26 ± 0.18	0.56 ± 0.10 (*)

(*) p≤0.05; (**) p≤0.01

6.8 NGF protein levels in SCG target organs of P5, P10 and 6-7 weeks old wt and mdx mice

To investigate whether structural and/or functional damages of the dystrophic SCG muscular targets might affect expression of neurotrophins and thus be responsible for ganglion neuron death in *mdx* mice, NGF protein levels were evaluated by ELISA. Levels of total NGF (Fig. 10) were not significantly different ($p>0.05$) in the iris and heart of wt P5 and P10 *mdx* mice compared to age-matched controls, but they were lower in the same organs of adult *mdx* mice compared to the wt, although statistical significance ($p\leq0.05$) was reached only in the heart.

As ELISA does not discriminate between different NGF species, we performed Western immunoblot to detect all the NGF forms in wt and *mdx* mouse SCG target organs (Fig. 11 and Fig. 12). Mature NGF (~13kDa and 16kDa) was not detectable in all P5 and P10 SCG target tissue extracts (Fig. 11 A and B). On the other hand, at least one proNGF form (molecular mass approximately 25 and 32 kDa) was detectable in all SCG target organs at any postnatal date examined, along with glycosylated-NGF (glyNGF, molecular mass more than 50 kDa) (Fig. 11 and Fig. 12). The 25 kDa proNGF form was seldom and slightly evident in SCG target organ extracts, while the 32 kDa form was always present. Densitometric analysis of immunoblot bands relative to the 32 kDa proNGF revealed that its level is approximately 2.5 fold higher in both P5 (Fig. 11A') and P10 (Fig. 11B') *mdx* iris compared to age-matched controls ($p\leq0.05$). As for the levels of proNGF in heart and in submandibular gland, there is no significant difference ($p>0.05$) between wt and *mdx* mice at both P5 (Fig. 11A') and P10 (Fig. 11B').

Different tissues from adult mice showed different patterns of expression of NGF species, as also reported by others (Bierl et al., 2005). High levels of mature NGF were detected in the submandibular gland of adult mice, although in *mdx* mice they were clearly reduced respect to the wt (Fig. 12B). Presence of mature NGF was also detected in adult mouse hearts, but its level was significantly lower in *mdx* mice compared to controls (Fig. 12C). We did not perform a densitometric analysis of the bands in the immunoblot representative of mature NGF in the submandibular gland because the high amount of NGF present in this organ gave rise to saturated bands. Nonetheless, repeated experiments always gave the same pattern of NGF expression.

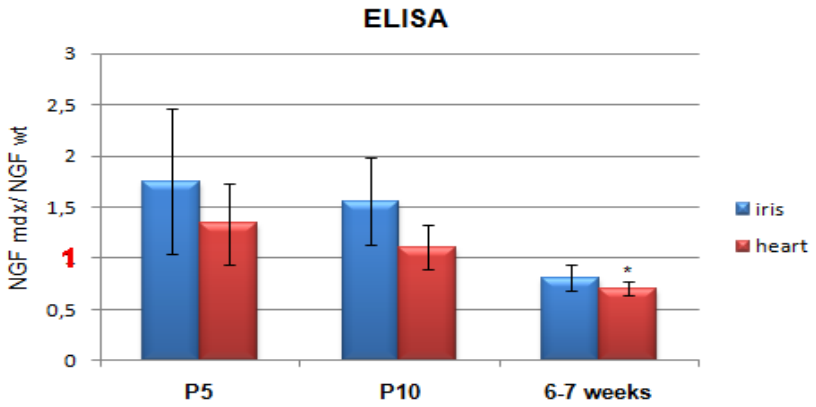

Fig. 10. Total NGF level in iris and heart of P5, P10 and 6-7 weeks old wt and *mdx* mice. The levels of total NGF, measured by the Elisa technique, are significantly lower in adult *mdx* mouse heart than in age-matched control mice. There are no differences in P5 and P10 *mdx* mouse iris and heart compared to the wt of the same age (n=4). * p≤0.05.

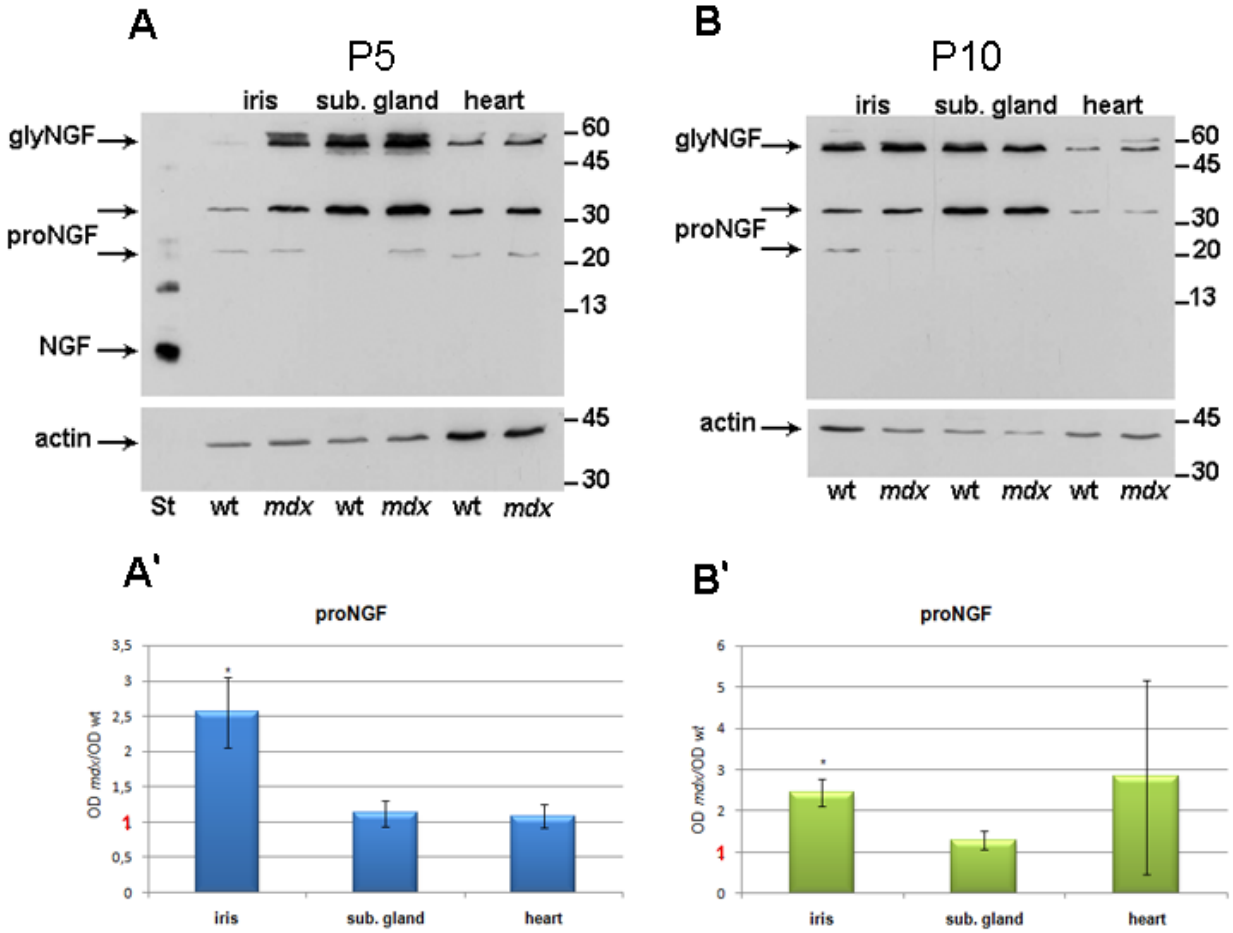

Fig. 11. Western immunoblot of NGF and densitometric analysis of proNGF in iris, submandibular gland and heart of P5 and P10 wt and *mdx* mice. The NGF antibody recognizes multiple bands, corresponding to mature NGF (approximately 13 kDa), proNGF (approximately 25 and 32 kDa) and glycosylated forms of proNGF (glyNGF, more than 50 kDa). Mature NGF is not detectable in tissue extracts from both P5 (A) and P10 (B) animals. The 32 kDa band of proNGF is expressed at high levels in all these tissues in both P5 (A) and P10 (B) mice. The 25 kDa band of proNGF is seldom and faintly detectable in Western immunoblot and has not been included in the quantitative analysis. Densitometric analysis of the 32 kDa proNGF band shows that its level is higher in P5 (A') and P10 (B') *mdx* iris compared to the age-matched wt (n=3). Molecular mass standards (/1000) are indicated on the right hand side. St: NGF standard (1 ng). OD: optical density. * p≤0.05.

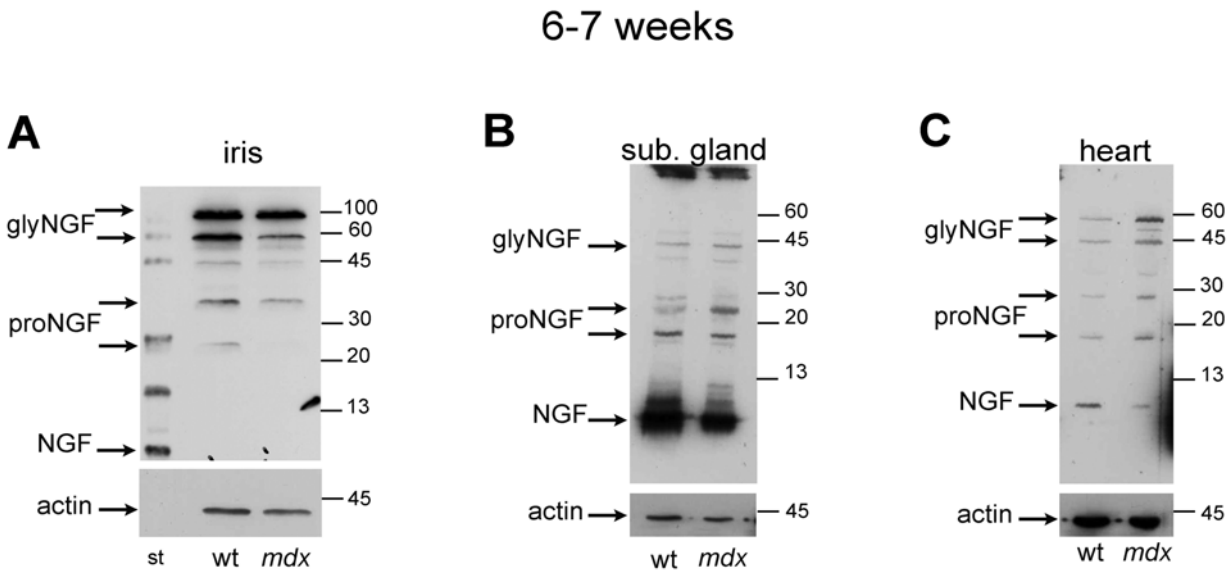

Fig. 12. Western immunoblot analysis of NGF in iris, submandibular gland and heart of 6-7 weeks old wt and *mdx* mice. The mature NGF band is clearly detectable in the submandibular gland (B) and in the heart (C). The intensity of the NGF band is lower in both these tissue extracts from *mdx* animals, compared to the same tissue extracts from wt mice. The mature NGF band is not detectable in irises (A). The other NGF forms show tissue specific patterns of expression in adult mice (A-C). The difference in the intensity of the bands in the standard lane between this Western immunoblot and the one shown in Fig. 10 is due to a different exposure time of the film. Molecular mass standards (/1000) are indicated on the right hand side. St: NGF standard (1 ng).

6.9 NGF and NGF receptors protein levels in SCG of P5, P10 and 6-7 weeks old wt and mdx mice

To verify if the levels of TrkA and p75, which are both expressed in sympathetic neurons (Enfors et al., 1992), are different in *mdx* mouse SCG neurons respect to wt animals (Fig13), Western immunoblot of SCG extracts from P5, P10 and 6-7 weeks old wt and *mdx* mice was performed. Fig. 13A shows a typical Western immunoblot for TrkA. The two bands of 140 kDa and 110 kDa molecular mass correspond to different glycosylated forms of the receptor (Martin-Zanca et al., 1989). The 140 kDa protein represents the membrane bound receptor fully glycosylated (Mischel et al., 2002). Densitometric analysis of these bands (Fig. 13A') highlights that TrkA protein level is approximately 60% lower in P5 and P10 *mdx* mouse SCG compared to controls of the same age ($p \leq 0.01$), while it is similar between adult *mdx* and wt mice. TrkA belongs to the family of tyrosine kinase receptors. Therefore, to evaluate the extent of the receptor activation in *mdx* mouse SCG, we analyzed by Western immunoblot the levels of phosphoTrkA, by using a specific antibody directed against the phosphotyrosine 490 (Fig. 13B). Densitometric analysis of immunopositive bands (Fig. 13B') revealed that the level of phosphoTrkA was approximately 50% lower in P5 *mdx* mouse SCG compared to the wt ($p \leq 0.05$), was still lower than controls at P10, although not significantly ($p=0.1$), showed no difference between adult wt and *mdx* mice.

In Fig. 13C, is shown a typical Western immunoblot for p75, the other NGF receptor. A single band was detected by the anti-p75 antibody used, which densitometric analysis (Fig. 13C') revealed that the protein levels are significantly lower in P10 and 6-7 weeks old *mdx* mouse SCG compared to controls of the same age ($p \leq 0.01$), while they are similar at P5.

As ganglion neurons produce and secrete NGF (Hasan et al., 2003), we also analyzed NGF protein levels of P5, P10 and 6-7 weeks old wt and *mdx* mouse SCG (Fig. 14A). Western immunoblot analysis showed that, as for peripheral targets, also the SCG does not express detectable levels of mature NGF. ProNGF forms, instead, were much more abundant and clearly visible, as also reported by others (Hasan et al., 2003; Jansen et al., 2007). Densitometric analysis of the 32 kDa band (Fig. 14A') revealed no difference in proNGF protein level between P5 and 6-7

weeks old wt and *mdx* mouse SCG. ProNGF protein level was, instead, slightly but significantly lower (p≤0.05) in P10 *mdx* mouse SCG compared to the wt.

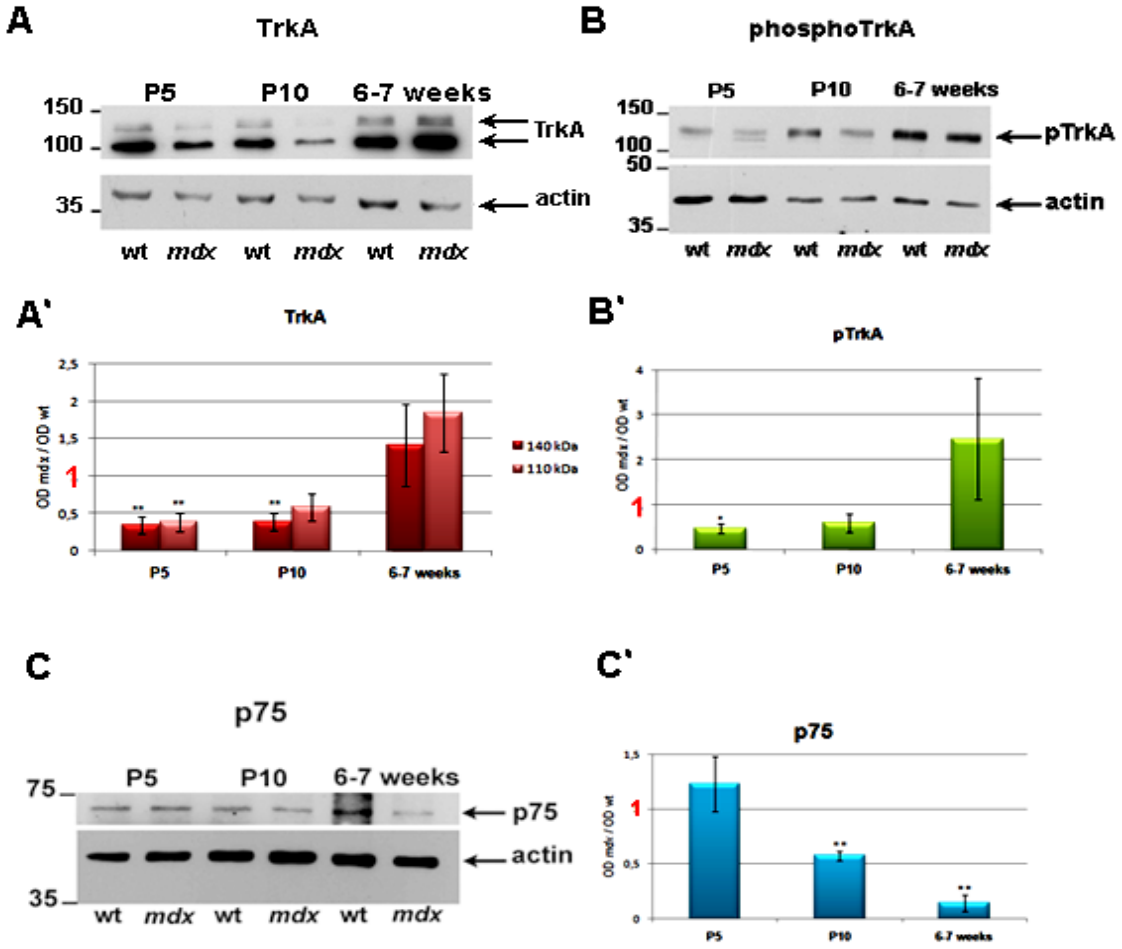

Fig. 13. Western immunoblot and densitometric analysis of NGF receptors in SCG of P5, P10 and 6-7 weeks old wt and *mdx* mice. The TrkA antibody (A) recognizes two bands of 110 and 140 kDa, that represent two differently glycosylated forms of the receptor. The 140 kDa form represent the membrane bound receptor. Densitometric analysis (A') of both bands shows that TrkA level is lower in P5 and P10 *mdx* mouse SCG compared to the age-matched wt (n=4). The phosphoTrkA (pTrkA) antibody (B) recognizes a single band of approximately 140 kDa, representing TrkA receptor phosphorylated in its tyrosine 490 residue. Densitometric analysis (B') reveals that pTrkA level is lower in P5 *mdx* mouse SCG (n=4). The p75 antibody (C) detects a quite faint band of approximately 70 kDa. Densitometric analysis shows that the p75 protein level is lower in P10 and 6-7 weeks old *mdx* mouse SCG compared to the wt (n=3). Molecular mass standards (/1000) are indicated on the left hand side. OD: optical density. * p≤0.05. ** p≤0.01.

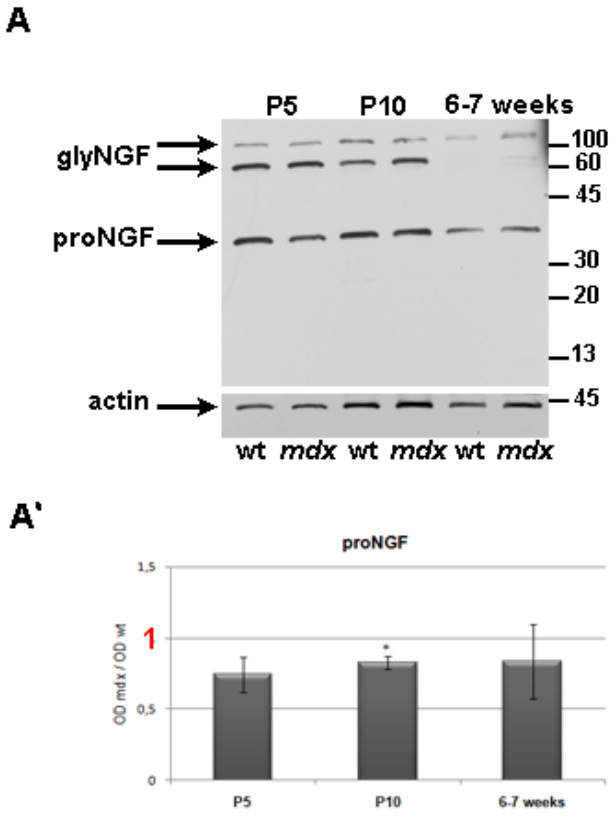

Fig. 14. Western immunoblot of NGF and densitometric analysis of proNGF in SCG of P5, P10 and 6-7 weeks old wt and *mdx* mice. Mature NGF is not detectable in mouse SCG extracts, while the 32 kDa form of proNGF is expressed (A), together with higher molecular mass glycosylated forms (glyNGF). Densitometric analysis (A') of the 32 kDa proNGF band shows that its level is not different in P5 and 6-7 weeks old *mdx* SCG compared to the age-matched wt, while it is lower in P10 *mdx* mouse SCG compared to the wt (n=4). Molecular mass standards (/1000) are indicated on the right hand side. OD: optical density. * p≤0.05.

6.10 Levels of neurofilament proteins and dynein in SCG of P5, P10 and 6-7 weeks old wt and mdx mice

Protein levels of some cytoskeletal components were analysed. Figure 15A shows a typical Western immunoblot for neurofilament proteins. NF-H antibody detects at least two bands of molecular mass of approximately 180 and 200 kDa, which represent multiple phosphorylation forms of the protein. Antibodies directed against NF-M and NF-L recognize bands of approximately 140 kDa and 68 kDa, respectively (Fig. 15A). Densitometric analysis of the immunoreacted bands (Fig. 15A') revealed that the level of all three NF proteins was lower in P5 *mdx* mouse SCG ($p \leq 0.05$) compared to control, and that remained lower for NF-H and NF-M in P10 *mdx* mouse SCG compared to the age-matched wt ($p \leq 0.01$). Differently, in adult mice SCG, NF-H protein level was higher in *mdx* than in control animals ($p \leq 0.05$). It has to be noted that the densitometric analysis on NF-H was performed on both the 180 and the 200 kDa bands; thus the reported results are representative for the total NF-H optical density (Fig. 15A').

A specific antibody (SMI 36) was used to evaluate the level of the phosphorylated form of the high molecular mass neurofilament protein (Fig. 15B). Densitometric analysis of the single band detected by this antibody showed that the level of phosphoNF-H is significantly lower in P10 *mdx* mouse SCG compared to the wt (Fig. 15 B'). The level of phosphoNF-H is lower in 6-7 weeks old *mdx* mouse SCG than in control as well, but it does not reach statistical significance ($p=0.07$).

The protein level of the molecular motor protein dynein heavy chain 1 (HC1) was also analysed in wt and *mdx* mouse SCG and a typical Western immunoblot is shown in Fig. 16A. No significant differences in dynein levels were ever detected by densitometric analysis (Fig. 16A').

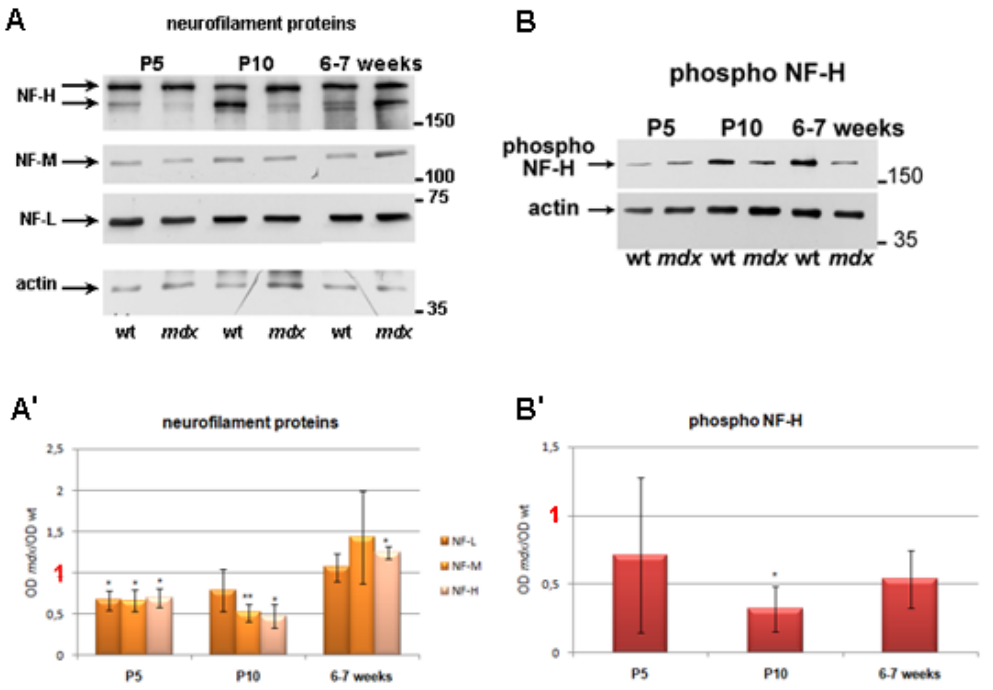

Fig. 15. Western immunoblot and densitometric analysis of neurofilament light, medium and high molecular mass proteins in SCG of P5, P10 and 6-7 weeks old wt and *mdx* mice. All three NF proteins were analyzed by Western immunoblot on the same nitrocellulose membrane by using specific antibodies (A). As expected, molecular mass of NF-L is approximately 68 kDa, that of NF-M is 140 kDa. The NF-H antibody recognizes at least two bands, of approximately 180 and 200 kDa, corresponding to different phosphorylation forms of the protein. Densitometric analysis (A') reveals that the level of all NF proteins is lower in P5 *mdx* mouse SCG compared to the wt. NF-M and NF-H protein levels are also lower in P10 *mdx* mouse SCG compared to the age-matched controls. Differently, the total protein level of NF-H is higher in 6-7 weeks old *mdx* mouse SCG compared to the wt. (n=4). SMI 36 antibody detects a single band of molecular mass higher than 150 kDa (B). Densitometric analysis (B') shows that its level is lower in P10 *mdx* mouse SCG compared to age-matched wt. (n=3). Molecular mass standards (/1000) are indicated on the right hand side. OD: optical density. * p≤0.05. ** p≤0.01.

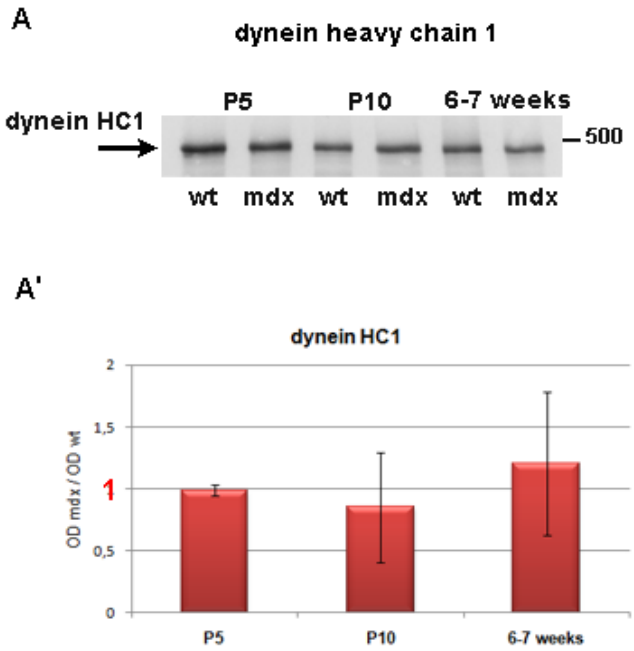

Fig. 16. Western immunoblot and densitometric analysis of dynein heavy chain 1 (HC1) in SCG of P5, P10 and 6-7 weeks old wt and *mdx* mice. Dynein HC1 antibody detects a single band of molecular mass approximately 500 kDa (A). Due to the high molecular mass of dynein, it has not been possible to analyze actin (molecular mass 43 kDa) levels in the same nitrocellulose membrane. Anyway protein loading is equal in all lanes. Densitometric analysis (A') shows that there is no difference between wt and *mdx* mouse SCG dynein levels, in any of the examined stages (n=4). Molecular mass standards (/1000) are indicated on the right hand side. OD: optical density.

7. DISCUSSION

7.1 Loss of SCG neurons in mdx mice

The present study shows that, in *mdx* mice, the lack of Dp427 causes intrinsic alterations to SCG neurons. When combined with dystrophy-associated damages of their muscular targets, this leads to ganglion neuron death. The SCG of adult *mdx* mice has 36% fewer neurons than that of wt mice. At P5, the earliest postnatal date examined for the neuronal count, no difference was observed in the number of ganglionic neurons between wt and *mdx* mice demonstrating that, in the latter, sympathetic neurons are generated in the correct number and all migrate to the appropriate position to form the ganglion. This excludes a role for dystrophin in these events of sympathetic neuron differentiation, in contrast to the aberrant neuroblast migration and orientation described for central neurons (Jagadha & Becker, 1988; Mehler & Kessler, 1998; Hatten, 1999). SCG neuron loss begins sometimes between P5 and P10, concomitantly to the physiological neuronal death (Wright, 1995). However, the remaining neurons are intrinsically affected by the lack of Dp427 (see below).

7.2 Alterations of axonal defasciculation and terminal sprouting in mdx mice

T-OH immunolabeling showed decreased axonal defasciculation and/or terminal sprouting in all SCG target organs examined as early as P5, when the number of ganglionic neurons is still at its full complement. These widespread changes in terminal axon architecture may be consequent to alterations in the dynamic link between the actin cortical cytoskeleton and the extracellular matrix (ECM), as also reported in different experimental models. Abnormal defasciculation of hippocampal axon terminals, for instance, has been observed in mice deficient in ephrin-B tyrosine kinase receptors (Chen et al., 2004), which normally provide the correct interaction between axons and extracellular environment (Kullander & Klein, 2002). Dystrophin is actively involved in the cytoskeleton-ECM linkage via the dystrophin–glycoprotein complex (Michele & Campbell, 2003). Lack of Dp427, by decreasing the plasma membrane expression of components of the complex itself (Ibraghimov-Beskrovnaya et al., 1992), dramatically alters this connection. The direct link between the basal lamina and the cytoskeleton of Schwann cells,

maintained by the dystroglycan interaction with Dp116 or utrophin and laminin-2, is disrupted in *mdx* mouse peripheral nerves (Hnia et al., 2006). Alterations in the cytoskeleton-ECM linkage in *mdx* mouse SCG are also suggested by the previously observed decrease in the number of intraganglionic synapses immunopositive for dystroglycan (Zaccaria et al., 2000).

In addition, an important contribution to aberrant axonal growth may derive from impairment of the fast ganglionic transmission consequent to the reduction in intraganglionic α3nAChRs (Del Signore et al., 2002). In support to this hypothesis, Rassadi and co-workers showed that in α3nAChR null mice, fast synaptic transmission in sympathetic ganglia is completely absent (Rassadi et al., 2005). Moreover, frequency alterations of the spontaneous rhythmic activity in chick motor neurons at early developmental stages result in altered fasciculation and axon pathfinding errors (Hanson & Landmesser, 2004; Hanson & Landmesser, 2006), underlining the significant contribution of synaptic activity in the formation of synaptic contacts.

Other molecules which might be involved in altered defasciculation are NCAM and its polysialic acid-conjugate form PSA-NCAM. Both the involvement of NCAM in the regulation of axon fasciculation and nerve branching during development, and the role of PSA in modulating such processes are, in fact, among the first-elucidated and best-studied PSA-NCAM functions (reviewed in Bonfanti, 2006). PSA appears for the most part to play a permissive role in axon guidance, reducing the fasciculative interactions between axons and thereby allowing them to respond more effectively to a variety of extrinsic signals, including those from their targets (reviewed in Brusés & Rutishauser, 2001). In the CNS, PSA expression increases specifically in the corticospinal tract (CST) when collateral branches begin to form (Daston et al., 1996). Thus, the sprouting and/or extension of the PSA-positive CST axons appears to be facilitated by the presence of PSA, possibly through the attenuation of axon-axon interactions in the CST (reviewed in Brusés & Rutishauser, 2001). In the PNS, limb motor neuron axon bundles up-regulate PSA as they enter the plexus region. During this process, they rearrange themselves into muscle-specific fascicles. When PSA is enzymatically removed during this period, this rearrangement is hindered, resulting in pathfinding errors (Tang et al., 1992). Based on our T-OH immunostaining data, it is possible to speculate that

defasciculation defects, observed in *mdx* mouse SCG targets, might be due to altered levels of PSA-NCAM or other adhesion molecules. Although NCAM mRNA level was not altered in *mdx* mouse SCG compared to the wt, it is strikingly important to evaluate NCAM protein levels and, above all, post-translational modifications. For this reason, PSA-NCAM expression is currently under investigation in wt and *mdx* SCG and its peripheral targets.

On the other hand, abnormalities in cytoskeletal components expression might as well be responsible for these intrinsic neuronal alterations, i.e. reduced defasciculation and terminal sprouting in all *mdx* mouse SCG targets and in *mdx* mice of all ages. Indeed, the mRNA levels of the neurofilament proteins were altered in *mdx* mouse SCG. Analysis of NF-L, NF-M and total NF-H protein levels revealed that they are reduced in P5 and P10 *mdx* mouse SCG compared to controls. In addition, the level of the phosphorylated form of NF-H protein is lower in P10 *mdx* mouse SCG compared to the wt. At P5, in *mdx* mouse SCG, the number of neurons is not yet different from that of the wt. However, the adrenergic fibres network of *mdx* iris is reduced compared to the wild-type, as already observed in P0 mice. This suggests that, in *mdx* mouse SCG, some neurons, probably engaged in the processes leading to their death, do not extend their axons and/or have already retracted them from the damaged iris muscle. This is consistent with the reduced levels of NF proteins, as NFs are the main cytoskeletal elements responsible for axonal architecture and diameter (reviewed in Lariviere & Julien, 2003). In 6-7 weeks old mice, NF-L and NF-M levels become comparable between wt and *mdx* SCGs, while the level of NF-H is still altered. It is reasonable to propose that some compensatory mechanism is operating in 6-7 weeks old *mdx* mouse SCG neurons, since these neurons are the surviving ones and most of them project to the submandibular gland, a non-muscular SCG peripheral target, undamaged by the lack of Dp427. Lately, it has been shown that in small diameter axons, an intact intermediate filament network is required for collateral sprouting (Belecky-Adams et al., 2003), and that neurofilament content is correlated with branch length and stability in cultured *Xenopus* spinal cord neurons (Smith et al., 2006). On the basis of these findings, it is possible to speculate that a reduced amount of NFs in *mdx* mouse SCG neurons may be in part responsible for the defects in defasciculation

and terminal sprouting observed in SCG peripheral targets of dystrophin-deficient mice.

7.3 Damages induced by the lack of Dp427 in SCG peripheral target organs

T-OH immunoreactivity revealed a reduction in the extension of the adrenergic fiber network only in the heart and iris of *mdx* mice of all examined ages. The adrenergic fibers density is dramatically reduced even in P0 *mdx* iris compared to the wt, strongly suggesting that some adrenergic fibers never reach this muscular target. In adult animals, the reduction in the extension of fiber network is partly consequent to the selective loss of SCG neurons projecting to muscular targets, as demonstrated by WGA-HRP retrograde labeling. The death-promoting signals may derive from the structural and/or functional damages induced in cardiomyocytes and iris smooth muscle cells by the lack of Dp427. Indeed, despite the absence of cell degeneration and/or apparent ultrastructural alterations, EBD labeling revealed damage to the plasma membrane of both heart and iris muscle cells as early as in P10 *mdx* mice. In both skeletal (Petrof et al., 1993) and heart (Danialou et al., 2001) muscle cells, the dystrophin–glycoprotein complex protects the plasma membrane from the mechanical stress that develops during contraction. In DMD patients and *mdx* mice, lack of this complex causes focal breakdown of the muscle plasma membrane, thought to be responsible for the initial events in muscle necrosis (reviewed in Blake et al., 2002). Damaged muscle cells show increased membrane permeability to macromolecules flowing in and out, thus affecting muscular function, contractile properties and survival (Kaye et al., 1996; Sapp et al., 1996; Iwata et al., 2003). Possible functional alterations in *mdx* mouse cardiomyocytes and iris smooth muscle cells, consequent to the plasma membrane damage revealed by EBD staining, may render them inhospitable to growing axons and induce synapse removal and sympathetic fiber retraction, as shown by the reduced extension of the adrenergic innervation observed already at P0 and P5. Weakened by the dystrophic phenotype, SCG neurons may be unable to redirect their axons onto undamaged muscle fibers and die. In support of this hypothesis is our unpublished observation that the poor adrenergic innervation of heart and iris does not recover in 10 month-old *mdx* mice, when cycles of muscle degeneration-

regeneration have ceased. Although we did not observe cell degeneration, or evident ultrastructural alterations, of *mdx* mouse cardiomyocytes and iris smooth muscle cells at P10 (data not shown), EBD staining revealed ruptures in their plasma membranes as the first sign of the pathology. Variable amounts of degenerating heart muscle cells were instead detected in 6–7 weeks old animals, as also reported by other authors (Grady et al., 1997; Megeney et al., 1999; Straub et al., 1997; Danialou et al., 2001). However, at this age, we still failed to demonstrate degeneration, or apparent ultrastructural alterations, of iris smooth muscle cells despite the damage to their plasma membrane caused by the lack of Dp427. Our findings are in agreement with those reported by other authors (Boland et al., 1995; Vannucchi et al., 2004). Boland et al. (1995) found no cell necrosis, fibrosis or other morphological alterations in different types of dystrophic smooth muscles. However, when compared with wild-type mice, the thickness of the gastrointestinal smooth muscle layers of *mdx* mice was significantly reduced, suggesting mild cell necrosis and muscular atrophy undetectable with the electron microscope (Boland et al., 1995), but possibly responsible for some of the gastrointestinal dysfunction episodes observed in DMD patients (Nowak et al., 1982; Leon et al., 1986; Barohn et al., 1988). Similarly, Faussone-Pellegrini's group described a number of ultrastructural and functional alterations, consequent to the lack of Dp427, in the myenteric neurons (Vannucchi et al., 2003) and in the interstitial cells of Cajal of *mdx* mice (Vannucchi et al., 2004), but reported absence of evident morphological alterations in the surrounding smooth muscle cells (Vannucchi et al., 2004). Altered biomechanical properties of carotid arteries have also been described in *mdx* mice (Dye et al., 2007). In addition, circular smooth muscle cells from colon segments, but not those from the duodenum of *mdx* mice, developed altered electrical (Serio et al., 2001) and mechanical activity (Mancinelli et al., 1995; Mulè et al., 1999; Azzena & Mancinelli, 1999), indicating that smooth muscles from different locations may be differently affected by the dystrophic pathology, as demonstrated for skeletal muscles (Porter et al., 2004). Smooth muscle cells from *mdx* mouse iris may be similar in this respect to those from the colon and it is reasonable to suggest that molecular and functional alterations occur that are undetectable at the ultrastructural level and that these may affect SCG neuron survival. Although the submandibular gland is listed among the non-

muscular SCG peripheral targets, it contains a component of smooth muscle-like cells, which express Dp427, as do other gland cell types (i.e. acinar cells). The absence of full-length dystrophin in *mdx* mice, however, does not induce evident structural damage in any of these cells. The lack of cellular EBD staining also demonstrates integrity of the plasma membranes, even in myoepithelial cells, whose modest mechanical activity cannot be compared to that of heart and iris muscle cells. Although we cannot exclude fine ultrastructural changes and/or functional alterations in myoepithelial cells, as well as in secretory cells, they may not be relevant for SCG neuron survival.

7.4 Trophic factors in SCG target organs

SCG neuron survival and differentiation (Wright, 1995; ElShamy et al., 1996; reviewed in Huang & Reichardt, 2001; reviewed in Glebova & Ginty, 2005), as well as density of innervation and collateral sprouting (Purves, 1988; Saffran & Crutcher, 1990; reviewed in Glebova & Ginty, 2005), strictly depend on target-derived neurotrophic factors (i.e. NGF, NT-3). Therefore, we hypothesized that excessive neuron death in *mdx* mouse SCG and reduced peripheral target innervation, may be triggered by an insufficient provision of these factors, attributable to their reduced synthesis by iris and heart muscle cells damaged by the lack of Dp427. Our experimental results partially confirm this hypothesis.

NT-3 is a member of the neurotrophin family of growth factors, which was initially shown to be crucial for sympathetic neuron survival *in vivo* (Enfors et al., 1994; Farinas et al., 1994). However, it does not directly support survival of postnatal sympathetic neurons, because it is not able to promote TrkA retrograde signalling (Kuruvilla et al., 2004). NT-3 does, instead, support proximal axon extension along the vasculature and SCG intermediate targets, and the subsequent innervation of effector organs (Kuruvilla et al., 2004). For this reason, the developmental period in which NT-3 principally exerts its action precedes that of our study (ElShamy et al., 1996; Kuruvilla et al., 2004; reviewed in Glebova & Ginty, 2005); therefore NT-3 was not taken into consideration in the present work. Instead, an extensive analysis of NGF levels, which is the neurotrophin principally involved in sympathetic neuron survival and target innervation in the considered time window, was performed. The measured levels of total NGF, analyzed by ELISA,

were not significantly different between wt and *mdx* P5 and P10 iris, nor in the heart. However, this technique does not discriminate mature NGF from the proNGF forms, because the employed antibody detects both (Peters et al., 2006; Bierl & Isaacson, 2007). Thus, although less-sensitive, Western blot analysis permits to define with precision all the molecular mass of the NGF forms (Bierl et al., 2005). Mature NGF was not detectable in P5 and P10 *mdx* mouse tissues, in accordance with the findings of others (Fahnestock et al., 2001; Bierl et al., 2005; Randolph et al., 2007). On the contrary, the 32 kDa proNGF form was increased approximately 2.5-fold in iris of both P5 and P10 *mdx* mice compared to the age-matched controls. Even though this is not a direct evidence, it is possible to hypothesize that the amount of mature NGF in irises of P5 and P10 *mdx* mice may be lower than in the same tissue of wild-type animals. Thus, it suggests that *mdx* mouse SCG neurons might receive a reduced quantity of trophic factor from irises, in a strikingly important period for neuron survival. The reduced amount of NGF produced by dystrophic irises may add to the greater distance of this target tissue from the SCG, compared to the submandibular gland, and explain the selective neuronal death of iris-projecting neurons observed in *mdx* mouse SCG. Sympathetic innervation of the heart in rodents is, instead, primarily provided by the stellate ganglion, with only minor contributions from the SCG and mid-thoracic paravertebral ganglia (Pardini et al., 1989), and our data on excessive neuron loss in *mdx* mouse SCG were obtained for iris-projecting neurons only. Thus, it is not possible to draw the same conclusion for the hearts of *mdx* mice.

The higher level of proNGF in P5 and P10 *mdx* irises also suggests that alterations in proNGF processing to generate mature NGF might be present. Why the lack of Dp427 induces such alterations is an open question. One possibility is an impairment in the cleavage of proNGF into NGF by proteases. Proneurotrophins can be cleaved both intracellularly by furin (Farhadi et al., 1997) and other members of the pro-protein convertase family (Seidah et al., 1996), and extracellularly by MMPs and plasmin (Lee et al., 2001; Pang et al., 2004; Bruno & Cuello, 2006). Recent studies demonstrate that proNGF can be released after adult CNS injury (Harrington et al., 2004) and detected in the brains of Alzheimer's disease patients (Fanhestock et al., 2001; Peng et al., 2004), suggesting that an increased proNGF level might be a feature of some pathological conditions.

In adult life, sympathetic neurons are relatively resistant to cell death. However they continue to require target-derived NGF for their maintenance, growth and neurotransmitter release (reviewed in Cowen & Gavazzi, 1998). Our data show that mature NGF is produced in great quantity by 6-7 weeks old mouse submandibular glands. This result was expected, since mouse submandibular gland served as the preferred starting material for isolation of NGF in most of the early studies on NGF (reviewed in Shooter, 2001), because of the large amount of this factor it contains. Nonetheless, NGF level was reduced in 6-7 weeks old *mdx* mouse submandibular gland compared to the wt, a result in accordance with the observed NGF mRNA level in this tissue. Anyway, the amount of NGF was very high, suggesting that it can be more than sufficient for neuron maintenance and survival. On the other hand, the total NGF levels are reduced in iris and heart of adult *mdx* mice compared to the controls and this may in part account for the innervation defects observed in these muscular target tissues in adult *mdx* mice.

7.5 NGF and NGF receptors in SCG neurons

Although the mRNA level for NGF TrkA receptor was higher in P5 and P10 *mdx* mouse SCG compared to the wt, the protein level of TrkA was lower, suggesting that post-transcriptional mechanisms affect TrkA production and/or degradation in dystrophin-deficient mice. Protein level of the phosphorylated form of TrkA receptor was lower as well. Phospho-TrkA is the ligand-activated receptor, likely transported back from axon terminals, by means of retrograde transport. It is well-known that TrkA receptor, when ligand-activated, transmits positive signals such as enhanced survival and growth (reviewed in Kaplan & Miller, 2000), allowing to propose that *mdx* mouse sympathetic neurons might receive a weak survival signal from the periphery. This is certainly due to the presence of a decreased number of receptors in SCG neurons membrane, but also to a lower activation of TrkA receptors, as demonstrated by our Western immunoblot data. Thus, at P5, when the neuron number in SCG of wt and *mdx* mice is still similar, just before the beginning of the greater neuron death in *mdx* mouse SCG, there are approximately 50% less “active” NGF receptors in *mdx* mouse SCG than in the wt.

SCG neurons express p75NTR receptor, together with TrkA (Enfors et al., 1992). While sympathetic neurons, between embryonic day 13 (E13) and E14,

become specified to up-regulate TrkA mRNA in culture, independently of added factors, p75 mRNA is up-regulated by NGF in the same conditions (Wyatt & Davies, 1995), demonstrating that NGF can transcriptionally regulate p75. NGF is also necessary for expression of p75 *in vivo* (Kuruvilla et al., 2004). Thus, it is possible to infer that the lower levels of both NGF and TrkA are responsible for the reduced expression of p75 observed in *mdx* SCG neurons compared to the wt, in P5 mice at the mRNA level and in P10 mice at both the mRNA and protein levels. In addition, p75 and TrkA are reported to interact and determine sensitivity and affinity of SCG neurons to NGF (reviewed in Nykjaer et al., 2005). Lee et al. (1994) showed that p75-deficient post-natal SCG neurons are less sensitive to sub-saturating concentrations of NGF than wild-type neurons, suggesting that a decreased sensitivity to NGF may lead to increased loss of SCG neurons *in vivo*. In addition, the number of high affinity sites for NGF can be modulated by changing the ratio of expression of the two NGF receptors (Esposito et al., 2001). Data presented here revealed that the protein levels of the NGF receptors (i.e. TrkA or p75) are altered in *mdx* mouse SCG neurons compared to the age-matched controls, in all the post-natal examined stages. This can probably lead to a reduced number of high affinity sites for NGF and thus to a reduced NGF survival signalling in *mdx* mice, at least partly explaining the higher number of neurons dying in *mdx* mouse SCG during the period of the physiological cell death. Such reduced survival signalling might also be due to alterations in cytoskeletal components in *mdx* mice neurons, since retrograde transport is strictly dependent on cytoskeleton. Although dynein protein levels were not different between wt and *mdx* SCGs, the reduced expression of NF proteins in *mdx* mice suggest that it is not possible to exclude this possibility.

p75 is also a death receptor (reviewed in Hempstead, 2002; reviewed in Nykjaer et al., 2005). Proneurotrophins bind to p75 with higher affinity than that exhibited by mature neurotrophins and induce apoptosis more effectively than mature neurotrophins do (Lee et al., 2001), in particular when p75 forms a complex with sortilin (Nykjaer et al., 2004; Teng et al., 2005). Nonetheless, various groups demonstrated that p75 death signalling is silenced by an ongoing TrkA activation in many cell types (Bamji et al., 1998; Yoon et al., 1998; Majdan et al., 2001; Teng et al., 2005). Thus, if a sympathetic neuron reaches the appropriate target and sequesters NGF, TrkA is robustly activated and this activation silences any ongoing

apoptotic signal deriving from p75. Conversely, if in a neuron TrkA is only weakly activated, as a consequence of the lack of NGF, a p75-mediated death signal would cause the rapid apoptotic elimination of that neuron (Majdan et al., 2001). We hypothesize that this is the case for *mdx* mouse SCG neurons reaching dystrophic muscular targets, in particular the iris. P5 *mdx* irises, in fact, contain a higher level of the pro-apoptotic factor proNGF compared to P5 wt irises, possibly contributing to the activation of p75 death signalling.

ProNGF is reported to be secreted also by SCG neurons, suggesting an autocrine or paracrine loop involving induction of cell death by activation of p75 signalling (Hasan et al., 2003). Nevertheless, proNGF protein level was not different in P5 and 6-7 weeks old *mdx* mouse SCG and, rather, it was slightly but significantly lower in P10 *mdx* mouse SCG compared to the age-matched wild-type. It is, thus, possible to exclude a higher autocrine and/or paracrine triggering of p75 death signalling in *mdx* mouse SCG neurons, at least in case this activation is due to proNGF. However, a very recent paper by Jansen and co-workers (2007) showed that in sortilin-deficient mice SCG neuron number during the period of the physiological cell death is not different from control animals, thus demonstrating that proneurotrophins are not accountable for developmental elimination of sympathetic neurons, even though they do not exclude that p75 death-signal may be activated by other ligands.

As already underlined, in addition to being the principal mediator of sympathetic neuron survival, NGF also controls final target innervation. Target expression of NGF and neuronal expression of TrkA and p75 are both required for appropriate sympathetic innervation of peripheral tissues. Studies of mice having one functional allele for NGF or TrkA, in fact, revealed that reductions both in levels of NGF receptors and neuronal number together hinder the capacity of terminal sympathetic axons to undergo compensatory collateral growth in peripheral tissues, resulting in lower densities of sympathetic axons (Ghasemlou et al., 2004). However, studies conducted by using mice deficient for NGF or p75 receptor showed that requirements of these molecules for innervation of sympathetic peripheral targets are heterogeneous (Lee et al., 1994; Glebova & Ginty, 2004; Jahed & Kawaja, 2005), suggesting that other factors might be involved (reviewed in Glebova & Ginty, 2005). Thus, we can not exclude that different molecules may

also contribute to the innervation defects that we observed in *mdx* mouse SCG peripheral targets. These studies also suggest that different target tissues might be differently susceptible to reduced levels of NGF or its receptors.

mRNA and protein levels of dynein heavy chain 1 (HC1), a component of the cytoplasmic dynein/dynactin complex, were also analyzed. Dynein is actually a 40 nm-long complex of molecular mass 1.6 x 10^6 Da, which includes two heavy chains and a number of light chains (reviewed in Brady et al., 1999). The dynein/dynactin complex is involved in retrograde transport of Trk receptors (Bhattacharyya et al., 2002; Heerssen et al., 2004) and in axonal transport of both microtubules and neurofilaments (He et al., 2005). To analyze whether reduced TrkA survival signalling in *mdx* mouse SCG neurons might depend on alterations in dynein expression, we evaluated mRNA and protein levels of this molecular motor. Changes in dynein levels might also have contributed to alterations in neuronal cytoskeleton, thus promoting the intrinsic defects observed in *mdx* mouse SCG neurons. Although the dynein mRNA level was slightly but significantly lower in P5 *mdx* mouse SCG than in the wt, the amount of expressed protein did not differ between wt and *mdx* mice, at P5, nor in the other examined ages. However, our data are only an evaluation of total protein levels. Even though dynein is present in equal amount in wt and *mdx* mouse SCG, it is still possible that alterations in its functioning exist. Dynein is a microtubule-based motor and tubulin expression appears to be altered as well in *mdx* mice SCG. Further studies are needed to examine the functional role of dynein and other cytoskeletal components in growth and maintenance of SCG neurons of mice lacking Dp427.

7.6 Conclusion

In summary, we have shown that, the SCG of adult *mdx* mice has 36% fewer neurons than that of wt mice. The greater neuron loss occurs during the period of the physiological neuronal death, between P5 and P10. Our data also show that the major alterations in the levels of molecules involved in neuronal growth and survival (NGF and its receptors, NF proteins) are evident in neonatal *mdx* mice, in a critical period for neuronal survival and the establishment of synaptic contacts. They, thus, may account both for the SCG increased neuronal death and target innervation defects. Most, but not all, of these alterations are not observed anymore in the adult,

suggesting that some compensatory mechanisms exist. In fact, those neurons present in 6-7 weeks old *mdx* mice are the surviving neurons, which have successfully passed the period of greater neuron death, and most of them project to the undamaged submandibular gland. However, they still show signs of an altered phenotype, in their inability to establish, or recover, a normal adrenergic fibres network in peripheral target organs. Our data show that axonal growth and terminal sprouting is impaired in all SCG neurons, independently on the type of target organ. This is probably caused by the lack of Dp427 that leads to the loss of DGC components, essential for the linkage between the cortical cytoskeleton and the ECM. These alterations do not per se induce neuronal death. However, when intrinsic alterations combine with the functional damages in SCG muscular targets (i.e. EBD permeable membranes and increased levels of proNGF), neuronal loss occurs. We, therefore, suggest that alterations of both the sympathetic neurons and their muscular targets consequent to the lack of Dp427 may contribute to the autonomic dysfunction described in DMD patients.

REFERENCES

Alderton J.M. and Steinhard R.A. (2000) Calcium influx through calcium leak channels is responsible for the elevated levels of calcium-dependent proteolysis in dystrophic myotubes. J Biol Chem 275, 9452-9460

Aloyz R.S., Bamji S.X., Pozniack C.D., Toma J.G., Atwal J., Kaplan D.R. and Miller F.D. (1998) p53 is essential for developmental neuron death as regulated by the TrkA and p75 neurotrophin receptors. J Cell Biol 143, 1691-1703

Ahmad F.J., Echeverri C.J., Valee R.B. and Baas P.W. (1998) Cytoplasmic dynein and dynactin are required for the transport of microtubules into the axon. J Cell Biol 140, 391-401

Ahmad F.J., He Y., Myers K.A., Hasaka T.P., Francis F., Black M.M. and Baas P.W. (2006) Effects of dynactin disruption and dynein depletion on axonal microtubules. Traffic 7, 524-537

Anderson J.L., Head S.I., Rae C. and Morley J.W. (2002) Brain function in Duchenne muscular dystrophy. Brain 125, 4-13

Anderson J.L., Head S.I. and Morley J.W. (2004) Long-term depressionis reduced in cerebellar Purkinje cells of dystrophin-deficient *mdx* mice. Brain Res 1019, 289-292

Andrews T.J., Thrasivoulou C., Nesbit W. and Cowen T. (1996) Target specific differences in the dendritic morphology and neuropeptide content of neuron in the rat SCG during development and aging. J Comp Neurol 368, 33-44

Azzena G.B. and Mancinelli R. (1999) Nitric oxide regenerates the normal colonic peristaltic activity in *mdx* dystrophic mouse. Neurosci Lett 261, 9-12

Baas P.W. and Buster D.W. (2003) Slow axonal transport and the genesis of neuronal morphology. J Neurobiol 58, 3-17

Baas P.W., Nadar C.V. and Myers K.A. (2006) Axonal transport of microtubules: the long and short of it. Traffic 7, 490-498

Baluk P. (1995) Structure of autonomic ganglia. In Autonomic Ganglia (McLachlan ed), 13-71 Harwood Academic Publishers Gmbh

Bamji S.X., Majdan M., Pozniak C.D., Belliveau D.J., Aloyz R., Kohn J., Causing C.G. and Miller F.D. (1998) The p75 neurotrophin receptor mediates neuronal apoptosis and is essential for naturally occurring sympathetic neuron death. J Cell Biol 140, 911-923

Barohn R.J., Levine E.J., Olson J.O. and Mendell J.R. (1988) Gastric hypomotility in Duchenne's muscular dystrophy. N Engl J Med 319, 15-18

Bhattacharyya A., Watson F.L., Pomeroy S.L., Zhang Y.Z., Stiles C.D. and Segal R.A. (2002) High-resolution imaging demonstrates dynein-based vescicular transport of activated Trk receptors. J Neurobiol 51, 302-312

Belecky-Adams T., Holmes M., Shan Y., Tedesco C.S., Mascari C., Kaul A., Wight D.C., Morris R.E., Sussman M., Diamond J. and Parysek L.M. (2003) An intact intermediate filament network is required for collateral sprouting of small diameter nerve fibers. J Neurosci 23, 9312-9319

Bennet M.R., Gibson W.G. & Lemon G. (2002) Neuronal cell death, nerve growth factor and neurotrophic models: 50 years on. Autonom Neurosci 95, 1-23

Bensen E.S., Jaffe K.M., and Tarr P.I. (1996) Acute gastric dilatation in Duchenne muscular dystrophy: a case report and review of the literature. Arch Phys Med Rehabil 77, 512-514

Berne R.M and Levy M.N. Principles of physiology (third edition). p.166 Casa Editrice Ambrosiana

Bierl M.A., Jones E.E., Crutcher K.A. and Isaacson L.G. (2005) “Mature” nerve growth factor is a minor species in most peripheral tissues. Neurosci Lett 380, 133-137

Bierl M.A. and Isaacson L.G. (2007) Increased NGF proforms in aged sympathetic neurons and their targets. Neurobiol Aging 28, 122-134

Black I.B., Hendry I.A. and Iversen L.L. (1971) Trans-synaptic regulation of growth and development of adrenergic neurons in a mouse sympathetic ganglion. Brain Res 34, 229-240

Black I.B. and Mytilineou C. (1976) Trans-synaptic regulation of the development of end organ innervation by sympathetic neurons. Brain Res 101, 503-521

Black M.M. and Lasek R.J. (1980) Slow components of axonal transport: two cytoskeletal networks. J Cell Biol 86, 616-623

Blake D.J. and Kroger S. (2000) The neurobiology of Duchenne muscular dystrophy: learning lessons from muscle? TINS 23, 92-99

Blake D.J., Weir A., Newey S.E. and Davies K.E. (2002) Function and genetics of dystrophin and dystrophin-related proteins in muscle. Physiol Rev 82, 291-329

Boland B., Himpens B., Denef J.F. and Gillis J.M. (1995) Site-dependent pathological differences in smooth muscles and skeletal muscles of the adult *mdx* mouse. Muscle Nerve 18, 649-657

Bonfanti L. (2006) PSA-NCAM in mammalian structural plasticity and neurogenesis. Progr Neurobiol 80, 129-164

Bowers C.W. and Zigmond R.E. (1979) Localization of neurons in the rat superior cervical ganglion that project into different postganglionic trunks. J Comp Neur 185, 381-392

Brady S.T. (2000) Neurofilaments run sprints not marathons. Nature Cell Biol 2, E43-E45

Brady S.T., Colman D.R. and Brophy P. (1999) Subcellular organization of the nervous system: organelles and their function. In Fundamental Neuroscience . 71-106. Academic Press

Bruno M.A. and Cuello A.C. (2006) Activity-dependent release of precursor nerve growth factor, conversion to mature nerve growth factor, and its degradation by a protease cascade. PNAS 103, 6735-6740

Brusés J.L. and Rutishauser U. (2001) Roles, regulation and mechanisms of polysialic acid function during neural development. Biochimie 83, 635-643

Byers T.J., Lidov H.G. and Kunkel L.M. (1993) An alternative dystrophin transcript specific to peripheral nerve. Nat Genet 4, 77-81

Campbell K.P. and Kahl S.D. (1989) Association of dystrophin and an integral membrane glycoprotein. Nature 338, 259-263

Campenot R.B. (1994) NGF and the local control of nerve terminal growth. J Neurobiol 25, 599-611

Cartaud A., Coutant S., Petrucci T.C. and Cartaud J. (1998) Evidence fon in situ and in vitro association between β-dystroglycan and the subsynaptic 43K rapsyn protein: consequence for acetylcholine receptor clustering at the synapse. J Biol Chem 273, 11321-11326

Casademunt E., Carter B.D., Benzel I., Frade J.M., Dechant G. and Barde Y.A. (1999) The zinc finger protein NRIF interacts with the neurotrophin receptor p75NTR and participates in programmed cell death. EMBO J 18, 6050-6061

Causing C.G., Gloster A., Aloyz R., Bamji S.X., Chang E., Fawcett J., Kuchel G. and Miller F.D. (1997) Synaptic innervations density is regulated by neuron-derived BDNF. Neuron, 18, 257-267

Chen Z.Y., Sun C., Reuhl K., Bergemann A., Henkemeyer M. and Zhou R. (2004) Abnormal hippocampal axon bundling in EphB receptor mutant mice. J Neurosci 24, 2366-2374

Chevalier-Larsen E. and Holzbaur E.L.F. (2006) Axonal transport and neurodegenerative disease. Biochimica Biophysica Acta 1762, 1094-1108

Coccurello R., Castellano C., Paggi P., Mele A. and Oliverio A. (2002) Genetically dystrophic *mdx*/*mdx* mice exhibit decreased response to nicotine in passive avoidance. Neuroreport 13, 1219-1222

Coral-Vazquez R., Cohn R.D., Moore S.A., Hill J.A., Weiss R.M., Davisson R.L., Straub V., Barresi R., Bansal D., Hrstka R.F., Williamson R. and Campbell K.P. (1999) Disruption of the sarcoglycan-sarcospan complex in vascular smooth muscle: a novel mechanism for cardiomyopathy and muscular dystrophy. Cell 98, 465-474

Cowen T. and Gavazzi I. (1998) Plasticity in adult and ageing sympathetic neurons. Progr Neurobiol 54, 249-288

Culligan K. and Ohlendieck K. (2002) Diversity of the brain dystrophin-glycoprotein complex. J Biomed Biotech 2, 31-36

Dail W.G. and Burton S. (1983) Structure and organization of mammalian sympathetic ganglia. In Autonomic Ganglia (Lars-Gösta Elfvin), 3-25 John Waley & Sons Ltd

Danialou G., Comtois A.S., Dudley R., Karpati G., Vincent G., Des Rosiers C. and Petrof B.J. (2001) Dystrophin-deficient cardiomyocytes are abnormally vulnerable to mechanical stress-induced contractile failure and injury. FASEB J 15, 1655-1657

Daston M.M., Bastmeyer M., Rutishauser U. and O'Leary D.D.M. (1996) Specially restricted increase in polysialic acid enhances corticospinal axon branching related to target recognition and innervation. J Neurosci 16, 5488-5497

De Biasi M. (2002) Nicotinic mechanisms in the autonomic control of organ systems. J Neurobiol 53, 568-579

Deconinck N. and Bernard D. (2007) Pathophysiology of Duchenne muscular dystrophy: current hypotheses. Pediatr Neurol 36, 1-7

De La Porte S., Morin S. and Koenig J. (1999) Charateristics of skeletal muscle in mdx mutant mice. Inter Rev Cytol 191, 99-148

Delcroix J.D., Valletta J.S., Wu C., Hunt S.V., Kowal A.S. and Mobley W.C. (2003) NGF signalling in sensory neurons: evidence that early endosomes carry NGF retrograde signals. Neuron 39, 69-84

Del Signore A., Gotti C., De Stefano M.E., Moretti M. and Paggi P. (2002) Dystrophin stabilizes α3 but not α7-containing nicotinic acetylcholine receptor subtypes at the postsynaptic apparatus in the mouse superior cervical ganglion. Neurobiol Disease 10, 54-66

Del Signore A., Gotti C., Rizzo A., Moretti M. and Paggi P. (2004) Nicotinic acetylcholine receptor subtypes in the rat sympathetic ganglion: pharmacological characterization, subcellular distribution and effect of pre- and postganglionic nerve crush. J Neuropathol Exp Neurol 63, 138-150

De Stefano M.E., Zaccaria M.L., Cavaldesi M., Petrucci T.C., Medori R. and Paggi P. (1997) Dystrophin and its isoforms in a sympathetic ganglion of normal and dystrophic *mdx* mice: immunolocalization by electron microscopy and biochemical characterization. Neurosci 80, 613-624

De Waegh S.M., Lee V.M. and Brady S.T. (1992) Local modulation of neurophilament phosphorylation, axonal caliber and slow axonal transport by myelinating Schwann cells. Cell 68, 451-463

Dubowitz V. and Crome L. (1969) The central nervous system in Duchenne muscular dystrophy. Brain 92, 805-808

Duchenne G. (1861) De l'electrisasion localiseè et de son application à la pathologie et à la thérapeutiche. Paris: Baillieère & Fills

Durbeej M. and Campbell K.P. Muscular dystrophies involving the dystrophin-glycoprotein complex: an overview of current mouse models. Curr Opin Gen Dev 12, 349-361

Dye W.W., Gleason R.L., Wilson E. and Humphrey J.D. (2007) Altered biomechanical properties of carotid arteries in two mouse models of muscular dystrophy. J Appl Physiol 103, 664-672

ElShamy W.M., Linnarsson S., Lee K.F., Jaenisch R. and Ernfors P. (1996) Prenatal and postnatal requirements of NT-3 for sympathetic neuroblast survival and innervation of specific targets. Development 122, 491-500

Enfors P., Lee K.F., Kucera J. and Jaenish R. (1994) Lack of neurotrophin-3 leads to deficiencies in the peripheral nervous system and loss of limb proprioceptive afferents. Cell 77, 503-512

Enfors P., Merlio J.P. and Persson H. (1992) Cells expressing mRNA for neurotrophins and their receptors during embryonic rat development. Eur J Neurosci 4, 1140-1158

Ervasti J.M. (2007) Dystrophin, its interactions with other proteins, and implications for muscular dystrophy. Biochim Biophys Acta 1772, 108-117

Esposito D., Patel P., Stephens R.M., Perez P., Chao M.V., Kaplan D.R. and Hempstead B.L. (2001) The cytoplasmic and transmembrane domain of the p75 and TrkA receptors regulate high affinity binding to nerve growth factor. J Biol Chem 276, 32687-32695

Fadic R. (2005) Cell surface and gene expression regulation molecules in dystrophynopathy: *mdx* vs. Duchenne. Biol Res 38, 375-380

Fahnestock M., Michalski B., Xu B. and Coughlin M.D. (2001) The precursor pro-nerve growth factor is the predominant form of nerve growth factor in brain and is increased in Alzheimer's disease. Mol Cell Neurosci 18, 210-220

Farhadi H., Pareek S., Day R., Dong W., Chrétien M., Bergeron J.J.M., Seidah N.G. and Murphy R.A. (1997) Prohormone convertases in mouse submandibular gland: co-localization of furin and nerve growth factor. J Histochem Cytochem 45, 759-804

Farinas I., Jones K.R., Backus C., Wang X.Y. and Reichardt L.F. (1994) Severe sensory and sympathetic deficits in mice lacking neurotrophin-3. Nature 369, 658-661

Feener C.A., Koenig M. and Kunkel L.M. (1989) Alternative splicing of human dystrophin mRNA generates isoforms at the carboxy terminus. Nature 338, 509-511

Francis N.J. and Landis S.C. (1999) Cellular and molecular determinants of sympathetic neuron development. Annu Rev Neurosci 22, 341-566

Ghasemlou N., Krol K.M., MacDonald D.R. and Kawaja M.D. (2004) Comparison of target innervation by sympathetic axons in adult wild type and heterozygous mice for nerve growth factor or its receptor TrkA. J Pineal Res 37, 230-240

Glebova N.O. and Ginty D.D. (2004) Heterogeneous requirement of NGF for sympathetic target innervation in vivo. J Neurosci 24, 743-751

Glebova N.O. and Ginty D.D. (2005) Growth and survival signals controlling sympathetic nervous system development. Annu Rev Neurosci 28, 191-222

Grady M.R., Teng H., Nichol M.C., Cunningham J.C., Wilkinson R.S., and Sanes J.R. (1997) Skeletal and cardiac myopathies in mice lacking utrophin and dystrophin: a model for Duchenne muscular dystrophy. Cell 90, 729-738

Haenggi T. and Fritschy J.-M. (2006) Role of dystrophin and utrophin for assembly and function of the dystrophin glycoprotein complex in non.muscle tissue. Cell Mol Life Sci 63, 1614-1631

Hamburger V. and Levi-Montalcini R. (1949) Proliferation, differentiation and degeneration in the spinal ganglia of the chick embryo under normal and experimental conditions. J Exp Zool 111, 457-502

Hanson M.G. and Landmesser L.T. (2004) Normal pattern of spontaneous activity are required for correct motor axon guidance and the expression of specific guidance molecules. Neuron 43, 687-701

Hanson M.G. and Landmesser L.T. (2006) Increasing the frequency of spontaneous rhythmic activity disrupts pool-specific axon fasciculation and pathfinding of embryonic spinal motoneurons. J Neurosci 26, 12769-12780

Harrington A.W., Leiner B., Blechschmitt C., Arevalo J.C., Lee R., Morl K., Meyer M., Hempstead B.L., Yoon S.O. and Giehl K.M. (2004) Secreted proNGF is a pathophysiological death-inducing ligand after adult CNS injury. Proc Natl Acad Sci USA 101, 6226-6230

Hasaka T.P., Myers K.A. and Baas P.W. (2004) Role of actin filaments in the axonal transport of microtubules. J Neurosci 24, 11291-11301

Hasan W., Pedchenko T., Krizsan-Agbas D., Baum L. and Smith P.G. (2003) Sympathetic neurons synthesize and secrete pro-nerve growth factor protein. J Neurobiol 57, 38-53

Hatten M.E. (1999) Central nervous system neuronal migration. Annu Rev Neurosci 22, 511-539

He Y., Francis F., Myers K.A., Yu W., Black M.M. and Baas P.W. (2005) Role of cytoplasmic dynein in the axonal transport of microtubules and neurofilaments. J Cell Biol 168, 697-703

Heerseen H.M., Pazyra M.F. and Segal R.A. (2004) Dynein motors transport activated Trks to promote survival of target-dependent neurons. Nature Neurosci 7, 596-604

Hempstead B.L. (2002) The many faces of p75NTR. Curr Opin Neurobiol 12, 260-267

Hirokawa N., Glicksman M.A. and Willard M.B. (1984) Organization of mammalian neurofilament polypeptides within the neuronal cytoskeleton. J Cell Biol 98, 1523-1526

Hnia K., Hugon G., Masmoudi A., Mercier J., Rivier F. and Mornet D. (2006) Effect of β-dystroglycan processing on utrophin/Dp116 anchorage in normal and *mdx* mouse Schwann cell membrane. Neurosci 14, 607-620

Hoffman E.P., Brown R.H. and Kunkel L.M. (1987) Dystrophin: the protein product of Duchenne muscular dystrophy locus. Cell 51, 919-928

Hoffman E.P., Hudeki M.S., Rosenberg P.A., Pollina C.M. and Kunkel L.M. (1988) Cell and fiber-type distribution of dystrophin. Neuron 1, 411-420

Honma Y., Araki T., Giannino S., Bruce A., Heuckeroth R., Johnson E.M. and Milbrand J. (2002) Artemin is a vascular-derived neurotrophic factor for developing sympathetic neurons. Neuron 35, 267-282

Howe C.L. and Mobley W.C. (2003) Signalling endosome hypothesis: a cellular mechanism for long distance communication. J Neurobiol 58, 207-216

Huang E.J. and Reichardt L.F. (2001) Neurotrophins: roles in neuronal development and function. Annu Rev Neurosci 24, 677-736

Huang E.J and Reichardt L.F. (2003) Trk receptors: roles in neuronal signal transduction. Annu Rev Biochem 72, 609-642

Ibraghimov-Beskrovnaya O., Ervasti J.M., Leveille C.J., Slaughter C.A., Sernett S.W. and Campbell K.P. (1992) Primary structure of dystrophin-associated glycoproteins linking dystrophin to the extracellular matrix. Nature 355, 696-702

Ibraghimov-Beskovraya O., Milatovich A., Ozcelic T., Yang B., Koepknik K., Franke U. and Campbell K.P. (1993) Human dystroglycan: skeletal muscle cDNA, genomic structure, origin of tissue specific isoforms and chromosomal localization. Hum Mol Genet 2, 1651-1657

Iwata Y., Katanosaka Y., Arai Y., Konamura K., Miyatake K. and Shigekawa M. (2003) A novel mechanism of myocyte degeneration involving the Ca2+-permeable growth factor-regulated channel. J Cell Biol 161, 957–967

Jagadha V. and Becker L.E. (1988) Brain morphology in Duchenne muscular dystrophy: a Golgi study. Pediatr Neurol 4, 87-92

Jahed A. and Kawaja D. (2005) The influences of p75 neurotrophin receptor and brain-derived neurotrophic factor in the sympathetic innervation of target tissues during murine postnatal development. Autonom Neurosci Basic Clin 118, 32-42

Jansen P., Giehl K., Nyengaard J.R., Teng K., Lioubinski O., Sjoegaard S.S., Breiderhoff T., Gotthardt M., Lin F., Eilers A., Petersen C.M., Lewin G.R., Hempstead B.L., Willnow T.E. and Nykjaer A. (2007) Roles of the pro-neurotrophin receptor sortilin in neuronal development, aging and brain injury. Nat Neurosci 10, 1449-1457

Julien J.P. and Mushynski W.E. (1983) Multiple phosphorylation sites among identified proteolytic fragments of mammalian neurofilaments. J Biol Chem 258, 4019-4025

Jung C., Chylinski T.M., Pimenta A., Ortiz D. and Shea T.B. (2004) Neurofilament transport is dependent on actin and myosin. J Neurosci 24, 9486-9496

Kaplan D.R. and Miller F.D. (2000) Neurotrophin signal transduction in the nervous system. Curr Opin Neurobiol 10, 381-391

Kaye D., Pimental D., Prasad S., Maki T., Berger H.J., McNeil P.L., Smith T.W. and Kelly R.A. (1996) Role of transiently altered sarcolemmal membrane permeability and basic fibroblast growth factor release in the hypertrophic response of adult rat ventricular myocytes to increased mechanical activity in vitro. J Clin Invest 97, 281–291

Kenchappa R.S., Zampieri N., Chao M.V., Barker P.A., Teng H.K., Hempstead B.L. and Carter B.D. (2006) Ligand-dependent cleveage of the p75 neurotrophin receptor is necessary forNRIF nuclear translocation and apoptosis in sympathetic neurons. Neuron 50, 219-232

Knuesel I., Mastoccola M., Zuellig R.A., Bornhauser B., Schaub M.C. and Fritschy J.M. (1999) Altered synaptic clustering of GABAA receptor in mice lacking dystrophin (*mdx* mice). Eur J Neurosci 11, 4457-4462

Kohn J., Aloyz R.S., Toma J.G., Haak-Frendscho M. and Miller F.D. (1999) Functionally antagonistic interactions between the TrkA and p75 neurotrophin receptors regulate sympathetic neuron growth and target innervation. J Neurosci 19, 5393-5408

Kullander K. and Klein R. (2002) Mechanisms and functions of Eph and ephrin signalling. Nat Rev Mol Cell Biol 3, 475-486

Kuruvilla R., Zweifel L.S., Glebova N.O., Lonze B.E., Valdez G. and Ginty D.D. (2004) A neurotrophin signalling cascade coordinates sympathetic neuron development through differential control of TrkA trafficking and retrograde signalling. Cell 118, 243-255

Lariviere R.C. and Julien J.P. (2003) Functions of intermediate filaments in neuronal development and disease. J Neurobiol 58, 131-148

Lee K.F., Bachman K., Landis S. and Jaenisch R. (1994) Dependence on p75 for innervations of some sympathetic targets. Science 263, 1447-1449

Lee K.F., Davies A.M. and Jaenisch R. (1994) p75-deficient embryonic dorsal root sensory and neonatal sympathetic neurons display a decreased sensitivity to NGF. Development 120, 1027-1033

Lee M.K., Xu Z., Wong P.C. and Cleveland D.W. (1993) Neurofilaments are obligate heteropolymers in vivo. J Cell Biol 122, 1337-1350

Lee M.K. and Cleveland D.W. (1996) Neuronal intermediate filaments. Annu Rev Neurosci 19, 187-217

Lee R., Kermani P., Teng K.K. and Hempstead B.L. (2001) Regulation of cell survival by secreted proneurotrophins. Science 294, 1945-1948

Leon S.H., Schuffler M.D., Kettler M. and Rohrmann C.A. (1986) Chronic intestinal pseudo-obstruction as a complication of Duchenne's muscular dystrophy. Gastroenterology 90, 455-459

Levitt M., Spector S., Sjoerdsma A. and Udenfriend S. (1965) Elucidation of the rate-limiting step in norepinephrine biosynthesis in the perfused guinea pig heart. J Pharmacol Exp Ther 148, 1-8

Lidov H.G.W., Byers T.J., Watkins S.C. and Kunkel L.M. (1990) Localization of dystrophin to postsynaptic regions of central nervous system cortical neurons. Nature 348, 725-728

Lidov H.G.W., Byers T.J. and Kunkel L.M. (1993) The distribution of dystrophin in the murine central nervous system: an immunocytochemical study. Neuroscience 54, 167-187

Liou J.C., Chen Y.H. and Fu W.M. (1999) Target-dependent regulation of acetylcholine secretion at developing motoneurons in Xenopus cell cultures. J Physiol 517.3, 721-730

Livak K.J and Schimttgen T.D. (2001) Analysis of relative gene expression data using real-time quantitative PCR and the $2^{-\Delta\Delta Ct}$ method. Methods 25, 402-408

Maisonpierre P.C., Belluscio L., Friedman B., Alderson R.F., Wiegand S.J., Furth M.E., Linsday R.M. and Yancopoulos G.D. (1990a) NT3, BDNF and NGF in the developing rat nervous system: parallel as well as reciprocal patterns of expression. Neuron 5, 501-509

Mallik R. and Gross S.P. (2004) Molecular motors: strategies to get along. Curr Biol 14, R971-R982

Mancinelli R., Tonali P., Servidei S. and Azzena G.B. (1995) Mechanical activity of small and large intestine in normal and *mdx* mice: a comparative analysis. Neurogastroenterol Motil 11, 133-139

Martin-Zanca D., Oskam R., Mitra G., Copeland T. and Barbacid M. (1989) Molecular and biochemical characterization ofthe human trk proto-oncogene. Mol Cell Biol 9, 24-33

Majdan M., Walsh G.S., Aloyz R. and Miller F.D. (2001) TrkA mediates developmental sympathetic neuron survival in vivo by silencing an ongoing p75NTR-mediated death signal. J Cell Biol 155, 1275-1285

Megeney L.A., Kablar B., Perry R.L.S., Ying C., May L. and Rudnicki M.A. (1999) Severe cardiomyopathy in mice lacking dystrophin and MyoD. Proc Natl Acad Sci U.S.A. 96, 220-225

Mehler M.F. (2000) Brain dystrophin, neurogenetics and mental retardation. Brain Res Rev 32, 277-307

Mehler M.F., Haas K.Z., Kessler J.A. and Stanton P.K. (1992) Enhanced sensitivity of hippocampal pyramidal neurons from *mdx* mice to hypoxia-induced loss of synaptic transmission. Proc Natl Acad Sci USA 89, 2461-2465

Mehler M.F. and Kessler J.A. (1998) Neural progenitor cells and developmental disorders. Ment Retard Dev Disabil Res Rev 4, 143-149

Michele D.E. and Campbell K.P. (2003) Dystrophin–glycoprotein complex: post-translational processing and dystroglycan function. J Biol Chem 278, 15457-15460

Mischel P.S., Smith S.G:, Vining E.R., Valletta J.S. and Mobley W.C. (2001) The extracellular domain of p75NTR is necessary to inhibit neurotrophin-3 signalling through TrkA. J Biol Chem 276, 11294-11301

Mischel P.S., Umbach J.A., Eskandari S., Smith S.G., Gundersen C.B. and Zampighi G.A. (2002) Nerve growth factor signals via preexisting TrkA receptor oligomers. Biophys J 83, 968-976

Mokri B. and Engel A.G. (1975) Duchenne dystrophy: electron microscopic findings pointing to a basic or early abnormality in the plasma membrane of the muscle fiber. Neurology 25, 1111-1120

Mulè F., D'Angelo S., Tabacchi G., Amato A. and Serio R. (1999) Mechanical activity of small and large intestine in normal and *mdx* mice: a comparative analysis. Neurogastroenterol Mot 11, 133-139

Mulè F., Vannucchi M.G., Corsani L., Serio R. and Faussone-Pellegrini M.S. (2001) Myogenic NOS and endogenous NO production are defective in colon from dystrophic (*mdx*) mice. Am J Physiol Gastrointest Liver Physiol 281, G1264-G1270

Mulè F., Amato A., Vannucchi M.G., Faussone-Pellegrini M.S. and Serio R. (2006) Altered tachykinergic influence on gastric mechanical activity in *mdx* mice. Neurogastroenterol Mot 18, 844-852

Nico B., Frigeri A., Nicchia G.P., Corsi P., Ribatti D., Quondamatteo F., Herken R., Girolamo F., Marzullo A., Svelto M. and Roncali L. (2003) Severe alterations of endothelial and glial cells in the blood-brain barrier of dystrophic *mdx* mice. Glia 42, 235-251

Nowak T.V., Ionasescu V. and Anura S. (1982) Gastrointestinal manifestations of the muscular dystrophies. Gastroenterology 82, 800-810

Nykjaer A., Lee R., Teng K.K., Jansen P., Madsen P., Nielsen M.S., Jacobsen C., Kliemannel M., Schwartz E., Willnow T.E. Hempstead B.L. and Petersen C.M. (2004) Sortilin is essential for proNGF-induced neuronal cell death. Nature 427, 843-848

Nykjaer A., Willnow T.E. and Petersen C.M. (2005) p75NTR – live or let die. Curr Opin Neurobiol 15, 49-57

Oppenheim R.W. (1991) Cell death during development of the nervous system. Annu Rev Neurosci 14, 453-501

Pang P.T., Teng H.K., Zaitsev E., Woo N.T., Sakata K., Zhen S., Teng K.K., Yung W.H., Hempstead B.L. and Lu B. (2004) Cleavage of proBDNF by tPA/plasmin is essential for long-term hippocampal plasticity. Science 306, 487-491

Pardini B.J., Lund D.D. and Schmid P.G. (1989) Organization of the sympathetic postganglionic innervation of the rat. J Auton Nerv Syst 28, 193-201

Peng S., Wuu J., Mufson E.J. and Fanhestock M. (2004) Increased proNGF levels in subjects with mild cognitive impairment and mild Alzheimer disease. J Neuropathol Exp Neurol 63, 641-649

Personius K.E. and Balice Gordon R.J. (2000) Activity-dependent editing of neuromuscular synaptic connections. Brain Res Bull 53, 513-522

Pescosolido N., Del Bianco G., De Feo G., Madia F., Risuleo G. and Scarsella G. (1998) Induced acute hypertension: mode of retinal cell degeneration. Acta Ophthalmol Scand 76, 20-21

Peters E.M.J., Hendrix S., Golz G., Klapp B.F., Arck P.C. and Paus R. (2006) Nerve growth factor and its precursor differentially regulate hair cycle progression in mice. J Histochem Cytochem 54, 275-288

Petrof B.J., Shrager J.B., Stedman H.H., Kelly A.M. and Sweeney H.L. (1993) Dystrophin protects the sarcolemma from stresses developed during muscle contraction. Proc Natl Acad Sci USA 90, 3710-3714

Porter J.D., Merriam A.P., Leahy P., Gong B., Feuerman J., Cheng G. and Khanna S. (2004) Temporal gene expression profiling of dystrophin deficient (*mdx*) mouse diaphragm identifies conserved and muscle group-specific mechanisms in the pathogenesis of muscular dystrophy. Hum Mol Genet 13, 257-269

Purves D. (1988) Body and brain, a trophic theory of neural connections. Harvard UP, Cambridge, MA.

Rando T. (2001) The dystrophin-glycoprotein complex, cellular signalling, and the regulation of cell survival in the muscular dystrophies. Muscle Nerve 24, 1575-1594

Randolph C.L., Bierl M.A. and Isaacson L.G. (2007) Regulation of NGF and NT-3 protein expression in peripheral targets by sympathetic input. Brain Res 1144, 59-69

Rassadi S., Krishnaswamy A., Pié B., McConnell R., Jacob M.H. and Cooper E. (2005) A null mutation for the □3 nicotinic acetycholine (ACh) receptor gene abolishes fast synaptic activity in sympathetic ganglia and reveals that ACh output from developing preganglionic terminals is regulated in an activity-dependent retrograde manner. J Neurosci 25, 8555-8566

Riccio A., Piechala B.A., Ciarallo C.L. and Ginty D.D. (1997) An NGF-TrkA-mediated retrograde signal to transcription factor CREB in sympathetic neurons. Science 277, 1097-1100

Rybakova I.N., Patel J.R. and Ervasti J.M. (2000) The dystrophin complex forms a mechanically strong link between the sarcolemma and costameric actin. J Cell Biol 150, 1209-1214

Sadoulet-Puccio H.M., Rajala M. and Kunkel L.M. (1997) Dystrobrevin and dystrophin: an interaction through coiled-coil motifs. Proc Acad Natl Sci USA 94, 12413-12418

Saffran B.N. and Crutcher K.A. (1990) NGF-induced remodeling of mature uninjured axon collaterals. Brain Res 525, 11-20

Sapp J.L., Bobet J. and Howlett S.E. (1996) Contractile properties of myocardium are altered in dystrophin-deficient *mdx* mice. J Neurol Sci 142, 17– 24

Sbriccoli A., Santarelli M., Carretta D., Pinto F., Granato A. and Minciacchi D. (1995) Architectural changes of the cortico-spinal system in the dystrophin detective *mdx* mouse. Neurosci Lett 200, 53-56

Seidah N.G., Benjannet S., Pareek S., Savaria D., Hamelin J., Goulet B., Laliberté J., Lazure C., Chrétien M. and Murphy R.A. (1996) Cellular processing of the nerve growth factor precursor by the mammalian pro-protein convertases. Biochem J 314, 951-960

Sekiguchi M. (2005) The role of dystrophin in the central nervous system. Acta Myol 24, 93-97

Senger D.L. and Campenot R.B. (1997) Rapid retrograde tyrosine phosphorylation of TrkA and other proteins in rat sympathetic neurons in compartmented cultures. J Cell Biol 138, 411-421

Shah J.V., Flanagan L.A., Janmey P.A. and Leterrier J. (2000) Bidirectional translocation of neurofilaments along microtubules mediated in part by dynein/dynactin. Mol Biol Cell 11, 3495-3508

Schinder A.F. and Poo M.M. (2000) The neurotrophin hypothesis for synaptic plasticity. Trends Neurosci 23, 639-645

Serio R., Bonvissuto F. and Mule` F. (2001) Altered electrical activity in colonic smooth muscle cells from dystrophic (*mdx*) mice. Neurogastroenterol Motil 13, 169-175

Shooter E.M. (2001) Early days of nerve growth factor proteins. Annu Rev Neurosci 24, 601-629

Sicinsky P., Geng Y., Ryder C.A., Barnard E.A., Darlison M.G. and Barnard P.J. (1989) The molecular basis of muscular dystrophy in the *mdx* mouse: a point mutation. Science 244, 1578-1580

Smith A. Gervasi C. and Szaro B.G. (2006) Neurofilament content is correlated with branch length in developing collateral branches of Xenopus spinal cord neurons. Neurosci Lett 403, 283-287

Stedman H., Sweeney H.L., Shrager J.B., Maguire H.C., Panettieri R.A., Petrof B., Narusawa M., Leferovich J.M., Sladky J.T. and Kelly A.M. (1991) The *mdx* diaphragm reproduces the degenerative changes of Duchenne muscular dystrophy. Nature 352, 536-539

Steel M.C. and Buckley N.J. (1993) Differential regulation of muscarinic receptor mRNA levels in neuroblastoma cells by chronic agonist exposure: a comparative polymerase chain reaction study. Mol Pharmacol 43, 694-701.

Straub V., Rafael J.A., Chamberlain J.S. and Campbell K.P. (1997) Animal models for muscular dystrophy show different patterns of sarcolemmal disruption. J Cell Biol 139, 375-385

Sugita S., Saito E., Tang J., Satz J., Campbell K.P. and Sudhof T.C. (2001) A stoichiometric complex of neurexins and dystroglycan in brain. J Cell Biol 154, 435-445

Tang J., Landmesser L. and Rutishauser U. (1992) Polysialic acid influences specific pathfinding by avian motorneurons. Neuron 8, 1031-1044

Taxi J. and Eugene D. (1995) Effects of axotomy, deafferentation and reinnervation on sympathetic ganglionic synapses: a comparative study. Int Rew Cytol 159, 195-263

Teng H.K., Teng K.K., Lee R., Wright S., Tevar S., Almeida R.D., Kermani P., Torkin R., Chen Z.Y., Lee F.S., Kraemer R.T., Nykjaer A. and Hempstead B.L. (2005) ProBDNF induces neuronal apoptosis via activation of a receptor complex of p75NTR and sortilin. J Neurosci 25, 5455-5463

Theiss C., Napirei M. and Meller K. (2005) Impairment of anterograde and retrograde neurofilament transport after anti-kinesin and anti-dynein antibody microinjection in chicken dorsal root ganglia. Eur J Cell Biol 84, 29-43

Vannucchi M.G., Zardo C., Corsani L. and Faussone-Pellegrini M.S. (2002) Interstitial cells of Cajal, enteric neurons, and smooth muscle and myoid cells of the murine gastrointestinal tract express full-length dystrophin. Histochem Cell Biol 118, 449-457

Vannucchi M.G., Corsani L. and Faussone-Pellegrini M.S. (2003) Synaptic vesicle morphology and recycling are altered in myenteric neurons of mice lacking dystrophin (*mdx* mice). J Cell Physiol 197, 232-242

Vannucchi M.G., Zizzo M.G., Zardo C., Pieri L., Serio R., Mule` F. and Faussone-Pellegrini M.S. (2004) Ultrastructural changes in the interstitial cells of Cajal and gastric dysrhythmias in mice lacking full length dystrophin (*mdx* mice). J Cell Physiol 199, 293- 309

Voyvodic J.T. (1989) Peripheral target regulation of dendritic geometry in the rat superior cervical ganglion. J Neurosci 9, 1997-2010

Wang L. and Brown A. (2002) Rapid movements of microtubules in axons. Curr Biol 12, 1496-1501

Wang L., Ho C., Sun D., Liem R.K.H. and Brown A. (2000) Rapid movement of axonal neurofilaments interrupted by prolonged pauses. Nature Cell Biol 2, 137-141

Watson F.L., Heerseen H.M., Bhattacharyya A., Klesse L., Lin M.Z. and Segal R.A. (2001) Neurotrophins use the Erk5 pathway to mediate a retrograde survival response. Nat Neurosci 4, 981-988

Wright L.L. (1995) Development and sexual differentiation of sympathetic ganglia. In Autonomic ganglia (McLachlan ed) 481-508 Harwood Academic Publishers Gmbh

Wright L.L., Cunningham T.J. and Smolen A.J. (1983) Developmental neuron death in the rat superior cervical sympathetic ganglion. Cell counts and ultrastructure. J Neurocytol 1, 739-750

Wyatt S. and Davies A. (1995) Regulation if nerve growth factor gene expression in sympathetic neurons during development. J Cell Biol 130, 1435-1446

Yabe J.T., Pimenta A. and Shea T.B. (1999) Kinesin-mediated transport of neurofilament protein oligomers in growing axons. J Cell Sci 112, 3799-3814

Yan Y. and Brown A. (2005) Neurofilament polymer transport in axons. J Neurosci 25, 7014-7021

Ye H., Kuruvilla R., Zweifel L.S. and Ginty D.D. (2003) Evidence in support of signalling endosome-based retrograde survival of sympathetic neurons. Neuron 39, 57-68

Yoon S.O., Casaccia-Bonnefil P., Carter B. and Chao M.V. (1998) Competitive signalling between TrkA and p75 nerve growth factor receptors determine survival. J Neurosci 18, 3273-3281

Yotsukura T., Sasaki K., Kachi L., Sasaki A., Ishihara T. and Ishikawa K. (1995) Circadian rhythm and variability of heart rate in Duchenne-type progressive muscular dystrophy. Am J Cardiol 76, 947-951

Zaccaria M.L., De Stefano M.E., Properzi F., Gotti C., Petrucci T.C. and Paggi P. (1998) Disassembly of the cholinergic postsynaptic apparatus induced by axotomy in mouse sympathetic neurons: the loss of dystrophin and β-dystroglycan immunoreactivity precedes that of the acetylcholine receptor. J Neuropathol Exp Neurol 57, 768-779

Zaccaria M.L., De Stefano M.E., Gotti C., Petrucci T.C. and Paggi P. (2000) Selective reduction in the nicotinic acetylcholine receptor and dystroglycan at the postsynaptic apparatus of *mdx* mouse superior cervical ganglion. J Neuropathol Exp Neurol 59, 103-112

Zaccaria M.L., Di Tommaso F., Brancaccio A., Paggi P. and Petrucci T.C. (2001) Dystroglycan distribution in adult mouse brain: a light and electron microscopy study. Neurosci 104, 311-324

Zweifel L.S., Kuruvilla R. and Ginty D.G. (2005) Functions and mechanisms of retrograde neurotrophin signalling. Nature Neurosci 6, 615-625

RINGRAZIAMENTI

Non sono molto brava a esprimere i miei pensieri, ma ci sono molte le persone che hanno, direttamente o indirettamente, contribuito alla realizzazione di questo lavoro e vorrei perciò ringraziarle tutte.

Innanzitutto ringrazio la Professoressa Paggi, mio docente guida, per la fiducia che ha sempre dimostrato nei miei confronti. Ho imparato da lei la precisione e l'attenzione ai dettagli.

Ringrazio la Professoressa Egle De Stefano. La sua dedizione alla ricerca è un grande insegnamento per me e rimane un esempio da imitare. Potermi confrontare con lei durante lo svolgimento degli esperimenti è stato preziosissimo, anzi direi indispensabile! Vorrei ringraziarla per tutto il tempo che mi ha dedicato e la pazienza che ha avuto con me.

Non potrei mancare di ringraziare tutte le persone che si sono succedute nel "Laboratorio Paggi" in questi tre anni : assegniste, dottorande e studenti. Il tempo passato con loro è stato intenso e impegnativo, ma sempre molto bello e arricchente. Ognuno di loro mi ha aiutato e sostenuto nel mio lavoro, materialmente o anche solo moralmente. Anche fuori dal laboratorio, la loro amicizia è stata, e continua ad essere, molto preziosa per me. Vorrei citarli tutti, sperando di non dimenticare nessuno : Arianna, Lucia, Michele, Sara, Francesca, Claudia, Marcello, Barbara, Valentina, Barbara, Tania, Matteo, Angela.

Infine, un ringraziamento a tutta la mia famiglia e in particolare a mamma, papà, Milena e nonna. Ognuno a modo suo mi ha sostenuto sempre, ascoltando, anche senza capire niente, i miei discorsi "scientifici"… Mi hanno incoraggiata quando ero demoralizzata e hanno gioito con me quando ero soddisfatta. E poi, Antonio, che è "arrivato" solo nell'ultimo anno, ma ha cambiato la mia vita e il modo in cui vedo il mio futuro: grazie!